AN ALL-PNEUMATIC ARTIFICIAL VENTRICLE DRIVING SYSTEM: ITS DEVELOPMENT AND SIMULATED PERFORMANCE AS A REPLACEMENT OF THE MYOCARDIAL FUNCTION

Seimer Hing Lau Tsang

A RESEARCH THESIS

IN THE

FACULTY OF ENGINEERING

Presented in Partial Fulfilment of the Requirements for the Degree of DOCTOR OF ENGINEERING

at

Concordia University

Montreal, Quebec

August 1976

© Seimer Hing Lau Tsang 1977

AN ALL-PNEUMATIC ARTIFICIAL VENTRICLE DRIVING SYSTEM: ITS DEVELOPMENT AND SIMULATED PERFORMANCE AS A REPLACEMENT OF THE MYOCARDIAL FUNCTION

Seimer Hing Lau Tsang

ABSTRACT

This thesis is involved with the development of an all-pneumatic driving system which provides the Starling's cardiac regulation function to a sac-type artificial left ventricle at constant frequency. The system, built basically from commercially available fluid operated devices, utilizes atrial pressure feedback to adjust the ventricle pumping air pressure, with the aid of a hydraulic/pneumatic pressure transducer developed especially for the application.

A mathematical model of an air-driven, sac-type artificial ventricle is presented. The model, derived from the energy and mass conservation equations of a deformable control volume, includes terms that can be identified as the ventricle sac elasticity, the ventricle hydrostatic head, the fluid kinetic energy, the fluid inertia and the driving air pressure. The model also includes the inlet and outlet flow rates as variables to allow for the transition period when both the inlet and outlet valves are open at the start of either the systolic or diastolic air pressure pulse. The equation gives the net pressure available for the fluid ejection process during systole, and indicates the contributing energy sources that help the ventricle to restore to its full volume during diastole. The model with a latex ventricle was evaluated in mock circulation tests, and it was later used in a digital simulation study of cardiovascular dynamics in which an artificial heart replaces the myocardial function.

ACKNOWLEDGEMENTS

The author wishes to express his gratitude to Dr. M.P. duPlessis, Professor and Chairman of the Department of Mechanical Engineering, for his assistance and support in this project and in the preparation of the thesis. The author also wishes to expres's his thanks to Mrs. Nancy Elliott in typing the manuscript.

This work was carried out under Grant No. 040-119 from the National Research Council of Canada to whom the author is indebted.

TABLE OF CONTENTS

Table of Contents (cont'd.)

Table of Contents (cont'd.)

LIST OF TABLES

LIST OF FIGURES

LIST OF SYMBOLS

A	ventricle output at $P_V = 0$
$\vec{A}$	flow area at control surface
A_{be}	effective area of bellows capsule
A_e	effective exit flow area of ventricle
A_i	average cross-sectional area of atrium and connecting tube
A_U	effective cross-sectional area of ventricle
A_o	ventricle output tube cross-sectional area
A_n	cross-sectional area, n = 1,2
B	ventricle sensitivity to venous pressure
C	capacitance (See Subscripts)
C_A	lumped arterial compliance
C_{ao}	capacitance of upper portion of ventricle
C_{at}	capacitance of atrium
C_n	capacitances, n = 0,1,2
C_V	lumped venous compliance
$C_{f1,f2,\ell}$	capacitances
d	tube diameter
d_e	sensor chamber diameter of h/p transducer
d_n	sensor nozzle diameter of h/p transducer
d_s	exit nozzle seat diameter of h/p transducer
$f(R_1)$	function of R_1
g	gravitational acceleration constant
h/p	hydraulic/pneumatic

$h_{i,r,t,n}$	vertical heights, n = 0,1,2,3
h_U	effective vertical component of ventricle depth, see Figure 39
h_{Uo}	initial ventricle depth with full ventricle volume
I	inertance (See Subscripts)
$I_{f,\ell,n}$	fluid inertances, n = 0,1,2,3
k	specific heat ratio of air
K	compliance ratio, C_V/C_A
k_{bS}	spring constant of bellows capsule, pressure per unit displacement
K_i, K_n	resistance coefficients, n = 0,1,2,3
ℓ	tube length
n_i, n_n	exponents, subscript n = 0,1,2,3
P, $\overline{P}$	pressure, mean pressure
P'	complementary of P
P_a	absolute pressure
P_A	arterial pressure
P_{ao}	ventricle output pressure, N/m^2
P_{at}, $\overline{P}_{at}$	atrial pressure, N/m^2, mean atrial pressure
P_E	ventricle-air exhaust pressure
P_i	blood pressures, i = 01,02,.....11,12 (see Figure 50)
P_o	pressure amplitude
P_n	pressure, n = 1,2, N/m^2
P_V	venous pressure
$P_{va,vaL,vaR}$	ventricle air pressures, N/m^2
$P_{vt,vtL,vtR}$	ventricle top pressures, N/m^2
P_{VAC}	ventricle air control pressure

P_{VAS}	ventricle air supply pressure
P_{03}	sensor output pressure of h/p transducer
P_{S1}	air supply pressure to air-piloted pressure regulator
P_{S2}	air supply pressure to pneumatic square-wave signal generator
P_{S3}	air supply pressure to h/p pressure transducer
P_{σ}	ventricle elastic stress, N/m^2
$P_{\sigma o}$	ventricle elastic stress constant, N/m^2
q	blood flow rate (See Subscripts)
Q	ventricle output, flow rate
Q_i, Q_n	flow rate, $n = 0,1,2,3$, m^3/sec
r	tube radius
R	circulatory resistance (See Subscripts)
R_v	output valve leakage resistance
$R_{f,\ell}$	resistances
R'	shunt resistance of arteries (See Subscripts)
R_1, R_2	pneumatic resistances
S	control surface
S_v	valve stroke
S_{ve}	effective valve stroke
S/D	systolic/diastolic time ratio
t	time
t_s	systolic time period
$t_{0,0L,0R}$	elapsed times before the opening of the outlet valve at the onset of systole
$t_{1,1L,1R}$	elapsed times before the outlet flow reverses its direction at the onset of diastole

$t_{2,2L,2R}$	elapsed times before the opening of the inlet valve at the onset of diastole
u	internal energy
V	velocity (voltage in Figure 3)
V_A	lumped volume of arteries
$\vec{V}_b$	velocity of moving control surface S
V_{bo}	initial volume of trapped air within bellows capsule
$\vec{V}_r$	fluid velocity relative to control surface S
V_{ST}	stroke volume
V_v	lumped volume of veins
V_υ	ventricle volume
$V_{\upsilon d}$, V_D	ventricle volume attained at the end of diastole
$V_{\upsilon o}$	initial full ventricle volume
$V_{\upsilon s}$, V_S	ventricle volume attained at the end of systole
W_n	natural frequency
$\dot{W}_{MECH}$	rate of mechanical work
$\dot{W}_{SHEAR}$	rate of shear work
X	distance between flapper sensor seat and bellows capsule as shown in Figures 19 and 21
X_0	set point adjusted when the inside of bellows capsule exposed to atmosphere
X_{01}, X_{02}, X_i	valve disc displacement
z	vertical dimension
α, α_o	resistance coefficients
β	ventricle capacitance coefficient
$\Delta P_i, \Delta P_n$	friction losses, n = 0,1,2,3
γ	ρg

λ	valve stroke coefficient
ρ	fluid density
υ_c	control volume
μ	fluid viscosity
η	multiplication factor of resistance
ζ	damping ratio
τ	time constant

Subscripts

ABAR	abdominal arteries
ABCP	abdominal capillaries
ABVE	abdominal veins
ASAO	ascending aorta
BRCP	bronchial capillaries
COAR	coronary arteries
HAAR	head and arms arteries
HACP	head and arms capillaries
HAVE	head and arms veins
INAR	intestinal arteries
INCP	intestinal capillaries
INVE	intestinal veins
INVC	inferior vena cava
LA	left atrium
LAVR	left atrium venous return
LEAR	legs arteries

LECP	legs capillaries
LEVE	legs veins
PUAR	pulmonary arteries
PUCP	pulmonary capillaries
PUVE	pulmonary veins
RA	right atrium
RAVR	right atrium venous return
SUVC	superior vena cava
THAO	thoracic aorta
THAR	thoracic arch

LIST OF PNEUMATIC CIRCUIT SYMBOLS

INHIBITOR

AND GATE

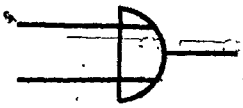

OR GATE

DIODE

ADJUSTABLE RESISTOR
(NEEDLEVALVE)

VOLUME

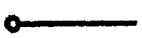

SUPPLY

INTRODUCTION

Coronary artery disease leading to a heart attack is the most common cause of death from heart diseases. Research in drug therapy for coronary thrombosis and preventive study on arteriosclerosis (hardening of the arteries) of the coronary arteries have made considerable advances in the combat of the disease. In cases when clinical procedures have either been administered too late or been unproductive, artificial hearts are good alternatives as replacements of the physiological hearts in the extension of life [1]. Artificial hearts are also potentially beneficial to patients stricken with poorly functioning myocardium (heart muscles).

The purpose of the artificial heart is to replace the myocardial function of the physiological heart of the recipient, either as a temporary substitute, or permanently. The physiological heart regulation characteristics, known as the Frank-Starling Law [2] of the heart, are usually described by function curves of the variations of cardiac output flow and the input pressure at the atrium, as shown in Figure 1. Details of the cardiac functions are described in the book by Guyton, et al. [3]. The operating points of the human heart are the respective intercepts of the left and right venous return curves with the left and right cardiac output curves where the venous return flow equals the cardiac output. The normal mean cardiac output is approximately 5 lit/min with a mean left atrial pressure of 4 mm Hg and

a mean right atrial pressure of 0 mm Hg. At these conditions, the sensitivity of the left ventricle function curve is 1.2 lit/min/mm Hg and 4.3 lit/min/mm Hg for the right ventricle. The outputs from an artificial heart must therefore possess these regulation characteristics. In addition, the artificial heart should also be able to provide the following fluid power output, mean aortic pressure and mean pulmonary pressure requirements.

	Minimum	Maximum
Fluid power output	1 watts	4 watts
Mean aortic pressure	60 mm Hg	140 mm Hg
Mean pulmonary pressure	12 mm Hg	28 mm Hg

This thesis involves the development of a sac-type artificial ventricle system to achieve Starling's Law response. An artificial ventricle system refers to the combination of the ventricle with its control and power source. Air is used as the driving fluid of the ventricle, as well as in the operation of the pressure transducer and in the control of the logic circuit. Potential advantages of the system are its simplicity, low cost and the low air pressure requirements of the driving system.

The first chapter of this thesis gives a review of existing artificial heart devices and systems. It is followed in the second chapter with a description of the presently developed artificial ventricle driving and control system, and its performance in a water cir-

culatory system. In the third chapter, a simple mathematical model of the physiological circulatory system is used to compare the simulated performance of the system with Starling's response of the natural left heart. A mathematical model of an air-driven, sac-type artificial ventricle, derived from the energy and mass conservation equations of a deformable control volume, is presented in the fourth chapter. The final chapter of the thesis is a further simulation study of the driving system in a complete model of the human cardiovascular system, using the derived ventricle model. Earlier mock circulation tests and the acquired simulation data indicate that the present artificial ventricle system could be developed further to replace the myocardial function of the physiological heart.

CHAPTER 1

A REVIEW OF EXISTING ARTIFICIAL HEARTS AND SYSTEMS

1.1 Human Cardiovascular System

A schematic diagram of the physiological heart and the cardiovascular system is shown in Figure 2. The left ventricle ejects freshly oxygenated blood through the aorta into arteries (the systemic circulatory system) leading to the head, internal organs, limbs, heart muscles and the bronchial capillary bed. Oxygen is diffused from the blood into the cells of the organs. The oxygen depleted blood then returns to the right atrium and right ventricle through veins and the vena cava. The right ventricle pumps the return blood into the lungs (the pulmonary circulatory system) where oxygen from the atmosphere diffuses into the blood. The oxygen-enriched blood flows into the left atrium and left ventricle for recirculation. The left and right ventricles contract and relax in unison at a normal heart rate of 75 beats per minute. An artificial heart is meant to substitute the physiological heart in the above described function.

1.2 Artificial Heart Classifications

Artificial hearts are basically blood pumps which deliver

blood from one circulation system to another. The left ventricle receives blood from the pulmonary circulatory system and delivers it to the systemic circulatory system. In terms of the manner in which blood is transported, existing blood pumps can be grouped into two basic classifications: kinetic pumps and positive displacement pumps. Kinetic pumps, utilizing rotating impellers, add energy to the blood by increasing its velocity as in a centrifugal pump [4-6]. The positive displacement pump achieves the pumping action by means of a displacement of the chamber containing blood. The volumetric displacement in the latter pump class is obtained either from rotary motion of mechanical mechanisms [7-13], from reciprocating motion of pistons [14, 15] or from direct displacement action of cylindrical chambers [16, 17], diaphragms [18-26], and ventricle sacs [27-40].

Table 1 is a summary of some typical positive displacement heart pumps. It gives the types of driving system for the actuating motion, which include electric motors, electromagnetic devices, hydraulic motors, electro-hydraulic systems, electro-pneumatic systems, all-pneumatic systems and electrical stimulation of piezo-electric crystals. All of the heart pumps can deliver the mean flow of 5 lit/min.

TABLE 1 Summary of Some Typical Positive Displacement Pumps.

HEART PUMP TYPE	TYPE OF ACTUATION	TYPE OF DRIVING SYSTEM
Fingers [7]	Rotary Mechanism	Electric Motor
Roller [7-12]	Rotary Mechanism	Electric Motor
Rotary [13]	Fixed Vane, Rotary Housing	Hydraulic Motor
Piston [14]	Reciprocating Mechanism	Electric Motor
Pendulum [15]	Reciprocating Mechanism	Electric Motor
Bladder [16]	Pulsatile Air Pressure	Electro-pneumatic System *
Wave-Pulsation [17]	Pulsatile Air Pressure	Electro-pneumatic System *
Diaphragm [18]	Hydraulic Fluid Motion	Electromagnetic System
Diaphragm [19-22]	Pulsatile Air Pressure	Electro-pneumatic System *
Diaphragm [23]	Pulsatile Air Pressure	Electric/Bellows Air Pump
Piezoelectric [24-26]	Bending of Crystal	Electrical Stimulation
Sac [27]	Motion of Bellows	Electromagnetic System
Sac [28]	Hydraulic Fluid Motion	Reciprocating Piston
Sac [29-36]	Pulsatile Air Pressure	Electro-pneumatic System *
Sac [37,38]	Pulsatile Air Pressure	All-pneumatic System *
Sac [39,40]	Hydraulic Fluid Motion	Electro-Hydraulic System

* See following Section for descriptions.

1.3 Air Driving And Regulating Systems

The major problems in the use of artificial hearts are the damage of red blood cells (hemolysis) and the formation of blood clots (thrombosis) [1, 41, 42]. The incompatibility of materials for prosthetic ventricles and heart valves with tissue and blood is identified as one of the causes of hemolysis and thrombosis. (Recent developments of new elastic materials for artificial hearts have reduced thrombosis and hemolysis [41, 43].) The other cause of hemolysis is the result of high shear stress induced on blood from the pumping action [42].

Among different types of artificial hearts, the diaphragm-type and the sac-type are generally considered the most suitable because of the gentle pumping action which produces a low rate of red blood cell hemolysis [1, 19]. Air is preferred as the driving fluid by many investigators because of the ease with which it can be handled and controlled in pulsatile systems.

Typical driving systems used for air-powered diaphragm-type or sac-type artificial hearts can be classified as either electro-pneumatic (E-P) or all-pneumatic (A-P).

(a) An electro-pneumatic driving system consists of voltage-controlled electro-pneumatic components which produce a pulsating air flow to actuate the ventricle. The frequency and the systolic (contraction) time period of the

air are controlled electronically.

(b) An all-pneumatic driving system uses only air-operated components to obtain the pulsating air flow. Simultaneous control of the systolic and diastolic (dilation) time periods of a pumping cycle is achieved by manual adjustment of flow restrictors in the pneumatic circuit.

Table 2 lists those publications containing information on Starling's Law response; it summarizes the main features of the driving and control systems and compares the degree of regulation achieved. The Detroit Coil Timer [30] and the computerized Servo System [34] (also reported in Ref. [44]) were designed to operate on manual selections of constant frequency and duty-cycle (time ratio of the systolic period to the total period of a single cycle). The output from the blood pumps are adjusted by varying the pressure amplitude of the air signal, either manually [30] or automatically [34] (see Table 2).

Other E-P systems [19, 32] employ ventricular position feedback to initiate an electronic systolic signal. The duration of the systolic signal is adjusted manually and the diastolic period is controlled intrinsically by the rate of ventricular filling which is dependent on the atrial pressure. As a result, the system operates with a fixed pressure amplitude, and a variable frequency.

Landis, et al. [45], developed a novel E-P system which uses

TABLE 2 Automatic Cardiac Regulation of Different Driving Systems: A Comparison Based on In-Vitro Data as Atrial Pressure Varies.

	ELECTROPNEUMATIC DRIVING SYSTEMS			ALL-PNEUMATIC DRIVING SYSTEMS	
	DETROIT COIL TIMER [30]	COMPUTERIZED SERVO SYSTEM [34]	SYSTEMS REPORTED IN REFS. [19,32]	FLUID AMPLIFIER SYSTEM [37]	DIAPHRAGM-EJECTOR AMPLIFIER SYSTEM [38]
Mode of Operation (Selection)	Constant Frequency (Manual)	Constant Frequency (Manual)	Var. Frequency (Automatic)	Var. Frequency (Automatic)	Var. Frequency (Automatic)
Systole	Const.	Const.	Const.	Var. Slightly	Const.(Approx.)
Diastole	Const.	Const.	Var.	Var.	Var.
Stroke Volume	Var.	Var.	Const.(Approx.)	Var.	Var.
Feedback	Nil	a. Atrial Pressure b. Ave. Ventricle Position	Ventricle Position	Ventricle Position	Ventricle Position
Primary Parameter Controlled by Feedback	Nil	a. Pressure Amplifier of Air Signal b. Ave. Air Pressure in Ventricle	Time of Initiation of Systole	Time of Initiation of Diastole	Time of Initiation of Systole
Pumping-Air Pressure (Selection)	Const. (Manual)	Var. (Automatic)	Const. (Manual)	Const. (Manual)	Const. (Manual)
Starling's Response *	Unsatisfactory	Achieved	Comparable to Normal Heart	Unsatisfactory	Unsatisfactory**

* -Based on reported in-vitro test results.

** Based on data not reported in Ref. [38].

the R-wave of the EKG to synchronize the pumping rate of a sac-type artificial ventricle with the natural heart. The pumping air pressure level in the system is adjusted manually. This system, therefore, operates with a fixed pressure amplitude, and a variable frequency. The system has been tested in total left ventricular bypass in calves [36].

There are other E-P systems which are not referenced here, since they have basically the same features as those listed in Table 2. Those systems either operate on a fixed pressure amplitude-fixed frequency mode, or on a fixed pressure-variable frequency mode, or on a variable pressure-fixed frequency mode.

The Fluid Amplifier (FA) system [37] and the Diaphragm-Ejector Amplifier DEA) system [38] are A-P systems which operate with a fixed pressure amplitude and a variable frequency in a manner similar to the E-P system developed by Kwan-Gett, et al. [19]. In both systems the frequency depends on the ventricle filling time which, although dependent on atrial pressure, is quite insensitive to it. These systems were not primarily designed to achieve Starling's Law response.

Kwan-Gett, et al. [19,32] have successfully used the variable frequency method to obtain satisfactory cardiac regulation with an E-P driving system. However, the A-P systems (the FA system [37] and the DEA systems [38]) which operate in the variable frequency mode, did not achieve the same kind of success. This is probably due to

the limited sensitivity of the frequency with respect to atrial pressure changes exhibited by these systems. Nosé and Kolff [30], Akutsu et al. [33] and Morris and Lock [46] have obtained varying degrees of Starling's response for the artificial hearts with the constant frequency method, using similar E-P driving systems with a manual selection of ventricle air pressure.

The reason behind the varying degrees of success achieved by different investigators in the use of the constant frequency method to achieve the inherent Starling's cardiac regulation characteristics is not clear. In-vitro experiments (described in the next chapter) were therefore conducted with an artificial ventricle to investigate the various factors associated with Starling's Law behaviour [47]. The acquired information is used in the development of an all-pneumatic driving system for sac-type and diaphragm-type artificial ventricles. Since air is used as the driving fluid, it can also be used to control the proportional and logic components, thereby eliminating the need for an additional electrical power source in the system. An all-pneumatic driving system offers such an advantage.

CHAPTER 2

DEVELOPMENT OF AN ALL-PNEUMATIC ARTIFICIAL VENTRICLE DRIVING SYSTEM

2.1 Factors Affecting Starling's Regulation of an Air-Driven Artificial Ventricle

The cardiac output (C.O., Q lit/min) can be related to the stroke volume of a pumping cycle (V_{ST} lit/beat) and the heart rate (H.R. beats/min) by the following expression:

$$Q = (H.R.) \times V_{ST} \qquad (2.1)$$

and $$V_{ST} = V_D - V_S \qquad (2.2)$$

where V_D and V_S are the ventricle volumes attained at the end of the diastolic period and at the end of the systolic period respectively.

Equation (2.1) shows that cardiac regulation can be obtained either by the variable frequency method with a constant stroke volume, or by the constant frequency method with a variable stroke volume. For Starling's Law response either the frequency or the stroke volume must be regulated automatically by the atrial pressure. Both of these methods have been discussed by Kwan-Gett, et al., [19]. Variable frequency with variable stroke volume is a third but less practical possibility.

The factors that affect the volume V_D are:

1. atrial pressure,
2. inflow valve impedance,
3. ventricle inside pressure,
4. effective compliance of the ventricle,
5. pressure and volume of the air in the ventricle housing,
6. impedance of the exhaust air path,
7. ventricle-air exhaust pressure, and
8. diastolic time.

The volume V_S can be affected by:

1. ventricle-air supply pressure (driving pressure),
2. impedance of the inlet air path,
3. pressure and volume of the air in the ventricle housing,
4. effective compliance of the ventricle,
5. ventricle inside pressure,
6. outflow valve impedance,
7. inflow valve regurgitation,
8. ventricle output pressure,
9. impedance of the circulatory system, and
10. systolic time.

The parameters which can be used most readily for control are the ventricular air evacuation rate, ventricle-air supply pressure, the systolic/diastolic time (S/D) ratio of a pumping cycle and the frequency.

An experimental investigation was carried out to determine the maximum sensitivity that can be obtained by "open-loop" adjust-

ment and optimization of the three parameters relative to one another.

2.2 "Open-Loop" In-Vitro Experiments [47]

A schematic of the apparatus is shown in Figure 3. The driving system used for this part of the experiments is a home-built E-P system similar to the Detroit Coil Timer [30]. It consists of two ¼ in. solenoid valves, a vacuum pump, a vacuum chamber and some assorted Tygon tubings. The on-off sequence of the solenoid valves is controlled by a relay switch, which in turn is driven by an electronic square-wave (see Figure 3). The ventricle with hinged disc valves and the plexiglas housing used in the experiments are shown in Figure 4. The ventricle and the atrium are made of latex rubber (Uniroyal Lot 1185) and have volumes of 200 ml and 45 ml, respectively. Figure 5 shows the shape of the original plasticine model and the mold from which a parafin wax duplicate was made. The ventricle and atrium are made by repeated application of latex on the wax model. The ventricle used in the tests has an average wall thickness of 1.1 mm. The inside diameters of the connecting tube to the atrium and of the ventricle output tube are 19 mm and 32 mm, respectively, and contain the disc valves shown in Figure 6. The valves have a large inside diameter of 24 mm and were developed at the University of Birmingham [48].

The prosthesis of the left heart was tested in a water cir-

culatory system similar to that used by Kwan-Gett, et al. [19]. In this system (Figure 7), the output from the ventricle passes through a restrictor and a closed reservoir before entering a series of U-columns of rectangular cross-section. Water leaving the final U-column flows through a rotameter and returns to an open reservoir for recirculation. Different values of atrial pressure are obtained by changing the water level in the open reservoir. The ventricle output pressure can be varied by regulating the volume of air trapped at each intersection between two U-columns. During the tests, the atrial pressure and the ventricle output pressure were measured with variable reluctance pressure transducers (Validyne). The mean ventricle output flow rate was measured with the rotameter (Fischer and Porter No. B5-27-10), which was dynamically calibrated at a pulse rate of 75 beats/min. The mean fluctuating readings indicated by the rotameter float agree closely with the supplier's static calibration data with errors less than ±2%.

Typical function curves obtained from the experiments at different ventricular air evacuation rates, ventricle-air supply pressures and systolic/diastolic time ratios at a constant pulse rate are compared with the normal function curve of the left heart in Figures 8, 9 and 10, respectively. Different air evacuation rates were obtained either by changing the exhaust air pressure, or by changing the exhaust path impedance (this can be achieved, for example, by using different line sizes and/or lengths).

The results in Figure 8 show the effect of air evacuation

rate on the relationship between ventricle output and atrial pressure at a pulse rate of 75 beats/min, a S/D ratio of unity, a ventricle output pressure of 115 mm Hg, and an air supply pressure of 250 mm Hg. It is postulated that the relaxation of the ventricle during diastole results from the resilience of the ventricle itself, the ventricle pressure at the end of systole and the rate of air evacuation through the exhaust port (see theoretical formulation in Chapter 4). If a vacuum source is used to exhaust the air rapidly during diastole, this will produce a negative pressure inside the ventricle for a period of time as shown by the pressure-time traces in Figure 11. By virtue of a large pressure difference across the inlet-valve, the ventricle expands and is filled quickly to attain a maximum volume V_D at the end of the diastolic period. In this case, the large pressure difference is mainly due to the vacuum source. Since the driving pressure during systole is constant, a near constant end-systolic volume V_S is obtained, which results in near constant stroke volume and flow rate for all atrial pressures. The dashed lines of Figure 8 show this effect.

When exhausting to atmosphere directly, the lower rate of air evacuation restricts the relaxation process of the ventricle. In this case, the net pressure that aids in the filling process is mainly due to the atrial pressure. (The pressure-time traces in Figure 12 show that the filling process produces a small, mean vacuum level in the ventricle during the initial phase of diastole. For a large portion

of the diastolic period, the ventricle pressure is near atmospheric. The filling pressure differential is therefore mainly due to the atrial pressure.) The ventricle may not reach its full volume before the arrival of the next systolic pulse, when the filling pressure is low. As a result, the stroke volume, hence the ventricle output, exhibits some sensitivity to the atrial pressure, as shown by the solid lines in Figure 8.

The effect of air supply pressure on the ventricle output function curve is shown typically in Figure 9. The number code associated with the experimental curve in the figure identifies the driving air line, the supply air pressure and the exhaust air line used in the tests. The number C250B, for example, indicates that line C was used for the transmission of 250 mm Hg of air pressure to drive the ventricle, and line B was used as the exhaust path. Driving-line C consists of a ¼" to ½" NPT bushing, a ¼" NPT Schrader male quick-connect fitting, a 6 mm i.d., 18 mm long Tygon tubing, a 3 mm i.d., 5 mm long Tygon tubing and a #10-32 to 1/8" Clipper hose fitting. Exhaust-line B consists of a 1/8" to ½" NPT bushing, a 1/8" NPT, 1½" long nipple, a ¼" to ½" NPT bushing, a 1/8" to ¼" NPT bushing and a 1/8" Schrader male quick-connect fitting.

The effect of increasing driving air pressure is to increase the ventricle output. The experimental results show that there is no significant increase in ventricle output at atrial pressures lower than approximately 5 mm Hg when the driving air pressure is increased beyond 250 mm Hg. The results also show that there

exists a supply pressure level above which any further increase in pressure will not produce any apparent effect on the sensitivity of the function curve.

In-vitro data obtained at S/D = 1 and 0.45 with different air supply pressure are shown in Figure 10. Driving-line B consisted of a ¼" to ½" NPT bushing, a ½" NPT Schrader male quick-connect fitting, a 6 mm i.d., 23 mm long Tygon tubing and a 1/8" NPT Schrader male quick-connect fitting and exhaust-line C consisted of exhaust-line B, plus a 6 mm i.d., 200 mm long Tygon tubing. The effect of decreasing the systolic period at a constant pulse rate (75 beats/min) is to increase the diastolic time. Consequently, the residual ventricle volume attained at the end of systole increases due to the shorter time allowed for the driving air to actuate the ventricle. The ventricle volume attained at the end of diastole also increases. The stroke volume to atrial pressure characteristics are therefore altered, producing the function curves as shown in Figure 10.

The experimental results show that, although the characteristics of ventricle output versus the mean atrial pressure function curve can be adjusted in an "open-loop" system, a sensitivity better than 0.7 lit/min/mm Hg at the normal operating point (as compared to 1.2 lit/min/mm Hg of the normal left heart) cannot be obtained by manual adjustment of the three parameters mentioned earlier. The maximum sensitivity is obtained by operating the ventricle assembly at an approximately constant value of V_S.

This is achieved by using a constant ventricle-air supply pressure and a constant S/D ratio. The volume V_D in this case is determined automatically by the atrial pressure, since all other parameters affecting the ventricular expansion process are held constant. The system is therefore inherently self-regulating, but the ventricle output does not have the required sensitivity to the atrial pressure.

The ventricle output characteristics can also be affected by the size of the atrium [49]. The ventricle output sensitivity to atrial pressure, however, remains virtually unchanged [50].

Sensitivity could be affected by the ventricle inlet valve impedance and the compliance of the ventricle sac. Previous work such as that by Klain, et al. [51], shows that artificial heart valve impedance has an insignificant effect on the sensitivity. Rodbard and Hochberg [52] demonstrated that the sac thickness alone can change the contractile behaviour of a spherical elastic sac. The varying degrees of sensitivity obtained by different investigators and in the "open-loop" study where the valve impedance is fixed, can in part be attributed to differences in the compliances of the ventricle sacs used in the experiments.

The effective compliance depends on factors such as the type of material, the thickness and the shape of a particular ventricle sac and it is therefore not a parameter that can be controlled easily to obtain the optimum ventricle sensitivity. The desired

driving system must be capable of achieving the required sensitivity with different compliances. Because the compliance influences both V_D and V_S, one way of minimizing its effect on the cardiac regulation characteristics is to ensure that V_D remains constant at its maximum value.

2.3 The All-Pneumatic Driving System

In the presently developed all-pneumatic system, maximum V_D is accomplished by reducing the exhaust-air path impedance, and by providing a vacuum assist for the evacuation of ventricular air when necessary. The ventricle therefore expands fully during diastole. The end-systolic volume V_S is variable, and it is controlled by a variable-air pressure amplitude (at a fixed systolic time), which in turn is regulated by the atrial pressure through a feedback scheme described as follows.

The atrial pressure feedback scheme is shown schematically in Figure 13. The feedback scheme consists of a hydraulic passive filter, a hydraulic/pneumatic (h/p) pressure transducer specifically developed for this application, and a one-to-one (1:1) air-piloted pressure regulator. The atrial pressure signal is filtered, transduced and amplified into a ventricular air control signal P_{VAC} through the h/p transducer. The pressure signal P_{VAC} in turn controls the air-piloted pressure regulator to provide the desired ventricle air pressure P_{VAS}. Air at the automatically regulated pressure P_{VAS} first passes through an air-

piloted, two-way diaphragm valve (FESTO, with enlarged flow area), and then actuates the ventricle to deliver the desired ventricle output corresponding with the mean atrial pressure $\bar{P}_{at}$. The ventricular air later exhausts through another air-piloted two-way diaphragm valve during the diastolic period. The pneumatic transmission lines have an inside diameter of 12.7 mm. A pneumatic square-wave generator is used to control the on-off sequence of the valves.

Any suitable pneumatic square-wave generator (or time delay relays) with adjustable frequency and duty-cycle can be used in the system. In the present work, two pneumatic square-wave generators built from diaphragm fluidic elements (FESTO) according to the pneumatic circuits shown in Figures 14 and 15 were used at different occasions. Generator #1 uses four diaphragm fluidic elements, a volume (pneumatic capacitor) and two needlevalves, as compared to seven diaphragm elements, one fluidic diode, two pneumatic capacitors and two needlevalves used in generator #2. Generator #1 (Figure 16) has a lower power consumption (typically 1.3 lit/min at STP for P_{S2} = 150 mm Hg gauge) than generator #2 (typically 3.5 lit/min at STP for P_{S2} = 150 mm Hg gauge). There is a mutual interaction between the frequency and the duty-cycle adjustments in the first generator. The interaction is insignificant in the second generator (Figure 17).

The h/p transducer, which is shown in Figure 18, operates on the principle of the single-jet flapper valve. A schematic diagram of the transducer is shown in the inset in Figure 19, which gives

the ejector-sensor characteristics. In this device, an ejector-sensor [53] is used, with a 7 cm dia. phosphor-bronze barometer capsule (Observator Barometer, Netherlands) which acts as the conventional flapper. The ejector-sensor (d_e = 1.52 mm, d_n = 1.02 mm and d_s = 3.18 mm) is used here because it is available from a previous work. The atrial pressure is applied to the barometer capsule through a connecting tube of pre-determined diameter and length, which together with the capsule volume and an orifice, serves as a passive filter. As the mean atrial pressure increases, the bellows expand over a pre-determined operating displacement range, thereby reducing the "curtain area" between the flapper and its nozzle. This in turn causes an increase in P_{VAC} and consequently an increase in the ventricle-air pressure P_{VAS} as described earlier. Typical characteristics of the h/p transducer are shown in Figure 20. The gain of the h/p transducer can be adjusted manually by changing its air supply pressure P_{S3} and its set point X_0. Typical values of the input/output gains at X_0 = 0.090 mm are 3.1 for P_{S3} = 100 mm Hg and 12.5 for P_{S3} = 400 mm Hg.

It was found later that, at the atrial pressure range > 6 mm Hg, the above h/p transducer cannot provide a ventricle air pressure to the ventricle system that is high enough (a) to overcome the higher losses in the pneumatic transmission line, and (b) to accelerate the ventricle and the fluid rapidly enough to produce a large stroke volume during systole. A new h/p transducer was subsequently built to rectify the shortcomings of the system. The modified transducer (Figure 21) uses a flapper-nozzle configuration

(d_e = 6.35 mm, d_n = 1.50 mm, d_s = 2.95 mm) as the sensor (instead of ejector) for the bellows capsule displacement. Figure 22 compares the P_{VAS} versus $\overline{P}_{at}$ characteristics of the modified transducer at different values of $\overline{P}_{at}$, P_{S3}, X_0 and d_s with the characteristics needed to obtain Starling's cardiac regulation. The desired conditions were obtained from open-loop measurements with the present latex ventricle in mock circulation. Note that the flapper-nozzle must have non-linear characteristics to achieve the desired function. The functional behaviour of the transducer can be varied either by adjusting the transducer supply pressure, P_{S3}, the set point X_0 and the sensor seat diameter, d_s, one at a time or simultaneously. The adjustment capability of the transducer should allow its use in other artificial ventricle systems with different effective compliances of the ventricle and the ventricle housing.

2.4 The Passive Hydraulic Filter

The passive hydraulic filter consists of the inside volume of the bellows capsule of the h/p transducer, the flexible tubing connecting the capsule with the atrium and some tubing fittings. Its function is to "average" the fluctuating pressure at the atrium, so that a mean atrial pressure can be obtained for the automatic selection of ventricle driving air pressure through the h/p pressure transducer.

An assumed, lumped parameter model of the passive hydraulic filter is given in Figure 23. Assuming laminar flow, the resistance R_f and the fluid inertance I_f of the tubes can be calculated from

$$R_f = \frac{128\mu\ell}{\pi d^4} \tag{2.3}$$

and

$$I_f = \frac{4\rho\ell}{\pi d^2}\left(\frac{4}{3}\right) \tag{2.4}$$

respectively [54]; where

μ = fluid viscosity,

ρ = fluid density,

ℓ = tube length; and

d = tube diameter.

The capacitance C_{f1}, due to the displacement of the bellows capsule, and the capacitance C_{f2}, resulting from the compressibility effect of air trapped within the capsule, can be calculated from (Ref. [54])

$$C_{f1} = \frac{A_{be}}{k_{bs}} \tag{2.5}$$

and

$$C_{f2} = \frac{V_{bo}}{kP_a} \tag{2.6}$$

where A_{be} = effective area of the bellows,

k_{bs} = spring constant of bellows (pressure/unit displacement, e.g. N/m^3),

V_{bo} = initial volume of trapped air,

P_a = absolute pressure (above atmosphere,) and

k = specific heat ratio of air.

Figure 23 also gives a schematic diagram of the apparatus for the study of step-response of the passive filter. The apparatus includes the filter assembly, a hose clamp, a constant head tank, two electronic pressure transducers (Validyne) and a storage oscilloscope. The input pressure "step" $P_i(t)$ is generated by a sudden release of the hose clamp. The resulting pressure response of the filter $P(t)$ is measured at the inlet to the bellows capsule. Distilled water is used for the tests. Typical photographs of the pressure-time traces obtained from the experiments are shown in Figure 24. The lengths of the connecting tubes used are 0.305 m and 0.610 m, with an inside tube diameter of 1.70×10^{-3}m. The high frequency oscillatory pressure appearing at the input port to the filter is due to the water hammer effect when the clamp was suddenly released. It is observed that the oscillatory pressure is effectively attenuated by the passive filter.

With a connecting tube of diameter $d = 1.70 \times 10^{-3}$m, and of length $\ell = 0.305$ m, it is calculated in Appendix A that $R_f = 2.6 \times 10^9$ N-sec/m^5, and $I_f = 2.24 \times 10^8$ N-sec^2/m^5 (including the fittings). From measurements, it is determined that: $k_{bs} = 1.41 \times 10^7$ N/m^3, the inside volume of the bellows capsule $V_b = 1.9 \times 10^{-5}$ m^3, and actual area of the capsule $A_b = 3.62 \times 10^{-3}$ m^2 (see Appendix B). By assuming $A_{be} = 0.5\ A_b$, $V_{bo} = 0.4\ V_b$ and $k = 1.0$, it is calculated in Appendix B that $C_{f1} = 1.28 \times 10^{-10}$ m^5/N and $C_{f2} = 7.5 \times 10^{-11}$m^5/N. Using the above R_f, I_f, C_{f1} and C_{f2} values, the undamped natural frequency of the second order, passive filter system is

$$W_n = \sqrt{\frac{1}{I_f(C_{f1} + C_{f2})}} = 4.69 \text{ rad/sec.} \qquad (2.7)$$

The associated damping ratio of the filter is

$$\zeta = \frac{R_f}{2}\sqrt{\frac{C_{f1} + C_{f2}}{I_f}} = 1.24$$

Similarly for $d = 1.70 \times 10^{-3}$ m, and $\ell = 0.610$ m, $W_n = 3.23$ rad/sec and $\zeta = 1.64$.

By solving the hydraulic analog circuit shown in Figure 23 for an overdamped system ($\zeta > 1$), the pressure response of the filter to the practical input pressure "step" (with a finite rise time) of

$$P_i(t) = P_o(1 - e^{-t/\tau}) \qquad (2.9)$$

is

$$P(t) = \frac{P_o W_n^2}{1 - 2\zeta W_n \tau + W_n^2 \tau^2}\left\{\frac{1 + \tau r_1}{r_2(r_1 - r_2)}(1 - e^{r_2 t})\right.$$

$$\left. - \frac{1 + \tau r_2}{r_1(r_1 - r_2)}(1 - e^{r_1 t}) + \tau^2(1 - e^{-t/\tau})\right\} \qquad (2.10)$$

where $r_{1,2} = -\zeta W_n \pm W_n\sqrt{\zeta^2 - 1}$ (see Appendix C). P_o is the pressure amplitude and τ is the time constant of the applied "step" input (it is determined from experiments that $\tau \approx 0.1$ second). Note that as $\tau \to 0$, Equation (2.10) becomes the solution for a "step"

pressure input.

The experimental results are compared with theory in Figures 25 and 26. The experimental curves are reproduced from photographs of pressure traces obtained from the storage oscilloscope. The reasonably good agreement between the theoretical and experimental results suggest that the model describes the hydraulic passive filter adequately. This model is useful in the design of the filter to obtain a mean atrial pressure.

In the design of a hydraulic low-pass filter for the h/p pressure transducer, the damping factor of the system can be increased by adding an orifice to the connecting tube or by pinching the tube with a hose clamp. The dominant frequencies of the fluctuating pressure at the atrium are around 75 cycles per minute, therefore, the present passive filter system is adequate for the averaging of the atrial pressure, as demonstrated in later "closed-loop" in-vitro experiments.

2.5 "Closed-Loop" In-Vitro Experiments [55]

Typical "closed-loop" in-vitro data obtained with the all-pneumatic driving system, using the h/p pressure transducer with the ejector-sensor system, are shown in Figures 27 to 29. The water

circulatory system and the artificial ventricle assembly have been described in Section 2.2. The figures illustrate the effects of the h/p pressure transducer air supply pressure P_{S3}, the systolic time period, the ventricle air exhaust pressure P_E and the transducer's set point X_0 on the ventricle output at different mean atrial pressures at a heart rate of 75 beats/min and a mean ventricle output pressure of 100 mm Hg.

For fixed values of P_{S3} and X_0, the ventricle-air pressure P_{VAS} increases for an increasing mean atrial pressure as a result of the characteristics of the h/p transducer as shown typically in Figure 20 and of the 1:1 air-piloted pressure regulator. The increasing P_{VAS} results in an increasing ventricle output from the artificial ventricle. The Starling's regulation achieved compares very well with the results obtained by Webb et al. [34], using a computerized servo system (Figure 29).

The effect of increasing P_{S3} is to increase the ventricle output generally, and to shift the ventricle output versus mean atrial pressure function curve to the left in a manner as shown in Figure 27. The sensitivity of the function curve can be varied by adjusting the initial displacement position X_0 of the h/p transducer. Typical sensitivity values, measured at $\bar{P}_{at}$ = 4 mm Hg from the function curves shown in Figure 29, are 1.2, 1.9 and 2.5 lit/min/mm·Hg for X_0 = 0.078, 0.102 and 0.125 mm, with P_{S3} = 190, 240 and 340 mm Hg, respectively.

The effect of increasing the systolic time at a fixed heart rate is to increase the work done on the ventricle by the ventricle-air, and consequently to increase the ventricle output over a range of atrial pressures as shown typically in Figure 28. However, when $P_E = 0$, the output reaches a maximum value of 4.8 lit/min at $\bar{P}_{at} = 2.7$ mm Hg for a systolic time = 0.40 second, as compared to a maximum value of 7.2 lit/min at $\bar{P}_{at} = 5.3$ mm Hg for a systolic time = 0.32 second. This characteristic is a result of the reduction in diastolic time which occurs when the systolic time is increased at a constant heart rate. A shorter diastolic period does not allow the ventricle-air to exhaust completely, thereby preventing the ventricle to return to its fully expanded condition before the arrival of the next systolic cycle. A vacuum source was therefore used to assist ventricular air evacuation, thus ensuring that the ventricle returns to its fully expanded state at the end of the diastolic period. As a result, improved function curve characteristics were obtained (Figure 28).

The results illustrated in Figure 29, however, are not satisfactory for the atrial pressure range > 6 mm Hg and < 3 mm Hg. The unsatisfactory characteristics can be attributed to the h/p transducer as mentioned earlier in Section 2.3. The ventricle output function curves shown in Figure 30 are obtained from the all-pneumatic driving system with the modified h/p transducer with the flapper-nozzle sensor. The results illustrate a marked improvement over the atrial pressure range of 0-9 mm Hg. For $\bar{P}_{at} > 9$ mm Hg,

improvement cannot be obtained. This is due to the limited air flow handling capability of the two FESTO diaphragm valves at high atrial pressures when the air flow rate requirement is high. A further development of diaphragm valves with large flow area could improve the results. In any event, the "closed-loop" results are markly improved over the results obtained with a constant driving air pressure.

2.6 Dynamic Response and Power Requirements

Figure 31 is a four-pen stripchart recording which shows the typical dynamic responses of the system in mock circulation. The circulatory system used in this part of the experiment is described in Chapter 4. The pressures were measured with variable reluctance pressure transducers (Validyne) and the ventricle output, with a 24 mm I.D. electromagnetic blood flowmeter (Statham Instruments). Saline solution (9 gm Sodium Chloride per litre of distilled water) was used. The figure illustrates the manner in which the ventricle-air pressure responds to changes in atrial pressure with the modified h/p pressure transducer (with P_{S3} = 250 mm Hg, X_0 = 0.132 mm and d_s = 3.78 mm). At point A, the mean atrial pressure is increased (from an initial mean atrial pressure of 0.40 mm Hg) to 5.5 mm Hg by adding saline solution to the input reservoir connected to the atrium. As a result, the ventricular air pressure amplitude increases from an initial value of 106 mm Hg to 145 mm Hg, the mean ventricle output pressure increases from a mean

value of 65 mm Hg to 90 mm Hg and the peak ventricle output increases from 7.60 lit/min to 8.85 lit/min (for a fixed ventricle loading, a heart rate of 75 beats/min and a S/D ratio of 0.6).

At point B, the hydraulic resistance of the mock circulation unit was reduced to show the effect of loading on the output side of the artificial ventricle. The reduction in hydraulic resistance was achieved by releasing a pinch-clamp which was originally pinching a 10 mm I.D. tube to simulate the dilation of the blood vessel. This gives rise to a decrease in the ventricle output pressure and an increase in the peak ventricle output as shown in the figure. Since the volume of saline solution in the mock circulation system remains constant, the increased ventricle output is indicative of a larger fluid circulation, a lower amount of fluid stored in the reservoir and, as a result, a decrease in atrial and ventricle air pressures.

The mean atrial pressure is decreased at point C by removing fluid from the circulation unit which results in decreases in the ventricle air pressure, output pressure and the peak ventricle output.

The dynamic results as illustrated in Figure 31 show that the h/p pressure transducer is able to adjust the ventricle air pressure amplitude in accordance with the atrial pressure nearly instantaneously. Since the dynamic response of a ventricle to the pumping air pressure depends so much on the rate of venous pressure change

and on the output loading, it is difficult to give quantitative comparisons between different artificial ventricle driving systems in mock circulation. Qualitatively, however, the above results show that the present all-pneumatic system gives adequate Starling's regulation, in comparison with the responses of the physiological heart (dog) to venous pressure changes given in Rushmer [2] and with the dynamic responses of the electropneumatic systems obtained by Pierce et al. [35] and Kwan-Gett et al. [56].

The mean atrial pressure as shown in the figure was measured at the inlet to the bellows capsule of the h/p pressure transducer. The results show that the hydraulic passive filter was functioning satisfactorily.

At the present stage of the development, the power consumption of the h/p pressure transducer is high; typically 20 watts, with P_{S3} = 250 mm Hg, and an air flow rate = 36.2 lit/min STP, at $\bar{P}_{at}$ = 0.04 mm Hg. (Air flow measurements were measured with a hot-film Thermo-System Mass Flowmeter.) It is possible, however, to reduce the power consumption by miniaturizing the device with further development work. The power required to drive the ventricle in mock circulation is 4.25 watts based on a ventricle air pressure = 106 mm Hg, an average ventricle air flow rate = 18 lit/min STP and $\bar{P}_{at}$ = 0.04 mm Hg. The pneumatic square-wave signal generator #2 requires 1.2 watts.

CHAPTER 3

SIMULATED PERFORMANCE OF THE ALL-PNEUMATIC ARTIFICIAL VENTRICLE SYSTEM IN A SIMPLE SYSTEMIC CIRCULATION MODEL

3.1 Introduction

In an attempt to compare the Starling's response achieved by the all-pneumatic driving system with that of the natural left heart, a simple mathematical model of the physiological circulatory system is used in a simulated performance study.

When the natural heart is totally replaced by an artificial heart in an animal, increased systemic resistance and decreased compliance can be caused by the compression of veins, arteries or of the artificial heart due to an imperfect fit, or it can be caused by the formation of scar tissue on the veins or atria. The animal commonly develops symptoms of heart failure such as steadily increasing venous or arterial pressures [19]. The model allows assessment of the relative importance of artificial heart sensitivity and of changes in systemic resistance in causing these symptoms of heart failure. It also shows the effect of the systemic compliance on the sensitivity of the artificial heart.

3.2 Comparison with Starling's Law of the Natural Heart

Around the normal operating conditions, cardiac performance at steady state is well represented by a linear function

$$Q = A + B P_V \qquad (3.1)$$

For Starling's Law, the sensitivity coefficient B is 1.2 lit/min/mm Hg and the coefficient A has a value of 0.2 lit/min to give the natural left ventricle output of 5 lit/min when P_V is 4 mm Hg.

A linear regression analysis of the artificial ventricle test results shown in Figure 30 with $P_{S3} \triangleq 300$ mm Hg yields A = 0.18 and B = 1.14 lit/min/mm Hg. A high correlation coefficient of 0.998 was obtained with these test results which covered mock circulation flow rates between 1 and 10 lit/min.

Comparison of the sensitivity coefficients shows that the present artificial ventricle system has a slightly lower sensitivity (1.14 lit/min/mm Hg) than the natural heart (1.2 lit/min/mm Hg). At the average atrial pressure of 4 mm Hg the corresponding flows are 4.74 and 5 lit/min. Both closer agreement at the average conditions and a higher sensitivity can be obtained by finer adjustment of P_{S3}, X_0 and P_E.

In order to determine how this deviation from Starling's Law would affect the arterial pressure, venous pressure and cardiac output in the normal system which is subject to changes in resis-

tance and compliance, a simple model [57] of the circulatory system as shown in Figure 32 is used. The model consists of a pump with lumped arterial compliance (C_A), venous compliance (C_V) and circulatory resistance (R). The system is passive since there is no reflex control by the autonomous nervous system (baroreceptor response). The independent variables are systemic resistance and compliance. A comparison of the steady state simulated performance of the artificial ventricle with the natural left heart can be made using the appropriate coefficients of the pump Equation (3.1).

The circuit equation is

$$Q = \frac{P_A - P_V}{R} \tag{3.2}$$

The incompressible mass conservation equation, $dV_A = -dV_V$ or $C_A dP_A = -C_V dP_V$ gives

$$dP_A = -\left(\frac{C_V}{C_A}\right) dP_V = -K dP_V \tag{3.3}$$

where compliance is defined as $C = \frac{dV}{dP}$ and K is the compliance ratio C_V/C_A.

Integration of Equation (3.3) with the boundary conditions $P_A = 100$ mm Hg for $P_V = 4$ mm Hg yields

$$P_A = 100 - K(P_V - 4) \tag{3.4}$$

Substitution of Equation (3.1) into Equation (3.2) gives

$$P_V = \frac{P_A - AR}{1 + BR} \tag{3.5}$$

From Equations (3.4) and (3.5)

$$P_A = \frac{100 + K\left(\frac{AR}{1 + BR} + 4\right)}{1 + \frac{K}{1 + BR}} \qquad (3.6)$$

$$P_V = \frac{100 + 4K - AR}{1 + BR + K} \qquad (3.7)$$

From Equations (3.2), (3.5) and (3.6)

$$\dot{Q} = \frac{100 + 4K + A(1 + K)/B}{R + \frac{1 + K}{B}} \qquad (3.8)$$

Equations (3.6), (3.7) and (3.8) give the arterial pressure, venous pressure and cardiac output as functions of the systemic resistance R, systemic compliance ratio K, and the function coefficients A and B (sensitivity) of the artificial ventricle and the natural heart. The ratio (K) of venous compliance to arterial compliance is given as 24 by Guyton [58]. From data given by Snyder and Rideout [59], K is 33.2, and by Reeve and Guyton [60], it has a value of 37.5. Figures 33, 34 and 35 give the simulated variations of arterial pressure, venous pressure and cardiac output with systemic resistance for three compliance ratios of 10, 24 and 38. At average conditions (Q = 5 lit/min) the simulated lumped resistance is about 19 mm Hg/lit/min. The comparison with the artificial heart (with A = 0.18, B = 1.14) is made with R varying from about one-third to three times the average value and with K = 24.

The variation of arterial pressure with systemic resistance

is shown in Figure 33. Throughout the range of resistance changes the simulated arterial pressure produced by the artificial heart corresponds closely to that of the natural heart although it is lower by about 2 mm Hg. This difference can be eliminated by a slight increase in the supply air pressure. Decreasing the resistance to half its average value would decrease the arterial pressure to about 68 mm Hg with the natural heart and 66 mm Hg with the artificial heart. Doubling the resistance results in corresponding pressures of 132 and 130 mm Hg. In the natural system, the baroreceptor response would act to restore normal arterial pressure. The artificial ventricle would therefore place a slightly more severe demand on the baroreceptor system when resistance decreases but there would be less demand on the system when resistance increases. Figure 33 also shows that an increased compliance ratio places less demand and a decreased ratio places more demand on the baroreceptor system for both decreased and increased values of the resistance. The corresponding changes in venous pressure and cardiac output are shown in Figures 34 and 35.

Figure 34 shows the variation of venous pressure with change in resistance. There is close agreement between the characteristics of the natural and artificial hearts. The artificial heart system has a simulated venous pressure which is about 0.08 mm Hg less than the natural heart. The venous pressure is relatively insensitive to large changes in systemic resistance. The sensitivity increases with decreased values of the compliance ratio K.

The variation of ventricle output with changes in resistance is shown in Figure 35. The output increases with decreased systemic resistance which is consistent with the physiological response where decreased resistance normally indicates an increased demand for cardiac output. The output becomes more sensitive to decreased systemic resistance for lower compliance ratios. The artificial ventricle output is about 0.25 lit/min lower than the natural heart output for resistances lower than the average value, but this difference decreases to less than 0.1 lit/min for resistances higher than the average.

3.3 Artificial Heart Sensitivity

Figures 36, 37 and 38 show the simulated effect of the ventricle sensitivity coefficient B on the ventricle output, the arterial pressure and the venous pressure. A constant compliance ratio of 24 is used. Three values of B are used, namely 0.2, 0.7 and 1.2. The value of 0.7 was chosen as the maximum auto regulation sensitivity that can be obtained at constant frequency (75 beats/min) with the artificial ventricle. A sensitivity of 0.2 is readily achievable with most sac-type artificial ventricles. In each case, the coefficient A has been adjusted to satisfy the average flow of 5 lit/min at 4 mm Hg atrial pressure. Figure 36 shows that at the sensitivity of 0.7, the output flow decreases from 6 lit/min to 3.6 lit/min when the resistance increases from half its average value to twice its average value. The required

output change is from 6.5 to 3.2 lit/min. The corresponding effect on the arterial pressure is to increase its value from 50 mm Hg to 175 mm Hg for the low sensitivity of 0.2 as compared to the natural ventricle change from 70 to 134 mm Hg. An artificial heart with 0.7 sensitivity will experience a change in arterial pressure from 65 to 147. These drastic changes in arterial pressure with insensitive artificial ventricles will place severe demands on the baroreceptor system of the recipient. The associated changes in venous pressure are from 5.7 mm Hg to 0.8 mm Hg for the sensitivity of 0.2, and from 5.5 mm Hg to 2 mm Hg for the 0.7 sensitivity, as compared to the natural ventricle change from 5.3 mm Hg to 2.6 mm Hg. The changes are more drastic when the artificial ventricle output is increased to match that of the normal heart (see Tables 3 and 4).

3.4 Conclusions

The above simple analysis leads to the following conclusions:

1. The steady state simulated performance of the artificial ventricle agrees well with that of the natural heart for outputs from 1 to 10 lit/min and for changes in systemic resistances from about one-third to three times the average value. Agreement with the natural heart is within 2 mm Hg for arterial pressure. No excessive demands would therefore be placed on the baroreceptor system of the recipient of the artificial ventricle. If necessary, closer agreement can be obtained by adjustment of the air supply pressure and set-point of the h/p transducer but this would result in a slight reduction of the upper flow limit of 10 lit/min above which

TABLE 3

Variation of P_A, P_V and Q as Functions of Pump Sensitivity

Sensitivity, B lit/min/mm Hg	Q lit/min		P_A mm Hg		P_V mm Hg	
	R=10	R=40	R=10	R=40	R=10	R=40
1. 0.2	5.3	4.3	59	175	5.7	0.8
Deviation, 3-1	-1.2	+1.1	-11	+21	+0.5	-1.8
2. 0.7	6.0	3.6	65	147	5.4	2.0
Deviation, 3-2	-0.5	+0.4	- 5	+13	+0.2	-0.6
3. 1.2	6.5	3.2	70	134	5.2	2.6

TABLE 4

Variation of P_A and P_V for Q Matching Natural Heart Output

	Half Normal Resistance				Twice Normal Resistance			
Sensitivity, B lit/min/mm Hg	Q lit/min	R	P_A mm Hg	P_V mm Hg	Q lit/min	R	P_A mm Hg	P_V mm Hg
2. 0.7	6.5	6.5	31	6.4	3.2	48	159	1.5
3. 1.2	6.5	10	70	5.2	3.2	40	134	2.6
Deviation, 2-3			-39	+1.2			+25	-1.1

the artificial ventricle characteristics would deviate from Starling's Law.

2. The sensitivity of an artificial heart has a pronounced effect on the output, arterial pressure and venous pressure at different systemic resistances. Table 3 compares the simulated values obtained with sensitivities of 0.2 and 0.7 with corresponding values for the natural heart sensitivity of 1.2 lit/min/mm Hg. In each case, the pump satisfies the average flow and pressures and the resistance is changed from half to twice the average value. For instance, at 0.2 sensitivity and half the average resistance, there is a flow deficiency of 1.2 lit/min, an arterial pressure deficiency of 11 mm Hg and an excess venous pressure of 0.5 mm Hg. The same sensitivity at twice the average resistance would result in a flow excess of 1.1 lit/min, an arterial pressure excess of 21 mm Hg and a venous pressure deficiency of 1.8 mm Hg. Although the deviations are less for the highest attainable auto-regulation sensitivity of 0.7, there is still a significant excess of arterial pressure at the highest impedance to justify use of the feedback control system which results in a minimum additional demand on the baroreceptor system of the recipient. If the artificial ventricle output is increased to match that of the normal heart, the deviations become more severe as shown in Table 4. Note for instance the high venous pressure predicted at half the normal resistance and the high arterial

pressure at twice the resistance. This characteristic of insensitive artificial heart pumps could contribute to the symptoms of heart failure such as the steadily increasing venous or arterial pressures observed in animals tested [19].

The simple analysis given in this chapter suggests that the presently developed artificial ventricle system can provide adequate Starling's regulation to the recipient. However, the analysis, which is based on a quasi steady state model of the blood circulation system, does not show the ventricle's ability to respond to a dynamic change of the peripheral resistance, for instance. In order to further evaluate the performance capability of the driving system, a mathematical model of the ventricle sac is developed, and it is described in the next chapter. The model is used in a dynamic study of the all-pneumatic system as a replacement of the natural heart (see Chapter 5).

CHAPTER 4

MODEL OF A SAC-TYPE ARTIFICIAL VENTRICLE*

4.1 Introduction

Previous works on blood circulation suggest a variety of mathematical models for the natural heart. The heart is generally modelled as (a) a time-varying compliance or elastance [61-64], (b) a pressure or/and flow source with internal impedances [65-68], and (c) a thick-walled muscle chamber [69, 70]. The models, derived from physiological data, were used primarily as tools to gain better insight into the physical phenomena of blood pressure and flow propagations in arteries and to obtain quantitative understanding of parameters associated with the circulatory system.

Modelling a cardiac prothesis in a hypothetical cardiovascular system has gained significant attention recently in studies related to mechanical assistance for circulation. The study is beneficial to patients suffering from acute heart failure who need cardiac assistance as therapy to their failing hearts. It helps to predict and evaluate the performance of the assist device in simulated conditions before it is used on patients. The data obtained from the study have applications in the design of the assist device [71] and in the selection of methods for cardiac assistance to achieve the optimum results [72]. In their work on counterpulsation

---

* Accepted for Presentation and Publication at the 1976 ASME Winter Annual Meeting, New York, Dec. 5-10, Paper No. 76-WA/Bio-7.

* Accepted for Publication in the ASME Journal of Bio-Mechanical Engineering.

assistance, Murthy, et al. [71] modelled the intra-aortic balloon pump as a "pressure-node-volume source". In a similar study by Wemple and Mockros [72], the assist device is modelled as a pulsatile flow source.

There has also been some interest in the mathematical modelling of diaphragm-type and sac-type cardiac prothesis. Spyker [73] modelled a diaphragm-type ventricular bypass pump as a time-varying pressure source, from the pneumatic driving system. On a sac-type prosthetic device, Johnson, et al. [74] represented the rubber heart as an elastic sphere, wherein the contractile pressure is obtained from the sudden release of the elastic stress stored in the distended sac. More recently, McDonald [75] presented a massless piston-pump model for a pulsatile heart pump, and Wade [76] used the control volume theory to model an artificial ventricle in the study of stroke work and efficiency of an artificial heart pump.

The models on cardiac prothesis mentioned above generally ignore the fluid inertia and the elastic capacitance effects of the ventricle. In addition, the inlet and outlet valves are treated as constant resistive elements without flow regurgitation (backflow).

In this chapter, a mathematical model of an air-driven, sac-type artificial ventricle is presented. The model, derived from the energy and mass conservation equations of a deformable control volume, includes terms that can be identified as the ventricle sac elasticity, the ventricle hydrostatic head, the fluid kinetic

energy, the fluid inertia and the driving air pressure. The inlet and outlet valves are represented as non-linear resistive elements with variable effective flow areas dependent on the openings of the valves. Flow regurgitation is also accounted for in the model. The results obtained from digital computer simulation of a sac-type artificial ventricle in a mock circulatory system are compared with experimental measurements. The model is used in a digital simulation study of the all-pneumatic driving system in a detailed model of the human cardiovascular circulatory system.

4.2 Mathematical Model of an Elastic Sac

Figure 39 is a schematic diagram of an air driven, sac-type artificial ventricle. During the contraction phase (systole) of a pumping cycle, air flows into the ventricle housing to displace the fluid contained within the elastic ventricle against a given load at the output port. During the dilation phase (diastole), air is exhausted from the housing to allow the filling of the ventricle in preparation for the next contraction phase. The problem is to find a suitable mathematical model to describe this pulsatile flow system. Since an exact solution involves the complex unsteady Navier-Stokes equations, an approximate method based on the theory of a deformable control volume is used.

Consider the elastic sac as shown in Figure 39. The control surface is taken as the inside wall of the sac and passes perpendicularly across the inlet and outlet flows. The control volume

does not enclose the valves. The mass conservation and energy equations for a deformable control volume are [77]

$$\frac{d}{dt}\int_{\upsilon_c} \rho d\upsilon_c + \int_s \rho \vec{V}_r \cdot d\vec{A} = 0 \tag{4.1}$$

$$\dot{Q}_{TH} = \dot{W}_{MECH} + \dot{W}_{SHEAR} + \frac{d}{dt}\int_{\upsilon_c} (u + \frac{V^2}{2} + gz)\rho d\upsilon_c$$

$$+ \int_s (u + \frac{P}{\rho} + \frac{V^2}{2} + gz)\rho \vec{V}_r \cdot d\vec{A} + \int_s P\vec{V}_b \cdot d\vec{A} \tag{4.2}$$

where $\dot{Q}_{TH}$ = rate of heat transfer into the control volume,

$\dot{W}_{MECH}$ = rate of mechanical work done on the control volume,

$\dot{W}_{SHEAR}$ = rate of shear work done on the control volume, and

υ_c = the control volume.

The third term on the right-hand-side of Equation (4.2) is associated with the rate of change of energy within the control volume, the fourth term is the net efflux of energy from the control volume and the last term is the work done on the moving control surface. The definitions of the symbols are given in the List of Symbols.

The fluid is incompressible so that the mass conservation equation, Equation (4.1), can be reduced to

$$\dot{V}_\upsilon = Q_i - Q_o \tag{4.3}$$

where Q_i = inlet of flow rate into the control volume, i.e. the ventricle,

Q_o = outlet flow rate, and

$\dot{V}_v$ = rate of change of ventricle volume.

Equation (4.3) indicates that the time of change of ventricle volume is equal to the net influx of fluid into the ventricle.

The following assumptions are made:

1. The velocity $\vec{V}_r$ is normal to the flow areas and is uniform across the flow areas.
2. The contraction and relaxation processes are adiabatic, i.e. $\dot{Q}_{TH} = 0$.
3. The shear work transmitted across the control surface is negligible, i.e. $\dot{W}_{SHEAR} = 0$.
4. The mechanical work is associated with the work done to deform the ventricle sac, i.e. $\dot{W}_{MECH} = -P_\sigma \dot{V}_v$, where P_σ, the elastic wall stress, is a function of the ventricle volume, the modulus of rigidity of the sac material and the sac thickness [74].
5. The air pressure acts uniformly on the ventricle, so that the term associated with the work done on the moving control surface can be represented by

$$\int_S \rho \vec{V}_b \cdot d\vec{A} = P_{va} \dot{V}_v.$$

6. The change in internal energy is negligible.

7. The potential energy of the control volume can be represented by $-gh_v/2$, where h_v is the vertical component of the ventricle depth shown in Figure 39.

8. The energy within the control volume is isotropic.

9. The fluid velocity within the control volume is $(Q_o - Q_i)/A_v$, where A_v is a constant, average effective cross-sectional area of the ventricle.

10. The velocity of fluid at the top control surface is $(Q_o - Q_i)/A_e$, where A_e is effective exit flow area.

With these assumptions, the energy equation reduces to the following momentum equation (see Appendix D):

$$P_{va} - P_{vt} - P_\sigma - \frac{1}{2}\gamma\left[h_v - \frac{V_v}{(Q_o - Q_i)}\dot{h}_v\right] + \frac{\rho(Q_o - Q_i)^2}{2A_v^2} - \frac{\rho(Q_o - Q_i)^2}{2A_e^2} = \frac{\rho V_v}{A_v^2}(\dot{Q}_o - \dot{Q}_i), \qquad (4.4)$$

where $\gamma = \rho g$ and P_{vt} is the ventricle pressure at the top control surface. The equation is applicable for both systole and diastole.

Equation (4.4) represents the ventricle as a time-varying inertive element. The left-hand-side of the equation gives the net pressure available for fluid ejection during systole and for the filling of the ventricle during diastole. The equation is similar to the momentum equation given by Beneken and DeWit [18] on the

natural heart wherein the natural ventricle is modelled as an inertive element, with a ventricle pressure derived from muscular contraction/dilation of the ventricle fibre. The inclusion of both Q_o and Q_i in the equation allows for the transition period when both the inlet and outlet valves are opened at the start of either the systolic or diastolic air pressure pulse. The parameter P_σ is important in that it determines the effective stroke volume of the ventricle, as will be shown later. In addition, it is one of the contributing energy sources that helps the ventricle to return to its full volume during the filling phase of the pumping cycle (as opposed to the rubber heart [74] which draws the contractile energy from the distended elastic sac). The other energy sources that aid in the filling phase are the potential energy of the ventricle, the rate of change of ventricle head and the kinetic energy of the fluid due to the regurgitation flow from the outlet valve. Equation (4.4) is used in a digital computer simulation study of a latex ventricle in mock circulation as described in the following section.

4.3 Experimental Apparatus

A sketch of the latex ventricle with attached atrium and the saline solution circulatory system is shown in Figure 40. The ventricle is enclosed in a plexiglas housing; it has a volume of 180 ml and an approximate wall thickness of 0.8 mm. The fabrication procedure of the ventricle, the hinged disc valves used and the all-pneumatic ventricle driving system to achieve Starling's Law Response have been described in Chapter 2. Figure 41 is a photograph

of the latest artificial ventricle used in this part of the experiment.

The circulatory system consists of a reservoir, an open, overhead tank and four different sizes of flexible tubings. The ventricle output passes through two flexible tubes (2.40 cm dia. by 16 cm long and 0.953 cm dia. by 60 cm long) into the open, overhead tank and returns to the reservoir through a 0.486 cm dia. by 78.6 cm long flexible tube. The saline solution from the reservoir flows into the ventricle through a 2.22 cm dia. by 54.2 cm long flexible tube. This simple circulation system was chosen so that the resistance and capacitance of each element of the circuit can be measured. During dynamic tests, pressures were measured with variable reluctance pressure transducers (Validyne) and the flow rates, with 2.4 cm dia. electromagnetic blood flowmeters (Statham Instruments, Type SP7517).

4.4 The Latex Ventricle Model

In the absence of a theoretical equation to describe P_σ, experiments were conducted to obtain some empirical information on the P_σ characteristics of the ventricle.

Steady state conditions applied to Equation (4.4) with $Q_o^* = Q_i = 0$, yields

$$P_\sigma = P_{va} - P_{vt} - \frac{1}{2}\gamma h_v \qquad (4.5)$$

which gives the elastic wall stress in hydrostatic equilibrium with the net pressure acting on the ventricle. By keeping a constant head of fluid in the apparatus during the experiments, and by stepwise variation of the ventricular air pressure P_{va}, different values of P_σ can be calculated from Equation (4.5). The associated changes in ventricle volume can also be measured.

Some typical photographs of the ventricle taken during the above experiments are shown in Figure 42. The photographs illustrate the various equilibrium configurations attained by the ventricle for different pairs of P_σ and V_U values. The pictures show that as the ventricle volume decreases due to increasing air pressure, the effective head h_U, defined by the portion of the ventricle that contains fluid, also decreases.

The P_σ and h_U results are plotted in Figures 43 and 44, respectively, as a function of V_U. For convenience, the data are approximated by the following empirical equations, whose coefficients were determined from curve-fitting routines, i.e.

$$P_\sigma = P_{\sigma o} \ln \left(\frac{V_{Uo}}{V_U}\right) \qquad (4.6)$$

with $P_{\sigma o} = 780$ N/m^2 for decreasing volume, and $P_{\sigma o} = 250$ N/m^2 for increasing volume (where $V_{Uo} = 180$ ml, the initial full volume). For 100 ml $\leq V_U \leq V_{Uo}$ ml, $h_U = h_{Uo} = 7.6$ cm, and for $V_U < 100$ ml, $h_U = 0.076\ V_U$.

By equating Equations (4.5) and (4.6), and after rearranging

terms, it results in the following relationship.

$$V_{\upsilon} = V_{\upsilon o} \exp \{- \frac{(P_{va} - P_{vt} - \frac{1}{2} \gamma h_{\upsilon})}{P_{\sigma o}} \} \qquad (4.7)$$

Equation (4.7) shows that for the given ventricle in a fixed circulation system where P_{vt} is defined, the ventricle volume attained at the end of systole ($V_{\upsilon s}$) depends on the pumping air pressure. It also shows that the ventricle volume reached at the end of diastole ($V_{\upsilon d}$) will depend on the exhaust air pressure in the ventricle housing at the time. It therefore in effect defines the stroke volume V_{ST} of a pumping cycle, where $V_{ST} = V_{\upsilon d} - V_{\upsilon s}$ (see Chapter 2). Equation (4.7) also gives the limiting stroke volume of the ventricle as $V_{ST} = V_{\upsilon o}$, if $P_{va} \to \infty$ in systole, and $P_{va} \leq P_{vt} + \frac{1}{2} \gamma h_{\upsilon}$ in diastole. The other parameter that restricts the stroke volume is the coefficient $P_{\sigma o}$. A "stiffer" ventricle sac would have a higher value of $P_{\sigma o}$ and a larger end-systolic volume $V_{\upsilon s}$. The above physical interpretation of the present ventricle model supports the mathematical procedure from which the model was derived.

Since $h_{\upsilon} = h_{\upsilon}[V_{\upsilon}(t)]$, the time rate of change of h_{υ} in Equation (4.4) can be expressed as

$$\dot{h}_{\upsilon} = \frac{dh_{\upsilon}}{dt} = \frac{\partial h_{\upsilon}}{\partial V_{\upsilon}} \frac{dV_{\upsilon}}{dt} \qquad (4.8)$$

where $\dot{h}_{\upsilon} = 0$, for 100 ml $\leq V_{\upsilon} \leq V_{\upsilon o}$, and $\dot{h}_{\upsilon} = 0.076 \dot{V}_{\upsilon}$ for $V_{\upsilon} < 100$ ml.

The ventricle pressures P_{vt_o} and P_{vt_i} of Equation (4.4) can be related to measured pressures and flows at the outlet and inlet of the ventricle by the energy equation applied along a streamline between sections 01-02 and il-i2 of the ventricle assembly shown in Figure 39.

$$P_{vt_o} = P_{ao} + \gamma h_o + \frac{\rho h_o}{A_o} \dot{Q}_o + \Delta P_o \tag{4.9}$$

and

$$P_{vt_i} = P_{at} + \gamma h_i - \frac{\rho h_i}{A_i} \dot{Q}_i - \Delta P_i \tag{4.10}$$

The friction losses in Equations (4.9) and (4.10) are represented by

$$\Delta P_o = K_o Q_o^{no} \, SIGN(Q_o) \tag{4.11}$$

$$\Delta P_i = K_i Q_i^{ni} \, SIGN(Q_i) \tag{4.12}$$

where K_o and K_i are coefficients related to the effective flow area of the valves. To account for the transient effect, the following coefficients are used:

$$K_o = \alpha_o \{1 + \alpha \exp (- \frac{x_{01}}{S_{ve}})\} \tag{4.13}$$

for the ejection phase, and

$$K_o = \alpha_o \{1 + \alpha [1 - \exp (- \frac{x_{02}}{S_{ve}})]\} \tag{4.14}$$

for the regurgitation phase, where α_o and α are constants.

Similarly for the filling phase

$$K_i = \alpha_o \{1 + \alpha \exp (- \frac{x_i}{S_{ve}})\} \qquad (4.15)$$

The constants, α_o and α, and the effective valve stroke $S_{ve} = \lambda S_v$ are assumed the same for both valves. From steady state measurements, it was determined that $\alpha_o = 1.0846 \times 10^9$, no ≈ ni = 1.7638, and the maximum $S_v \approx 3.3$ cm for the present valve assemblies. The values for α and λ(≈1.5) are determined by fitting the simulation results with experimental data.

The valve position parameters x_{01}, x_{02} and x_i appearing in Equations (4.13) to (4.15) are calculated from the following equations:

$$x_{01} = \frac{1}{A_e} \int_{t_o}^{t} Q_o \, dt \qquad (4.16)$$

$$x_{02} = \frac{1}{A_e} \int_{t_s+t_1}^{t} - Q_o \, dt \qquad (4.17)$$

$$x_i = \frac{1}{A_e} \int_{t_s+t_2}^{t} Q_i \, dt \qquad (4.18)$$

(See List of Symbols for definitions of time parameters.)

The momentum equation for the ejection phase (systole) is obtained by substituting Equation (4.9) into Equation (4.4) with $Q_i = 0$,

$$\left(\frac{\rho h_o}{A_o} + \frac{\rho V_\upsilon}{A^2_\upsilon}\right) \dot{Q}_o = P_{va} - P_{ao} - P_\sigma - \gamma h_o - \Delta P_o$$

$$- \frac{1}{2}\gamma \left[h_\upsilon - \frac{V_\upsilon}{Q_o} \dot{h}_\upsilon\right] + \frac{1}{2}\frac{\rho Q_o^2}{A_\upsilon^2}$$

$$- \frac{1}{2}\frac{\rho Q_o^2}{A_e^2} \qquad (4.19)$$

Flow ejection, however, does not begin until the right-hand-side of Equation (4.19) is greater than zero. This in turn depends on the time it takes for P_{va} to become greater than $(P_\sigma + P_{ao} + \gamma h_o + \frac{1}{2}\gamma h_\upsilon)$.

At the onset of diastole, Equation (4.19) is applicable until the inlet valve opens. The inlet valve will open if P_{vt}, defined by Equation (4.9), is less than $(P_{at} + \gamma h_i)$. For the period when both the inlet and outlet valves are open, the applicable momentum equation for the filling phase is

$$\left(\frac{\rho h_i}{A_i} + \frac{\rho V_\upsilon}{A^2_\upsilon}\right) \dot{Q}_i = - P_{va} + P_{at} + P_\sigma + \gamma h_i - \Delta P_i$$

$$+ \frac{1}{2}\gamma \left[h_v - \frac{V_\upsilon}{(Q_o - Q_i)} \dot{h}_\upsilon\right] - \frac{1}{2}\frac{\rho(Q_o - Q_i)^2}{A_\upsilon^2}$$

$$+ \frac{1}{2}\frac{(Q_o - Q_i)^2}{A_e^2} + \frac{\rho V_\upsilon}{A^2_\upsilon} \dot{Q}_o \qquad (4.20)$$

which is obtained from Equations (4.4) and (4.10). The variable Q_o can be determined from Equation (4.9), wherein $P_{vt_o} = P_{vt_i}$ is given by Equation (4.10).

The outlet valve is considered closed when the volume of backflow into the ventricle is equal to the product of effective valve stroke and effective valve area. After the valve closure, a leakage flow with linear fluid resistance of $R_v = 3 \times 10^9$ N-sec/m^5, obtained experimentally, is assumed.

4.5 Model of the Mock Circulatory System

Figure 45 is a symbolic circuit analogy of the latex ventricle and the circulatory system. The simplified, lumped-parameter representations of the flexible tubes are modelled after existing work on arteries [66], with the exception that experimental values of fluid resistances and tube capacitance C_o are used instead of theoretical quantities. The constant hydrostatic heads of fluid in the tubes are represented symbolically as "batteries" in the model. The fluid inertances are calculated from $I = \rho\ell/\pi r^2$, with an assumed momentum correction factor of unity. C_1 and C_2, the fluid capacitances of the open, overhead tank and the reservoir, respectively, are calculated from $C_n = A_n/\gamma$. The measured capacitances of the return tube (3), and of the tube (4) connecting the reservoir and the atrium, are small in comparison with C_1 and C_2, and are therefore neglected. $C_{ao}(= \beta C_o)$ is a lumped capacitance accounting for the stretching effect of the upper part of the ventricle, and its magnitude is determined by comparing the simulation P_{ao} results with measurements.

By solving the circuit model of the circulation system, the

following momentum and continuity equations are obtained

$$(C_{ao} + C_o)\,\dot{P}_{ao} = Q_o - Q_1 \tag{4.21}$$

$$I_1\dot{Q}_1 + \Delta P_1 + \gamma h_1 = P_{ao} - P_1 \tag{4.22}$$

$$C_1\dot{P}_1 = Q_1 - Q_2 \tag{4.23}$$

$$I_2\dot{Q}_2 + \Delta P_2 - \gamma h_2 = P_1 \tag{4.24}$$

$$C_2\dot{P}_2 = Q_2 - Q_3 \tag{4.25}$$

$$I_3\dot{Q}_3 + \Delta P_3 - \gamma h_3 = P_2 - P_{at} \tag{4.26}$$

$$C_{at}\,\dot{P}_{at} = Q_3 - Q_i \tag{4.27}$$

where

$$\Delta P_1 = K_1\,Q_1^{n1}\,\mathrm{SIGN}(Q_1) \tag{4.28}$$

$$\Delta P_2 = K_2\,Q_2^{n2}\,\mathrm{SIGN}(Q_2) \tag{4.29}$$

$$\Delta P_3 = K_3\,Q_3^{n3}\,\mathrm{SIGN}(Q_3) \tag{4.30}$$

Table 5 is a list of the numerical data pertaining to the circulatory system. The numerical value for C_{at}, the capacitance of the atrium, is obtained from pressure-volume measurements.

4.6 Method of Solution

With P_σ given by Equation (4.6), h_v and $\dot{h}_v$ related to V_v and $\dot{V}_v$, the momentum equations of the ventricle assembly, Equations (4.19) and (4.20), contain only the variables P_{at}, Q_i, Q_o and P_{ao}.

TABLE 5

Data Pertaining to Circulatory System

INERTANCES, $N\text{-}s^2/m^5$	
I_o	1.32×10^5
I_1	8.78×10^6
I_2	4.41×10^7
I_3	1.40×10^6
I_i	5.13×10^4

HEADS, cm	
h_{vo}	7.62
h_o	6.67
h_1	76.20
h_2	57.20
h_3	5.57
h_i	2.25

CAPACITANCES, m^5/N	
C_o	1.01×10^{-10}
C_1	4.65×10^{-7}
C_2	2.53×10^{-6}
C_{at}	4.40×10^{-9}

RADII, cm	
Tube (1)	1.20
Tube (2)	0.48
Tube (3)	0.24
Tube (4)	1.10
Reservoir	8.90
Overhead Tank	3.81
Output Tube	1.27

RESISTANCE COEFFICIENTS	
R_v	3×10^9 N-s/m ^{5}
K_1	1.62×10^{11}
K_2	1.64×10^{11}
K_3	7.61×10^9
ηo, ηi	1.764
$\eta 1$	1.915
$\eta 2$	1.576
$\eta 3$	1.764

DISC VALVE	
S_v	3.30 cm
A_e	3.94 cm^2

With the additional Equations (4.21) to (4.30) involving the variables Q_1, P_1, Q_2, P_2 and Q_3, pressure-flow dynamics of the ventricle and the circulatory system can be simulated mathematically. In the present study, Euler's numerical method, with a step size $\Delta t = 20\mu$ sec, was used to solve the nine simultaneous differential equations. The reasons for using Euler's method are that its error of the order $(\Delta t)^2$ is acceptably small, and that it does not involve too many numerical evaluations for each incremental time step, thereby saving computation time. A time-varying air pressure P_{va} based on experimental pressure-time recordings is used as the input to the numerical solution (see Section 5.4). The Fortran program written for the simulation work consumes about 150 seconds of execution time and 11 seconds of compilation time on a CDC 6000 series digital computer, for a pumping cycle of 2 seconds.

Starting conditions at the onset of the systolic phase are as follows:

$$Q_i = 0,\ Q_o = 0,\ P_{ao} = \gamma(h_1 + h_t),\ P_{at} = \gamma h_r,\ V_U = 180 \text{ ml},$$

where $(h_1 + h_t)$ and h_r are the static heads above the points of pressure measurement in the outlet and inlet tubes respectively. Measurements showed that there is no measurable regurgitation flow through the inlet valve. The simulation therefore starts with Equation (4.19) directly, i.e. the inlet valve is assumed to close instantly at the onset of systole.

4.7 Discussions

To evaluate the mathematical model of the ventricle, simulated results are compared with experimental measurements of P_{ao}, Q_1, Q_3 and P_{at}. Figure 46 shows typical results with a driving air pressure P_{VAS} = 130 mm Hg and a pumping rate of 30 beats/min. The measured results are reproduced from four-pen stripchart recordings as shown typically in Figure 47. At this pumping rate all pressure and flow fluctuations are damped out at the end of diastole thus providing a convenient steady starting pressure for the computer solution. The values of $\beta = 3$ and $\alpha = 10$ are chosen such that, with $A_U = 1.5\ A_e$ ($A_e \simeq 3.94\ cm^2$), the first overshoot of the calculated P_{ao} coincides with the experimental trace and the corresponding magnitude of the pressure peak is comparable with the measured value (Figure 46, points A & B). Figure 46 also shows the effect of $A_U = V_{UO}/2h_{UO}$ which generally gives poorer agreement with measurements.

Figure 48 shows the effect of the coefficient α on the calculated ventricle output pressure (P_{ao}) and the ventricle output flow rate (Q_1) at an expanded time scale with $\beta = 0$ and $A_U = V_{UO}/2h_{UO}$, in comparison with the measured traces. The results show that an increased value of α reduces the amplitude of the oscillations of P_{ao} and Q_1. The parameter α, however, has no effect on the time (t_p) at which the first pressure overshoot occurs. The predicted first-overshoot times of t_p = 31 msec for $\beta = 0$, and t_p = 50 msec for $\beta = 3$ (Figure 46), using $A_U = V_{UO}/2h_{UO}$, do not compare well with the experimental value of 60 msec. The comparison is better with $\beta = 3$, $\alpha = 10$

and $A_u = 1.5\ A_e$.

In comparing the simulation results with measurements, the following observations are made:

- The model predicts the time parameters $t_o = 6.6$ msec, $t_1 = 120$ msec, and $t_2 = 22$ msec very well, as compared to the measured values of 7, 120, and 20 msec, respectively. These values cannot be identified on the time scale used in Figure 46.
- The model predicts an outlet valve closure time of 0.715 sec (the time at which P_{ao} begins to increase rapidly, measured from the onset of systole, Figure 46, point C) which compares well with the measured value of 0.765 sec (Figure 46, point D). After the sudden closure of the outlet valve, P_{ao} reaches a peak pressure of 232 mm Hg at $t = 0.785$ sec (point E), as compared to 238 mm Hg at $t = 0.820$ sec (point F) obtained experimentally.
- The ventricle output pressure periodically becomes subatmospheric due to the "water-hammer" effect when the outlet valve closes abruptly. Rigidity of the wall prevents the collapse of the tube which is observed to oscillate slightly under the action of peak and sub-atmospheric pressures.
- The model predicts flow regurgitation at the outlet valve at the onset of diastole. The results indicate that the outlet valve opens and closes a few times during the diastolic period, just as indicated in the experimental trace of Q_1.
- The simple lumped parameter model of the outlet tube does not

provide sufficient pressure and flow dissipation as indicated by the non-zero amplitudes of P_{ao} and Q_1 after completion of diastole. No attempt was made to improve the aortic tube resistance model because it does not affect the solution of the ventricle equations after the outlet valve closes.

- The model predicts the ventricle return flow and atrial pressure dynamic characteristics reasonably well in comparison with experimental traces. It gives a time t_F of 0.95 sec (the time at which P_{at} begins to increase, and Q_3 to decrease), as compared to an experimental value of 0.99 sec. The parameter t_F is indicative of the time at which the ventricle is totally full (point K). The stroke volume is 56 ml, with V_{Ud} = 180 ml and V_{Us} = 124 ml.

- The atrial pressure starts dropping after the inlet valve opens (G). The atrium remains fully extended until the pressure becomes subatmospheric when it is observed to first flex inward (H to I) and then outward (I to J) under the restoring elastic stress of the wall. Several more wall oscillations occur before the ventricle is full (K). The simulated results with a linear capacitive element follow these pressure oscillations reasonably well.

In general, the simulation results of the latex ventricle in mock circulation compare well with experiments. Similar observations can also be drawn from Figure 49, where the pumping air pressure is 120 mm Hg.

4.8 Conclusion

Although the presently derived mathematical model of a sac-type artificial ventricle and the assumed model of the hinged disc valve are only approximate representations of the actual systems, they provide simulation results in good agreement with measurements of the actual dynamic situation. The ventricle model can be applied to any sac-type ventricle, providing the appropriate P_σ and h_υ functions are used. It can also be applied to diaphragm-type artificial ventricles.

The mathematical model has application in the study of cardiac assistance to circulation with sac-type or diaphragm-type artificial hearts. Since the model associates with actual physical quantities such as the sac elasticity (P_σ) and the ventricle dimensions (A_υ, hu and V_υ), it can be used to gain relevant information on the design of artificial heart systems for the achievement of optimal cardiac assistance results. The static model as given by Equation (4.6), for example, illustrates the parameters that can be achieved to control the limiting stroke volume of a pumping cycle.

The present study shows that the pressure peak occurring at the ventricle output tube during diastole is a result of the sudden closure of the disc valve, causing the regurgitation flow to terminate abruptly; the model is able to give good predictions of the magnitude of the pressure peak and the subsequent dynamic pressure characteristics. It suggests that the model can be extended to the study of the regurgitation flow phenomena and the dynamics of passive prosthetic heart valves.

CHAPTER 5

SIMULATION OF CARDIOVASCULAR DYNAMICS WITH THE ALL-PNEUMATIC ARTIFICIAL VENTRICLE SYSTEM AS A REPLACEMENT OF THE MYOCARDIAL FUNCTION

5.1 Introduction

The steady state simulation study on the Starling's cardiac regulation characteristics of the physiological heart, and of the artificial heart (Chapter 3), demonstrated the importance of having an artificial ventricle with a response to the venous return that closely duplicates that of the natural heart. It was assumed that the mock circulation regulation characteristics shown in Figure 30 will remain unchanged when the artificial ventricle system is used as a replacement for the myocardial function of the natural left heart, irrespective of the completely different load that the artificial heart pump has to pump against. In the analysis, it was also assumed that the physiological right heart functions normally (i.e. the flow rate leaving the ventricle is exactly equal to the venous return flow), so that the right heart and the associated pulmonary circulation system can be treated as lumped passive elements in the model. The second assumption could be interpreted as having an artificial ventricle system which can duplicate exactly the muscular function of the natural right heart. The simulation results given

in Chapter 3 appear to indicate that the present all-pneumatic ventricle driving system could provide adequate Starling's regulation to the recipient for circulation flow rates between 1 and 10 lit/min at steady state. However, it is not clear how the system would respond in reality, for instance, to a change of the systemic resistance, when the important independent variable time t is considered. In addition, the assumed artificial ventricle system that could respond to the right-venous return as sensitively as the physiological right heart has yet to be developed. Therefore, the previous study should only be treated as a preliminary investigation into the more complex regulation functions demanded in an artificial heart system for temporary or total replacement of the physiological heart.

In order (a) to gain better insight into the regulation capability of the all-pneumatic artificial ventricle system as temporary or permanent replacement of the physiological heart, and (b) to obtain design data for an artificial right ventricle system that could respond to the right venous return flow in accordance to Starling's Law of the heart, a mathematical simulation of hemodynamics, with the natural heart being replaced by an artificial heart, is carried out. Details of the mathematical models used in the dynamic simulation and the simulation results are given in the following sections.

5.2 Mathematical Model of the Cardiovascular System

Figure 50 is a passive, lumped-parameter circuit representation of the human cardiovascular system, where gravitational effects are not considered. A typical segment of the artery is modelled as an inertance I and a resistance R in series, and a shunt resistance R' in series with a shunt capacitance C. The ascending aorta and the pulmonary artery are exceptions because the resistances R are neglected (see Figure 50). The quantities R and I are determined by the vascular dimensions, blood viscosity and density. R' and C are related to vascular dimensions and elastic and viscous properties of the vessel wall. From measurements by Peterson [78,79] the product R' C is 0.04 sec for all systemic arterial segments. The capillaries are modelled as ideal purely resistive elements, and the veins, including the superior and inferior vena cava, are modelled as series resistances with shunt capacitances.

The most extensive passive description of the human systemic arterial tree is given by Westerhof, et al. [66]. Each arterial segment is represented by longitudinal and transverse impedances, consisting of numerous resistive, inertive and capacitive elements. The number of elements involved depends on the arterial diameter and length, the vessel wall thickness and its Young's modulus of rigidity. The representation is derived from Navier-Stokes equations, the continuity equation of fluid motion, the equation of motion of the vessel wall, and Hooke's Law for elastic material. Details of the governing equations (partial differential equations) can also be

obtained from Reference [80].

A less extensive description of the physiological circulation system is given by Snyder, et al. [61]. The passive model of each segment of the arterial tree is the same as the one used in this study, which is based on the work by Beneken and De Wit [60]. The model of the systemic arterial tree used by Snyder and his co-workers, however, contains more segments than the present model.

By solving the circuit shown in Figure 50, the following momentum and continuity equations are obtained. The subscript attached to q identifies the flow rate associated with the appropriate arteries, veins, etc. (see List of Symbols). For examples, q_{ASAO} is the flow rate in the AScending AOrta, and q_{THAR} is the flow rate in the THoracic ARch. It applies similarly to the resistances, inertances and capacitances of the vascular segments.

$$q_{01} = q_{ASAO} - q_{THAR} - q_{COAR} \tag{5.1}$$

$$C_{ASAO}\,\dot{P}_{01} = q_{01} + R'_{ASAO}\,C_{ASAO}\,\dot{q}_{01} \tag{5.2}$$

$$I_{THAR}\,\dot{q}_{THAR} = P_{01} - P_{02} - R_{THAR}\,q_{THAR} \tag{5.3}$$

$$q_{02} = q_{THAR} - q_{THAO} - q_{HAAR} \tag{5.4}$$

$$C_{THAR}\,\dot{P}_{02} = q_{02} + R'_{THAR}\,C_{THAR}\,\dot{q}_{02} \tag{5.5}$$

$$I_{THAO}\,\dot{q}_{THAO} = P_{02} - P_{03} - R_{THAO}\,q_{THAO} \tag{5.6}$$

$$q_{03} = q_{THAO} - q_{ABAR} - q_{INAR} - q_{BRCP} \quad (5.7)$$

$$C_{THAO}\,\dot{P}_{03} = q_{03} + R'_{THAO}\,C_{THAO}\,\dot{q}_{03} \quad (5.8)$$

$$I_{ABAR}\,\dot{q}_{ABAR} = P_{03} - P_{04} - R_{ABAR}\,q_{ABAR} \quad (5.9)$$

$$q_{04} = q_{ABAR} - q_{LEAR} - q_{ABVE} \quad (5.10)$$

$$C_{ABAR}\,\dot{P}_{04} = q_{04} + R'_{ABAR}\,C_{ABAR}\,\dot{q}_{04} \quad (5.11)$$

$$I_{LEAR}\,\dot{q}_{LEAR} = P_{04} - P_{05} - R_{LEAR}\,q_{LEAR} \quad (5.12)$$

$$q_{05} = q_{LEAR} - q_{LEVE} \quad (5.13)$$

$$C_{LEAR}\,\dot{P}_{05} = q_{05} + R'_{LEAR}\,C_{LEAR}\,\dot{q}_{05} \quad (5.14)$$

$$q_{LEVE} = (P_{05} - P_{06})/(R_{LECP} + R_{LEVE}) \quad (5.15)$$

$$q_{ABVE} = (P_{04} - P_{06})/(R_{ABCP} + R_{ABVE}) \quad (5.16)$$

$$q_{13} = q_{INAR} - q_{INVE} \quad (5.17)$$

$$C_{INAR}\,\dot{P}_{12} = q_{12} + R'_{INAR}\,C_{INAR}\,\dot{q}_{13} \quad (5.18)$$

$$q_{INVE} = (P_{12} - P_{06})/(R_{INCP} + R_{INVE}) \quad (5.19)$$

$$I_{INAR}\,\dot{q}_{INAR} = P_{03} - P_{12} - R_{INAR}\,q_{INAR} \quad (5.20)$$

$$(C_{LEVE} + C_{ABVE} + C_{INVE})\,\dot{P}_{06} = q_{LEVE} + q_{ABVE} + q_{INVE} - q_{INVC} \quad (5.21)$$

$$q_{INVC} = (P_{06} - P_{07})/R_{INVC} \quad (5.22)$$

$$q_{BRCP} = (P_{03} - P_{07})/R_{BRCP} \quad (5.23)$$

$$q_{COAR} = (P_{01} - P_{07})/R_{COAR} \tag{5.24}$$

$$(C_{INVC} + C_{SUVC} + C_{RA})\dot{P}_{07} = q_{INVC} + q_{SUVC} + q_{COAR} + q_{BRCP} - q_{RAVR} \tag{5.25}$$

$$q_{08} = q_{PUAR} - q_{PUVE} \tag{5.26}$$

$$C_{PUAR}\,\dot{P}_{08} = q_{08} + R'_{PUAR}\,C_{PUAR}\,\dot{q}_{08} \tag{5.27}$$

$$q_{PUVE} = (P_{08} - P_{09})/(R_{PUCP} + R_{PUVE}) \tag{5.28}$$

$$(C_{PUVE} + C_{LA})\dot{P}_{09} = q_{PUVE} - q_{LAVR} \tag{5.29}$$

$$I_{HAAR}\,\dot{q}_{HAAR} = P_{02} - P_{10} - R'_{HAAR}\,q_{HAAR} \tag{5.30}$$

$$q_{10} = q_{HAAR} - q_{HAVE} \tag{5.31}$$

$$C_{HAAR}\,\dot{P}_{10} = q_{10} + R'_{HAAR}\,C_{HAAR}\,\dot{q}_{10} \tag{5.32}$$

$$q_{HAVE} = (P_{10} - P_{11})/(R_{HACP} + R_{HAVE}) \tag{5.33}$$

$$C_{HAVE}\,\dot{P}_{11} = q_{HAVE} - q_{SUVC} \tag{5.34}$$

$$q_{SUVC} = (P_{11} - P_{07})/R_{SUVC} \tag{5.35}$$

Table 6 is a list of the numerical values of resistances, inertances and capacitances pertaining to the cardiovascular system. The data are obtained from Reference [60]: C_{RA} and C_{LA} are the capacitances of the right and left artificial ventricles, respectively.

TABLE 6a Numerical Values Used in the Description of the Cardiovascular System.

	Resistance $N\text{-}s/m^5$	Inertance $N\text{-}s^2/m^5$	Capacitance m^5/N
Ascending aorta	-	2.93×10^4	2.10×10^{-9}
Thoracic arch	4.00×10^3	5.74×10^4	2.17×10^{-9}
Thoracic aorta	1.20×10^5	5.07×10^5	2.17×10^{-9}
Abdominal aorta	1.60×10^6	1.87×10^6	1.57×10^{-9}
Intestinal arteries	1.87×10^5	3.60×10^5	4.50×10^{-10}
Leg arteries	2.40×10^7	4.13×10^6	9.00×10^{-10}
Head & arm arteries	6.27×10^6	1.87×10^6	2.47×10^{-9}
Head & arm veins	3.01×10^7	-	7.05×10^{-8}
Leg veins	4.00×10^7	-	3.60×10^{-8}
Abdominal veins	7.95×10^7	-	3.82×10^{-8}
Intestinal veins	2.21×10^7	-	7.95×10^{-8}
Inferior vena cava	2.00×10^6	-	6.22×10^{-8}
Superior vena cava	8.00×10^6	-	6.22×10^{-8}
Pulmonary arteries	-	2.40×10^4	3.22×10^{-8}
Pulmonary veins	9.34×10^5	-	6.22×10^{-8}

TABLE 6b Numerical Values of Resistances in Capillaries.

	Resistance $N\text{-}s/m^5$
Coronary	1.60×10^9
Bronchial	1.60×10^9
Intestinal	3.07×10^8
Abdominal	7.60×10^9
Legs	2.00×10^9
Head and arms	8.00×10^8
Pulmonary	1.47×10^7

5.3 Model of the Artificial Heart

In the model, both the left and right artificial ventricles with their inlet and outlet valves are represented by the previously derived equations (Chapter 4).

The valves are passive devices that open and close under the action of the pressures acting on them. These pressures are the atrial and ventricle-top pressures for the left and right inlet valves. In Figure 50, these pressures are identified respectively as P_{09} and P_{vtL} and P_{07} and P_{vtR}. For the outlet valves the relevant pressures are the ventricle-top pressures P_{vtL} and P_{vtR}, and the pressures in the ascending aorta (P_{01}) for the left ventricle and P_{08} in the pulmonary artery for the right ventricle. The left and right ventricles are actuated at the same frequency, phase and systolic/diastolic time ratio at the driving pressures required to achieve identical mean ventricle outputs. However, the inlet and outlet valves open and close independently of one another under the action of the dynamic pressures. Regurgitation can occur during the time required for the valves to close. Previous mock circulation work was conducted with the ventricle in the vertical position where the buoyant force assists the rapid closing of the inlet valves. This simulation assumes instant closing of the inlet valves without regurgitation but accounts for regurgitation during closing of the outlet valves. In the simulation program, the ventricle and the inlet/outlet pressures are compared and the appropriate equations are selected. For convenience, the equations are grouped in six (6) sets based on

the open and closed positions of the inlet and outlet valves. The governing equations are written for the left ventricle only. Identical equations apply to the right ventricle.

Set (1). The following equations apply during the ejection phase when there is positive flow out of the ventricle, i.e. the inlet valve is closed and the outlet valve is open ($P_{vtL} > P_{09}$ and $P_{vtL} > P_{01}$).

The momentum equations are:

$$\left(\frac{\rho h_o}{A_o} + \frac{\rho V_{uL}}{A_u^2} + I_{ASAO}\right) \dot{q}_{ASAO} = P_{vaL} - P_\sigma - P_{01} - \Delta P_{OL} + \frac{1}{2}\frac{\rho q_{ASAO}^2}{A_u^2} - \frac{1}{2}\frac{\rho q_{ASAO}^2}{A_e^2} \qquad (5.36)$$

$$q_{LAVR} = 0 \qquad (5.37)$$

The valve resistance equation is:

$$\Delta P_{OL} = \alpha_0 \left[1 + \alpha \, EXP\left(-\frac{X_{01L}}{S_{ve}}\right)\right] (q_{ASAO})^{no} \, SIGN(q_{ASAO}) \qquad (5.38)$$

The valve-disc position equation is:

$$X_{01L} = \frac{1}{A_e} \int_{t_{OL}}^{t} q_{ASAO} \, dt \qquad (5.39)$$

(See Chapter 4 and the List of Symbols for explanations of symbols.)

Set (2). This set applies when air starts being evacuated from the ventricle housing. The inlet valves remain closed but because of the inertia effects, the blood outflow continues for a short period

during which Equations (5.36) to (5.39) apply ($P_{vtL} > P_{09}$ and $P_{vtL} > P_{01}$). When the blood outflow is reduced to zero and then reverses its direction, Equation (5.36) describes the regurgitation flow but the valve resistance equation and the valve position equation are replaced by the following equations.

The valve resistance equation is:

$$\Delta P_{OL} = \alpha_o \left\{ 1 + \alpha \left[1\text{-EXP } \left(- \frac{X_{02L}}{S_{ve}} \right) \right] \right\} (q_{ASAO})^{no} \text{ SIGN}(q_{ASAO}) \quad (5.40)$$

The valve position equation is:

$$X_{02L} = \frac{1}{A_e} \int_{t_s+t_{1L}}^{t} - q_{ASAO} \, dt \quad (5.41)$$

Equation (5.37) for the closed inlet valve is still valid.

Set (3). The following equations apply when the inlet valve is open while the outlet valve remains open ($P_{vtL} < P_{09}$ and $P_{vtL} < P_{01}$). This represents regurgitation flow plus diastolic inlet flow.

The momentum equations are:

$$\left(\frac{\rho h_o}{A_o} + I_{ASAO} \right) \dot{q}_{ASAO} = P_{vtL} - P_{01} - \Delta P_{OL} \quad (5.42)$$

$$\left(\frac{\rho h_i}{A_i} + \frac{\rho V_{uL}}{A_u^2} \right) \dot{q}_{LAVR} = P_{09} + P_\sigma + \frac{\rho V_{uL}}{A_u^2} \dot{q}_{ASAO} - \Delta P_{iL} - P_{vaL}$$

$$+ \frac{1}{2} \frac{\rho (q_{ASAO} - q_{LAVR})^2}{A_e^2} \quad (5.43)$$

$$- \frac{1}{2} \frac{\rho (q_{ASAO} - q_{LAVR})^2}{A_u^2}$$

where

$$P_{vtL} = P_{09} - \frac{\rho h_i}{A_i} \dot{q}_{LAVR} - \Delta P_{iL} \tag{5.44}$$

$$\Delta P_{iL} = \alpha_0 \left[1+\alpha \text{ EXP } \left(- \frac{X_{iL}}{S_{ve}}\right) \right] (q_{LAVR})^{no} \text{ SIGN}(q_{LAVR}) \tag{5.45}$$

$$X_{iL} = \frac{1}{A_e} \int_{t_s+t_{2L}}^{t} q_{LAVR} \, dt \tag{5.46}$$

ΔP_{0L} in Equation (5.42) is given by Equation (5.40) with the valve position equation, Equation (5.41). Note that Equations (5.42) and (5.43) determine the rate of dilation of the ventricle.

Set (4). This set applies when the outlet valve has closed and the inlet valve remains open ($P_{vtL} < P_{09}$ and $P_{vtL} < P_{01}$) as the ventricle is being filled. The outlet valve is closed when the volume of backflow into the ventricle is equal to the product of the effective valve stroke and valve area. After the valve has closed, an experimentally determined leakage flow with linear resistance $R_v \approx 3 \times 10^9$ N-sec/m^5 is used.

The leakage flow equation is:

$$q_{ASAO} = (P_{vtL} - P_{01})/R_v \tag{5.47}$$

The momentum equation, Equation (5.43), the valve resistance equation, Equation (5.45) and the valve position equation, Equation (5.46), for the filling process are still applicable.

The filling process continues until the integrated total in flow plus the end-systolic volume equals the maximum ventricle

volume. If the ventricle reaches its maximum volume before the onset of the next systolic phase, the leakage flow enters the atrium, i.e. $q_{LAVR} = q_{ASAO}$. This flow adds incrementally to the pulmonary flow entering the artificial atrium.

Set (5). This set applies in the case where the ventricle is completely full. Air starts to enter the ventricle housing and the inlet valves closes instantaneously when $P_{vaL} = P_{vtL} \geq P_{09}$, i.e. $q_{LAVR} = 0$. The outlet valve remains closed until $P_{vaL} = P_{vtL} \geq P_{01}$. Zero leakage flow occurs for a short period ($\approx 10^{-4}$ second) when $P_{vtL} > P_{09}$ and $P_{vtL} < P_{01}$. When $P_{vtL} > P_{01}$, the ejection process commences and Equations (5.36) to (5.39) of Set (1) are applicable.

Set (6). This set applies when the ventricle is only partially filled as air starts entering the ventricle housing. The equations of Set (4) apply until $P_{vtL} = P_{09}$, after which the equations of Set (5) become applicable.

5.4 Model of the Pneumatic Driving System

A simple, lumped parameter circuit model as shown schematically in Figure 51 is assumed for the representation of the pneumatic driving system. Detailed models of pneumatic transmission lines have been given by Nichols [81], Brown [82], Hougen, et al. [83], Brown, et al. [84], and Margolis and Brown [85]. For convenience, the pneumatic air line is presently represented by a constant series impedance, consisting of an inertance I_ℓ and a resistance R_ℓ, and a

constant shunt capacitance C_ℓ, neglecting terms which are frequencies dependent. C_U in the figure is a lumped capacitance due to the compressibility effect of an averaged volume created in the ventricle housing as a result of ventricular displacement. An ideal square-wave is assumed as the pressure source to the pneumatic system, with a pressure amplitude dependent on the driving air pressure P_{VAS} and the exhaust air pressure P_E. As illustrated by the typical dynamic air pressure-time trace shown in Figure 47, the present pneumatic system can be adequately represented by the second order line model.

Based on the assumed second order transmisstion line model, and from the dynamic pressure measurements, the natural frequency of the system can be deduced to be $W_n = 1/\sqrt{I_\ell(C_\ell + C_U)} = 238\ \text{sec}^{-1}$, and the associated damping ratio is $\zeta = \frac{1}{2} R_\ell \sqrt{(C_\ell + C_U)/I_\ell} = 0.6$, approximately. For the underdamped system ($\zeta < 1$), the time varying ventricle air pressures P_{vaL} and P_{vaR} can therefore be calculated from the following equations:

$$P_{va} = P_E + (P_{VAS} - P_E)\left\{1 - \frac{e^{-\zeta W_n t}}{\sqrt{1-\zeta^2}} \sin(W_n\sqrt{1-\zeta^2}\ t + \phi)\right\} \quad (5.40)$$

for systole, and

$$P_{va} = P_E + (P_{VAS} - P_E)\left\{\frac{e^{-\zeta W_n (t-t_s)}}{\sqrt{1-\zeta^2}} \sin\left[W_n\sqrt{1-\zeta^2}\ (t-t_s) + \phi\right]\right\} \quad (5.41)$$

for diastole, where

$$\phi = \tan^{-1}\ \frac{\sqrt{1-\zeta^2}}{\zeta} \quad (5.42)$$

The above equations can be obtained from any text book of automatic control, or physical networks theories.

5.5 The Simulation Study

Euler's numerical method was used for the hemodynamics simulation (see Section 4.6) at a constant heart rate of 72.3 beats/min with a systolic/diastolic time ratio S/D = 0.57. The objectives of the simulation study include the following:

(a) To determine the required driving air pressures and exhaust air pressures for the left and right ventricle systems, so that when the heart pump is driving against a normal cardiovascular load (i.e. with the normal resistances, inertances and capacitances given in Tables 6a and 6b), the mean output flow rate from both ventricles is 5 lit/min approximately, with a mean aortic pressure of 100 mm Hg and full ventricular volumes attained at the end of diastole.

(b) To determine the required driving air pressures and exhaust air pressures for the same artificial heart system when the systemic resistances have half ($\eta = 0.5$) and double ($\eta = 2.0$) their normal values ($\eta = 1.0$). The coefficient η is the resistance multiplication factor. The mean aortic pressure is maintained at 100 mm Hg, with the same mean output from both ventricles and full end-diastolic ventricular volumes. This information is needed to determine the required characteristics of the atrial pressure feedback system which automatically adjusts the driving air pressure to obtain Starling's Law response.

(c) To investigate the dynamic regulation capability of the artificial heart system when all the vascular resistances vary exponentially with time to half or double their normal values. A time constant of 2 seconds is used [60].

5.6 Results and Discussions

Table 7 is a summary of the results obtained for parts (a) and (b) of the simulation study. The starting conditions at the onset of systole are listed in Table 8. The values given in Table 7 are obtained after six complete pumping cycles from start-up when all the system variables reach repetitive values. The pressures and flow rates obtained at the end of the sixth cycle in part (a) are used as the starting conditions for part (c).

The required left ventricle driving air pressures for the multiplication factors, $\eta = 0.5, 1.0, 2.0$, are 150, 127, 119 mm Hg, with resulting mean left ventricle output flow rates of 9.24, 4.85 and 2.71 lit/min, respectively. The right ventricle driving air pressures are 54, 33 and 27 mm Hg, for the delivery of mean right ventricle outputs of 9.25, 4.78 and 2.70 lit/min, respectively, which are nearly the same as the outputs from the left ventricle. Better results can be obtained by finer adjustments of the driving pressure amplitudes. The obtained driving air pressures are also plotted as a function of mean atrial pressures in Figure 52. The indicated characteristics and the pressure levels of interest are obtainable by further development work on the hydraulic/pneumatic pressure transducers, which are used basically for the selection of driving air pressures at different mean atrial pressures.

The simulation results of Table 7 show that it is sufficient for the left ventricle air to exhaust to atmosphere directly and for the

TABLE 7

Driving and Exhaust Air Pressures Requirements for the Artificial Heart System - Performance Results.

		Multiplication Factor of Normal Vascular Resistance Values		
		0.5	1.0	2.0
Left Ventricle	Driving Air Pressure, mm Hg	150	127	119
	Exhaust Air Pressure, mm Hg	0	0	0
	Mean Atrial Pressure, mm Hg	9.009	5.580	4.772
	Mean Aortic Pressure, mm Hg	100.83	100.16	100.87
	Mean Ventricle Output, lit/min	9.24	4.85	2.71
	Stroke Volume, ml	127.86	67.07	37.45
Right Ventricle	Driving Air Pressure, mm Hg	54	33	27
	Exhaust Air Pressure, mm Hg	-5	-5	-5
	Mean Atrial Pressure, mm Hg	0.314	0.164	-0.386
	Mean Pulmonary Pressure, mm Hg	18.03	14.92	15.31
	Mean Ventricle Output, lit/min	9.25	4.78	2.70
	Stroke Volume, ml	128.00	66.03	37.36

TABLE 8

Starting Conditions for the Digital Simulation.

	Parts (a) and (b)	Part (c)		Parts (a) and (b)	Part (c)
P_{01}	96	83.89	q_{ASAO}, q_{LAVR}	-0.245	-0.213
P_{02}	96	83.89	q_{THAR}	0	0.139
P_{03}	96	84.08	q_{COAR}	0.480	0.421
P_{04}	96	84.65	q_{THAO}	0	1.308
P_{05}	96	84.86	q_{HAAR}	0	-0.368
P_{06}	0.1	0.62	q_{BRCP}	0.960	0.422
P_{07}	0	-0.37	q_{INAR}	0	1.876
P_{08}	8	10.04	q_{ABAO}	0	-0.240
P_{09}	4	4.15	q_{LEAR}	0	0.126
P_{10}	96	83.69	q_{LEVE}	0.752	0.330
P_{11}	1	0.97	q_{ABVE}	0.181	0.088
P_{12}	96	84.08	q_{INVE}	4.667	2.031
P_{vtL}	4	4.15	q_{INVC}	0.800	3.960
P_{vtR}	0	-0.37	q_{HAVE}	1.831	0.797
			q_{SUVC}	2.000	1.342
			q_{PUAR}, q_{RAVR}	-0.021	-0.028
			q_{PUVE}	4.103	3.023

NOTE: Pressure in mm Hg, Flow Rates in lit/min.

right ventricle air to exhaust to a 5 mm Hg vacuum. It is not necessary to use an excessively low vacuum source to assist air evacuation to achieve the maximum end-diastole volumes. A lower than required vacuum in the ventricle housing is undesirable since it causes a reduction of the ventricle output; at the onset of systole additional time is needed for the ventricle air pressure to build to the level required for flow ejection.

It is noted that the largest stroke volume utilized is 128 ml, associated with a mean flow rate of 9.25 lit/min and $\eta = 0.5$; as compared with the maximum achievable stroke volume of 180 ml. It is therefore possible to obtain a flow rate greater than 9.25 lit/min from the present artificial heart system. Practically, it has been demonstrated that 10 lit/min is obtainable (see Figure 30).

The mean ventricle outputs delivered by the artificial heart system in simulation are compared with the normal cardiac outputs at different mean atrial pressures in Figure 53. The behaviour and the sensitivities (i.e. the gradients) of the simulation curves compare reasonably well with the normal Starling's function curves. The results show that the artificial heart system possesses the Starling's cardiac regulation capability but the left ventricle characteristic is displaced from the normal function curve.

Typical dynamic traces of pressures and flows from the sixth pumping cycle with a normal cardiovascular loading (i.e. $\eta = 1$) are shown in Figures 54a and 54b. The figures illustrate the pressure deficiencies between the ventricle air pressures, the ventricle

pressures and the ventricle output pressures. The deficiencies are more pronounced in the right ventricle system (see Figure 54b), indicating that it is a less efficient pumping unit in comparison with the left ventricle system (see Figure 54a). The inefficiency is mainly caused by the high friction losses associated with the disc valve, especially in the initial transient state, and the acceleration effect from the mass of blood within the ventricle and in the connecting tube. Although the two ventricle systems are assumed identical, since the flow rates from both systems are the same, the friction losses and inertial losses are therefore affecting the right ventricle system to a larger extent due to its generally lower pressure levels.

The dynamic results also indicate the presence of flow regurgitation, a consequence of the passive disc valves used in the system. The valves do not reopen and close again as observed in the mock circulation tests described in Chapter 4. In addition, the high pressure-peaks observed in the output tube of the mock circulation tests, caused by the abrupt closure of the valve, is noticeably reduced in the simulated pressure-time traces in the ascending aorta and in the pulmonary arteries. This attenuation of the peak pressure is attributed to the relatively higher effective impedance and damping of the human cardiovascular system.

The mean blood flow rates and the mean blood pressures obtained from the simulation study are comparable with the actual physiological values (see Table 7). The general shapes of the dynamic traces shown in Figures 54a and 54b differ from those of the actual hemodynamics

simulation obtained by Beneken and DeWit [60]. The difference is basically due to the myocardial functions used for the pumping of blood between the two simulation studies. In the present study, the pumping force is derived from the pulsatile air pressure of nearly the shape of a square-wave, whereas the muscular driving force in the work by Beneken and DeWit, which is based on physiological data of heart muscle, is of near triangular-wave shape. Different input wave shapes can be used in the present calculation scheme so that the simulated dynamic traces display characteristics similar to the physiological traces.

The simulation results for part (c) are shown in Figures 55 to 58. In the simulation, the two (one for the left ventricle system and the other for the right) hydraulic/pneumatic (h/p) pressure transducers for the automatic selection of driving air pressures (P_{VAS}) have the P_{VAS} versus $\overline{P}_{at}$ (the mean atrial pressures) characteristics shown in Figure 52. The characteristics of Figure 52 are mathematically modelled by a piece-wise linear approximation method. The maximum allowable driving pressure for the right ventricle is limited to 54 mm Hg because of the steep slope of its characteristic curve. The mean atrial pressures are obtained with the second order, passive hydraulic filter model described in Section 2.4. Figure 59 compares the mean atrial pressures with the pulsatile pressures at the left and right atriums, indicating that averaged pressures are obtainable from the passive filters.

Figure 55 shows the dynamic response of the mean atrial pressure

when the resistance multiplication factor η is varied exponentially from 1 to 2, and from 1 to 0.5. The response is presented as a function of the number of pumping cycles (equivalent to the number of heart beats). The figure also gives the asymptotic mean atrial pressure levels for $\eta = 2$ and $\eta = 0.5$ obtained previously in parts (a) and (b) of the study. The corresponding changes in the driving air pressures, the mean aortic and pulmonary pressures and the mean ventricle outputs are given in Figures 56, 57 and 58, respectively, together with their corresponding asymptotic values. In general, the results show that the artificial heart system follows the exponential variation of η from 1 to 2 very well. The regulation behaviour of the system, however, is not satisfactory when η is varied from 1 to 0.5. The inadequacy of the model in describing the "steep-slope" characteristic of the right atrial pressure feedback system is the most probable cause for the variables of Figures 55 to 58 not reaching their steady-state mean values within a reasonable number of cycles when the resistances decrease.

5.7 Conclusions

The performance capability of the pneumatic artificial heart system as a replacement for the physiological heart was studied. Based on the results of the simulation of the hemodynamics, the following conclusions are drawn.

- The system can maintain the required physiological mean blood flow rates and mean blood pressures.

- The system exhibits regulation characteristics similar to the physiological heart. The driving system adequately follows an exponential increase of the resistances (vascular contraction) by a factor of two. However, the model needs further refinement for the case of an exponential decrease of resistances (vascular dilation) of one-half.

- The model accounts for regurgitation and leakage and enables assessment of their effects on the output pressure-flow characteristics of the left and right ventricles. For the disc-type valves of this study, regurgitation occurs during a significant time period: 50 msec for the left and 80 msec for the right outlet valves, Figures 54a and 54b. The amount of back-flow can be obtained and its effect, for instance, on the pumping efficiency can be determined. On the other hand, the leakage flow is insignificant: 0.213 lit/min for the left and 0.029 lit/min for the right ventricles, respectively.

- The pressure and flow traces of Figures 54a and 54b contain all the information needed to calculate the power outputs from both ventricles, the pressure and power losses across the valves and the power losses across the ventricle sacs. For instance, the larger areas between the air-ventricle pressure traces and ventricle-output pressure traces for the right ventricle as compared to the corresponding traces for the left ventricle indicate the lower efficiency of the right

ventricle system.

- Because of the detail of the model, it is possible to investigate separately the effects of parameters such as inlet valve resistance, atrium compliance, sac elasticity, etc., on the overall cardiovascular characteristics.

This study has been carried out at constant frequency. The same simulation program can be used to study the system performance with variable frequency. This can be achieved by statically or dynamically varying the systolic and/or the diastolic time in the program.

CONCLUSIONS AND RECOMMENDATIONS FOR FURTHER WORK

An all-pneumatic driving system which uses only fluid-operated devices has been developed for sac-type artificial ventricles. The system provides good Starling's cardiac regulation characteristics to a latex left ventricle in mock circulation. The system was built from commercially available hardware. It is economical and simple to operate. It accomplishes the cardiac function without electronic interfacing devices.

A mathematical model of the sac-type artificial ventricle has been derived, and a model of the prosthetic disc valve has been proposed. Both models have been evaluated in a simulation study of a latex ventricle in mock circulation and they give dynamic predictions in good agreement with measurements. Since the models include actual physical quantities such as the ventricle sac elasticity, and dimensions of the ventricle and of the valve, they are useful in studies relating to the design of artificial heart systems to achieve the best possible cardiac assistance results.

The mathematical models were used in a simulation study for the evaluation of the regulation capability of the all-pneumatic artificial ventricle system as a replacement of the myocardial function, and for the acquisition of design data to construct a right artificial ventricle system with Starling's autoregulation characteristics. Based on the in-vitro experiments and simulation studies

accomplished in this thesis, the following general conclusions can be drawn.

1. For temporary or permanent cardiac replacement, it is important to have an artificial heart that responds to the venous return in accordance with Starling's Law of the physiological heart.

2. The all-pneumatic artificial ventricle driving system provides the Starling's cardiac autoregulation function.

3. The derived model of an elastic sac is a reasonably accurate mathematical representation of the sac-type artificial ventricle.

4. The derived simple expression, which relates the ventricle volume to the ventricle air pressure, the ventricle pressure, the maximum ventricle volume and a parameter associated with the elastic property of the ventricular material, gives a qualitative understanding of the governing parameters that affect the stroke volume of an artificial ventricle.

5. The proposed model of the hinged disc valve gives good predictions regarding the opening and closing dynamics of the valve, and the regurgitation and leakage phenomena.

This thesis has made some significant contributions to the disciplines of cardiac prosthesis and cardiac assistance. There are some aspects of the work, however, that need further research and development. For example, (a) the power consumption of the hydraulic/pneumatic pressure transducer is high and it should be reduced, and (b) the all-pneumatic artificial ventricle system has been tested only in a mock circulatory system and it should be tested further in experiments involving live animals. The following is a list of recommendations for further work.

1. The functional characteristics of the hydraulic/pneumatic pressure transducer are acceptable for the automatic adjustment of ventricle driving air pressure. Miniaturization can help to reduce the size and power consumption of the device. The recommended power level for the miniaturized transducer is about one half watt, a level common to most miniature fluidic elements.
2. The present all-pneumatic artificial ventricle system can be used as it is for left ventricular bypass experiments with animals. It is therefore recommended to have such experiments conducted so that further evaluation of the system can be made.
3. It is recommended to build a duplicate driving system so that total heart replacement experiments (in-vitro and/or in-vivo) can be materialized.

4. The mathematical models of the elastic sac should be utilized in further simulation work on total heart replacement. The studies may include (a) efficiency study of the all-pneumatic driving system, (b) the effects of flow regurgitation, (c) the effects of ventricle sac elasticity and atrium compliance on the pumping performance of an artificial heart system, and (d) the effects of different types of prosthetic heart valves on the performance of an artificial ventricle system.

REFERENCES

1. Blumberg, M.S., Gardiner, K.W., Lyman, D.J. and Newgard, P.M., Artificial Heart Devices and Systems: A Conceptual Phase Study. Report PB 169832, Jan. 1966, Stanford Research Institute, California, Distributed by Clearinghouse.

2. Rushmer, R.F., Cardiovascular Dynamics. W.B. Saunders, 1970.

3. Guyton, A.C., Jones, C.E. and Coleman, T.G., Circulatory Physiology: Cardiac Output and Its Regulation. W.B. Saunders, 1973.

4. Saxton, G.A. and Andrews, C.B., An Ideal Heart Pump with Hydrodynamic Characteristics Analogous to the Mammalian Heart. Trans. Amer. Soc. Art. Int. Organs, Vol. 6, pp. 288-290, 1960.

5. Bernstein, E.F., Castaneda, A.R., Blackshear, P.L. and Varco, R.L., Prolonged Mechanical Circulatory Support: Analysis of Certain Physical and Physiological Considerations. Surgery, Vol. 57, pp. 103-122, Jan. 1965.

6. Dorman, F., Bernstein, E.F., Blackshear, P.L., Sovilj, R., and Scott, D.R., Progress in the Design of a Centrifugal Cardiac Assist Pump with Trans-Cutaneous Energy Transmission by Magnetic Coupling. Trans. Amer. Soc. Art. Int. Organs, Vol. 15, pp. 441-448, 1969.

7. Cappelletti, R.R., Domingo, R.T., Dennis, C., Amer, N.S. and Stuckey, J.H., Controlled Studies in Three Pumping Systems. Trans. Amer. Soc. Art. Int. Organs, Vol. 7, pp. 162-166, 1961.

8. Galletti, P.M. and Brecher, G.A., Heart-Lung Bypass. Grune and Stratton, N.Y., 1962.

9. Pierson, R.M., Camp, G.B. and Mathis, M.V., Roller Pump for Artificial Hearts Using Multichamber Rubber Tubing. Trans. Amer. Soc. Art. Int. Organs, Vol. 11, pp. 68-73, 1965.

10. Pierce, W.S., Turner, Jr., M.C., Boretos, J.W., Metz, H.D., Nolan, S.P. and Morrow, A.G., Mechanical Left Ventricle Assistance: Experimental Studies Using an Implantable Roller

Pump. Trans. Amer. Soc. Art. Int. Organs, Vol. 13, pp. 299-305, 1967.

11. Turner, M.C., Pierce, W.S., Metz, H.D. and Goodman, L., An Implantable Valveless Heart Assist Pump. ASME Paper No, 68-WA/Aut-10.

12. Klopp, E.H., Jacobs, L.A., Hoffman, B.F., Seamone, W. and Gott, V.L., Use of Left Atrial Pressure as a Control Parameter for Total Left Heart Bypass. Trans. Amer. Soc. Art. Int. Organs, Vol. 15, pp. 391-397, 1969.

13. Ostberg, B.N., Ostberg, G. N. and Ostberg, M., A Rotary Implantable Pump. Med. Bio.Eng., pp. 768-772, Nov. 1974.

14. Backman, D.K., Donovan, F.M., Sandquist, G., Kessler, T. and Kolff, W.J., The Design and Evaluation of Ventricles for the AEC Artificial Heart Nuclear Power Source. Trans. Amer. Soc. Art. Int. Organs, Vol. 19, pp. 542-559, 1973.

15. Akutsu, T., Seidel, W., Mirkovitch, V., Feller, J. and Kolff, W.J., An Electromotor-Driven Pendulum-Type Artificial Heart Inside the Chest. Trans. Amer. Soc. Art. Int. Organs, Vol. 7, pp. 374-377, 1961.

16. Robinson, W.J., Migliore, J.J., Arthur, J., Fugua, J.M., Dove, G.B., Coleman, S., Huffman, F.N. and Norman, J.C., An Abdominal Left Ventricular Assist Device: Experimental Physiologic Analysis II. Trans. Amer. Soc. Art. Int. Organs, Vol. 19, pp. 229-234, 1973.

17. Klain, M., Ogawa, H., Wright, J., Webb, J., Mrava, G., von Bally, K., Urbanek, K., Carse, C., Sagawa, K. and Nosé, Y., Valveless Orthotopic Cardiac Prosthesis - A Wave-Pulsating Total Heart. Trans. Amer. Soc. Art. Int. Organs, Vol. 16, pp. 400-408, 1970.

18. Portner, P.M., Dong, Jr., E., Jassawalla, J.S. and LaForge, D.H., Performance of an Implantable Controlled Solenoid Circulatory Assist System. Trans. Amer. Soc. Art. Int. Organs, Vol. 19, pp. 235-242, 1973.

19. Kwan-Gett, C.S., Zwart, H.J., Kralios, A.C., Kessler, T.R., Backman, D.K. and Kolff, W.J., A Prosthetic Heart With Hemispherical Ventricles Designed for Low Hemolytic Action. Trans. Amer. Soc. Art. Int. Organs, Vol. 16, pp. 409-415, 1970.

20. Lyman, D.J., Kwan-Gett, C., Zwart, H.H.J., Bland, A., Eastwood, N., Kawai, J. and Kolff, W.J., The Development and

Implantation of a Polyurethane Hemispherical Artificial Heart. Trans. Amer. Soc. Art. Int. Organs, Vol. 17, pp. 456-463, 1971.

21. Peters, J.L., Donovan, F.M. and Kawai, J., Consequences of the Diaphragm Driven Artificial Heart - Animal Implantation and Mock Circulation Studies. Chest, Vol. 63, pp. 589-597, 1973.

22. Donovan, F.M., Greenhalgh, S. and Volder, J.G.R., Efficiency and Power Requirements of the Diaphragm-Type Artificial Heart. Med. Instrumentation, Vol. 8, No. 2, pp. 77-83, 1974.

23. Nosé, Y. and Levine, S.N., Editors, Advances in Biomedical Engineering and Medical Physics, Vol. 3, Cardiac Engineering, Chapter 2 (written by Norton, S.H.), Interscience, 1970.

24. Loeha, M.L., Kosch III, W.F., Pierce, W.S. and Kirby, C.K., The Piezoelectric Artificial Heart. Trans. Amer. Art. Int. Organs, Vol. 10, pp. 147-150, 1964.

25. Williams, Jr., M.J., A Piezoelectric Heart Assist Device. Ph.D. Thesis, 1972, Rutgers University, New Brunswick, N.J.

26. Williams, Jr., M.J., Welkowitz, W., Fich, S., Molony, D.A., Jaron, D. and Kantrowitz, A., The Design of a Piezoelectric Heart Assist Drive. IEEE Trans., BIO-ENG., Vol. BME 22, No. 4, pp. 40-46, 1975.

27. Freebairn, D. and Heggs, T., Solenoid Design for a Prosthetic Heart. Trans. Amer. Soc. Art. Organs, Vol. 10, pp. 166-170, 1964.

28. Klopp, E.H., Seamone, W., Carlson, R.S., Hoffman, B.F. and Gott, V.L., The Development of an Automatically Controlled Intrathoracic Total Left-Heart Bypass System. Trans. Amer. Soc. Art. Int. Organs, Vol. 17, pp. 201-206, 1971.

29. Nosé, Y., Topaz, S., Sen Gupta, A., Tretbar, L.L. and Kolff, W.J., Artificial Hearts Inside the Pericardial Sac in Calves. Trans. Amer. Soc. Art. Int. Organs, Vol. 11, pp. 255-262, 1965.

30. Nosé, Y. and Kolff, W.J., The Intracorporeal Mechanical Heart. Vasc. Dis., Vol. 3, pp. 25-32, 1966.

31. Akutsu, T., Chaptal, P.A., Agrawal, G. and Kantrowitz, A., Compact Prosthetic Total Heart. Trans. Amer. Soc. Art. Int. Organs, Vol. 12, pp. 288-293, 1966.

32. Kwan-Gett, C.S., Wu, Y., Collan, R., Jacobson, S. and Kolff, W.J., Total Replacement Artificial Heart and Driving System with Inherent Regulation of Cardiac Output. Trans. Amer. Soc. Art. Int. Organs, Vol. 15, 1969.

33. Akutsu, T., Takagi, H. and Takano, H., Total Artificial Heart with Built-In Valves. Trans. Amer. Soc. Art. Int. Organs, Vol. 16, pp. 392-397, 1970.

34. Webb, J.A., Crosby, M.J. and Dustin, M.O., Pneumatic Artificial Heart Driving System Providing Quasi-Steady-State Regulation and Pressure Waveform Control. Lewis Research Center, NASA, Cleveland, Ohio, Oct. 12, 1970, Report 720-03, p. 27.

35. Pierce, W.S., Burney, R.G., Williams, K.R. and Kirby, C., A Servomechanism to Control Output of an Artificial Ventricle. J. Applied Physio., Vol. 18, No. 5, pp. 1029-1032, 1963.

36. Pierce, W.S., Brighton, J.A., O'Bannon, W., Donachy, J.H., Phillips, W.N., Landis, D.L., White, W.J. and Walhausen, J.A., Complete Left Ventricle Bypass With a Paracoporeal Pump: Design and Evaluation. Annals of Surgery, Vol. 180, No. 4, pp. 418-426, 1974.

37. Woodward, K.E., Straub, H., Nosé, Y. and Kolff, W.J., An Intrathoracic Artificial Heart Controlled by Fluid Amplifiers. Trans. Amer. Soc. Art. Int. Organs, Vol. 12, pp. 294-300, 1966.

38. duPlessis, M.P., Kwok, C.K. and Lin, S., The Diaphragm-Ejector Amplifier Heart Pump. Preprints of IFAC 5th World Congress, Paris, France, June 12-17, 1972, Session 25-3, p.7.

39. Burns, W.H., Loubier, R. and Bergstedt, The Development of an Electrohydraulic Implantable Artificial Heart. Trans. Amer. Soc. Art. Int. Organs, Vol. 11, pp. 265-268, 1965.

40. Burns, W.H., Loubier, R. and Farlow, J.M., The Development of an Intrapericardial Cardiac Replacement - Phase II, Trans. Amer. Soc. Art. Int. Organs, Vol. 12, pp. 272-274, 1966.

41. Peters, J.L., Seare, W., Donovan, F.M., Greenhalgh, S., Rowley, K. and Hershgold, E.J., A New In-Vitro Blood Damage Evaluation System for Artificial Hearts. Med. Instrumentation, Vol. 7, p. 72, Jan.-Feb.,1973.

42. Brest, A.N., Editor, Heart Substitutes - Mechanical and Transplant. Charles C. Thomas (Publisher), 1966.

43. Imai, Y., von Bally, K. and Nosé, Y., New Elastic Materials for Artificial Heart. Trans. Amer. Soc. Art. Int. Organs, Vol. 16, pp. 17-25, 1970.

44. Nosé, Y., Crosby, M., Woodward, K., Kwan-Gett, C.S., Hino, K. and Kolff, W.J., Respect the Integrity of the Large Veins and Starling's Law. Trans. Amer. Soc. Art. Int. Organs, Vol. 13, pp. 273-279, 1967.

45. Landis, D.L., Brighton, J.A., O'Bannon, W. and Pierce, W.S., A Synchronization Unit for Use With a Left Ventricle-Aortic Assist Pump: Design and Evaluation. ASME Publication, Paper 73-WA/Bio-24, 1973.

46. Morris, D.T. and Lock, G.S.M., Performance of a Pneumatically Driven Total Replacement Heart. Proc. Third Can. Med. and Biol. Eng. Conf., Halifax, N.S., Sept. 9-11, 1970.

47. Tsang, S. and duPlessis, M.P., Experimental Investigation of the Control for Pneumatically Driven Artificial Hearts. Proc. 4th Can. Cong. of Applied Mechanics, Montreal, Quebec, May 28-June 1, 1973, p. 855.

48. Clark, D.B., Ashton, F. and Abrahams, (Unpublished Work), Department of Surgery, The University of Birmingham, England.

49. Brighton, J.A., Wade, Z.A., Pierce, W.S., Phillips, W.M. and O'Bannon, W., Effect of Atrial Volume on the Performance of a Sac-Type Artificial Heart. Trans. Amer. Soc. Art. Int. Organs, Vol. 19, pp. 567-572, 1973.

50. Peters, J.L., Donovan, Jr., F.M., Backman, D.K., Kessler, T.R. and Kolff, W.J., Effects of Atria on the Function of the Artificial Heart. 24th ACEMB, Session 27.6, 1971.

51. Klain, M., Leitz, H., Phillips, P.M. and Kolff, W.J., A Functional Evaluation of Artificial Heart Valves. Proc. Biomed Symp. Eng. Med., 1966, p. 283.

52. Rodhard, S. and Hochberg, H.M., The Contractile Mechanism of an Elastic Sac. Cardiologia, Vol. 46, No. 2, pp. 85-103, 1965.

53. Brychta, O., Suresh, N. and Callaghan, J.C., The Diaphragm-Ejector Proportional Amplifier and Its Application to Fluidic Operational Circuits. 5th Cranfield Fluidics Conference, June 13-16, 1972, Uppsala, Sweden, Paper E6.

54. Zalmanzon, A., Components for Pneumatic Control Instruments. Pergamon Press, 1965.

55. Tsang, S. and duPlessis, M.P., An All-Pneumatic Artificial Ventricle Driving System. ASME Publication, Paper No. 75 WA/Flcs-2, 1975.

56. Kwan-Gett, C.S., Crosby, M.J., Schoenberg, A., Jacobsen, S.C. and Kolff, W.J., Control Systems for Artificial Hearts. Trans. Amer. Soc. Art. Int. Organs, Vol. 14, pp. 284-290, 1968.

57. Donovan, Jr., F.M., In-Vitro Investigation of the Effects of Venous Compliance, Venous Compression and Artificial Heart Sensitivity on the Circulation. Medical Instrumentation, Vol. 8, No. 2, pp. 70-76, March-April 1974.

58. Guyton, A.C., Textbook of Medical Physiology. W.B. Saunder, 1971, p. 214.

59. Snyder, M.F. and Rideout, V.C., Computer Simulation Studies of the Venous Circulation. IEEE Trans. Bio-Medical Engineering, Vol. BME-16, No. 4, pp. 325-334, Oct. 1969.

60. Reeve, E.B. and Guyton, A.C., Editors, Physical Bases of Circulatory Transport: Regulation and Exchange. W.B. Saunders, Chapter 1, 1967.

61. Snyder, M.F., Rideout, V.C. and Hillestad, R.J., Computer Modelling of the Human Systemic Arterial Tree. J. Biomachanics, Vol. 1, pp. 341-353, 1968.

62. Beneken, J.E.W. and Rideout, V.V., The Use of Multiple Models in Cardiovascular System Studies: Transport and Perturbation Methods. IEEE Trans. Bio-Med. Eng., Vol. BME-4, No. 4, pp. 281-289, Oct. 1968.

63. Suga, H., Theoretical Analysis of a Left-Ventricle Pumping Model Based on the Systolic Time-Varying Pressure/Volume Ratio. IEEE Trans. Bio-Med. Eng., Vol. BME-18, No. 1, pp. 47-55, Jan. 1971.

64. Green, M.E. and Clarke, J.W., The Innervated Left Ventricle: A Mathematical Model of Function. Med. Bio, Eng., pp. 464-468, July 1973.

65. Abel, F.L., An Analysis of the Left Ventricle as a Pressure and Flow Generator in the Intact Systemic Circulation. IEEE Trans. Bio-Med. Eng., Vol. BME-13, pp. 182-188, Oct. 1966.

66. Westerhof, N., Bosman, F., DeVries, C.J. and Noordergraaf, A., Analog Studies of the Human Systemic Arterial Tree. J. Bio-mechanics, Vol. 2, pp. 212-143, 1969.

67. Guier, W.H., Friesinger, G.C. and Ross, R.S., Beat-by-Beat Stroke Volume from Aortic-Pulse-Pressure Analysis. IEEE Trans. Bio-Med. Eng., Vol. BME-21, No. 4, pp. 285-292, July 1974.

68. Buoncristiani, J.F., Liedtke, A.J., Strong, R.M. and Urschel, C.W., Parameter Estimates of a Left Ventricular Model During Ejection. IEEE Trans. Bio-Med. Eng., Vol. BME-20, No. 2, pp. 110-114, Mar. 1973.

69. Ghista, D.N. and Sandler, H., An Analytic Elastic-Visco-elastic Model for the Shape and Forces of the Left Ventricle. J. Bio-mechanics, Vol. 2, pp. 35-47, 1969.

70. Corey, P.D. and Wemple, R.R., A Combined Left Ventricular/Systemic Arterial Model. J. Biomechanics, Vol. 8, pp. 9-15, Jan. 1975.

71. Murthy, V.S., McMahon, T.A., Jaffrin, M.Y. and Shapiro, A.H., The Intra-Aortic Balloon for Left Heart Assistance: An Analytical Model. J. Biomechanics, Vol. 4, pp. 351-367, 1971.

72. Wemple, R.R. and Mockros, L.F., An Analysis of Mechanical Cardiac Assistance. J. Biomechanics, Vol. 6, pp. 99-108, 1973.

73. Spyker, D.A., Simulation in the Analysis and Control of a Cardio-Circulatory Assist Device. Simulation, Vol. 15, No. 5, pp. 196-205, Nov. 1971.

74. Johnson, W., Soden, P.D. and Al-Hassani, S.T.S., Analysis of a Simple Heart-Aorta Analogue. Int. J. Mech. Sci., Vol. 12, pp. 615-626, 1970.

75. McDonald, J., A Study of Displacement Limiting in Sac-Type Pulsatile Pumps. Master Thesis, Penn. State University, Penn., 1974.

76. Wade, Z.A., The Effect of an Atrium on the Performance of an Artificial Heart. Master Thesis, Penn. State University, Penn., 1973.

77. Hansen, A.G., Fluid Mechanics. John Wiley and Sons, 1967.

78. Peterson, L.H., Jensen, R.E. and Parnell, J., Mechanical Properties of Arteries in-Vitro. Cir. Res., Vol. 8, pp. 622-639, 1960.

79. Peterson, L.H., Vessel Wall Stress-Strain Relationship In Pulsatile Blood Flow. Edited by Attinger, E.O., McGraw-Hill, pp. 263-274, 1964.

80. Biomedical Fluid Mechanics Symposium, Fluids Engineering Conference, Denver, Colorada, April 25-27, 1966. ASME Publication.

81. Nichols, N.B., The Linear Properties of Pneumatic Transmission Lines. ISA Trans., Vol. 1, pp. 5-14, 1962.

82. Brown, F.T., The Transient Response of Fluid Lines. J. of Basic Eng., Trans. ASME, Series D, Vol. 84, No. 3, pp. 547-553, 1962.

83. Hougen, J.O., Martin, O.R. and Walsh, R.A., Dynamics of Pneumatic Transmission Lines. Control Eng., pp. 114-117, 1963.

84. Brown, F.T., Margolis, D.L. and Shah, R.P., Small-Amplitude Frequency Bevior of Fluid Lines With Turbulent Flow. J. of Basic Eng., Trans. ASME, Vol. 91, No. 4, pp. 678-693, 1969.

85. Margolis, D.L. and Brown, F.T., Measurement of the Propagation of Long-Wavelength Disturbances Through Turbulent Flow in Tubes. ASME Paper 75-FE-22.

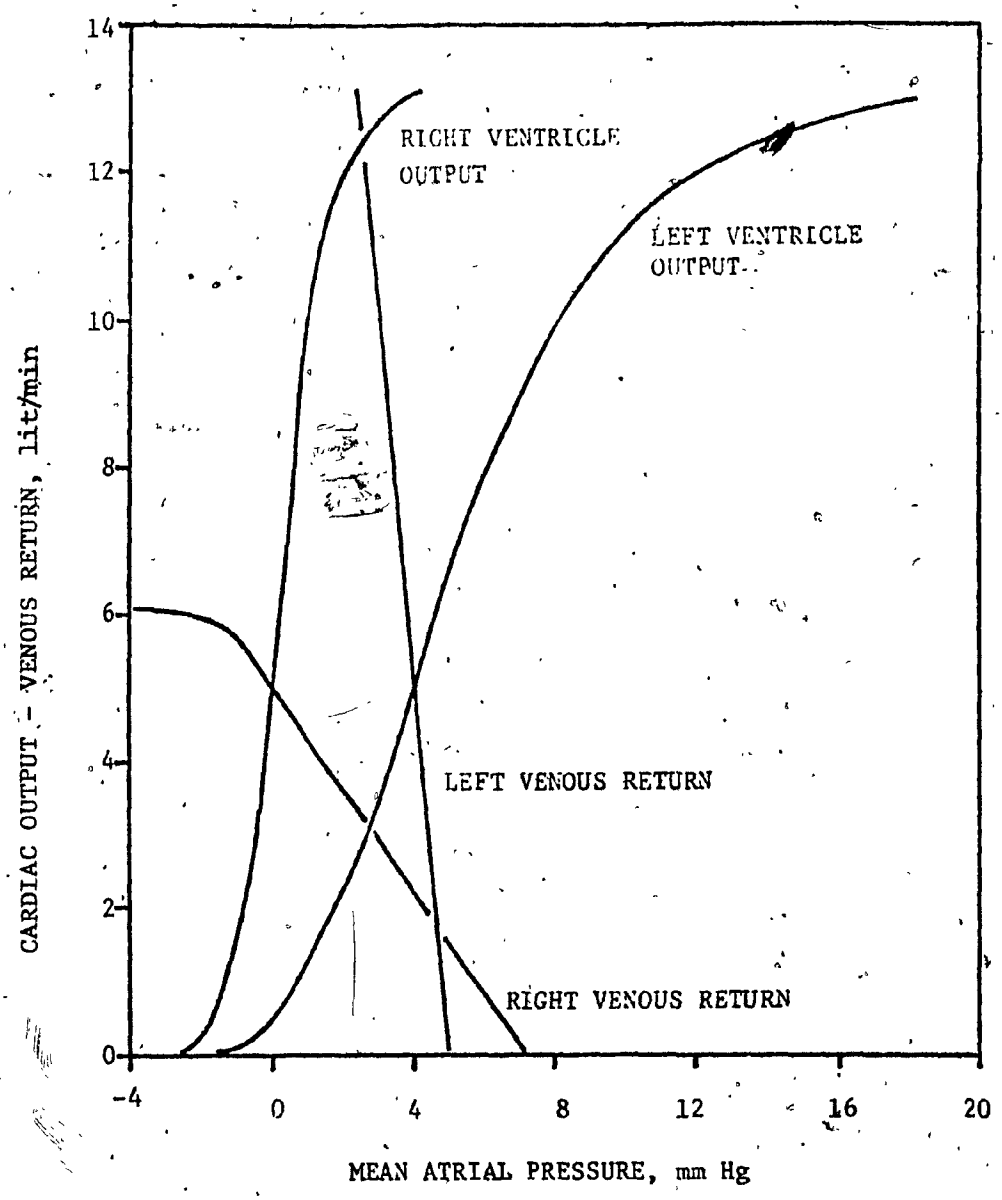

Fig. 1 - Typical cardiac output and venous return function curves of the heart [3].

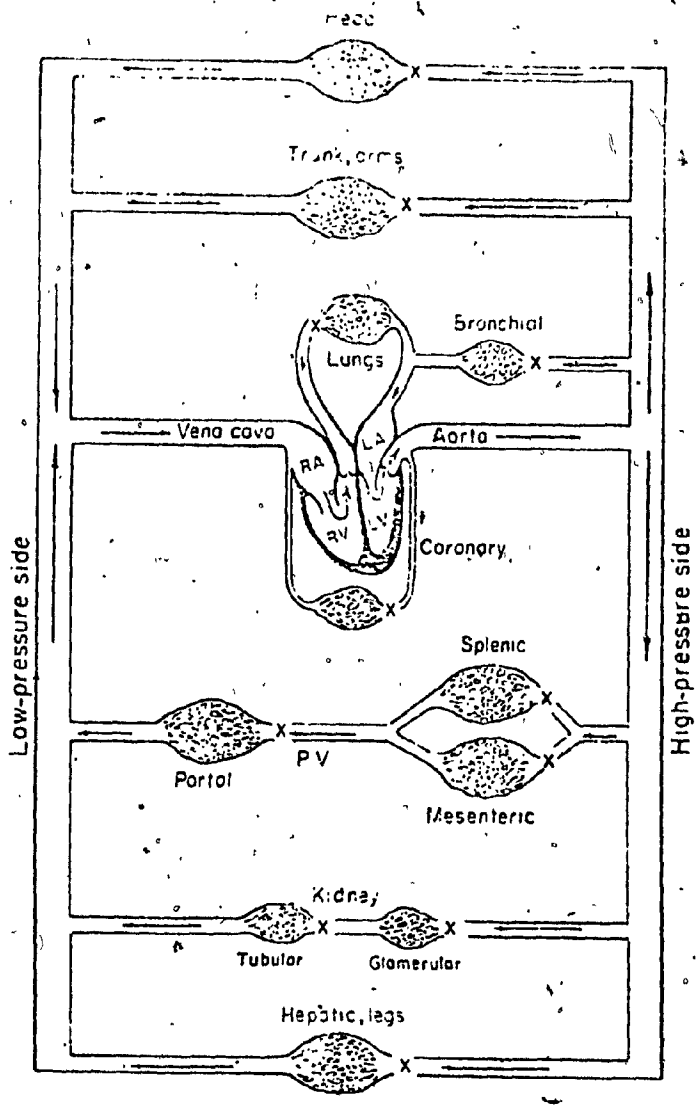

Fig. 2 - Schematic diagram of the human cardiovascular system. (From Glasser, O., Editor, "Medical Physics," Vol. I, Circulation: Physical Principles, by Green, H. D., The Year Book Publishers, Inc., 1949, p. 210.)

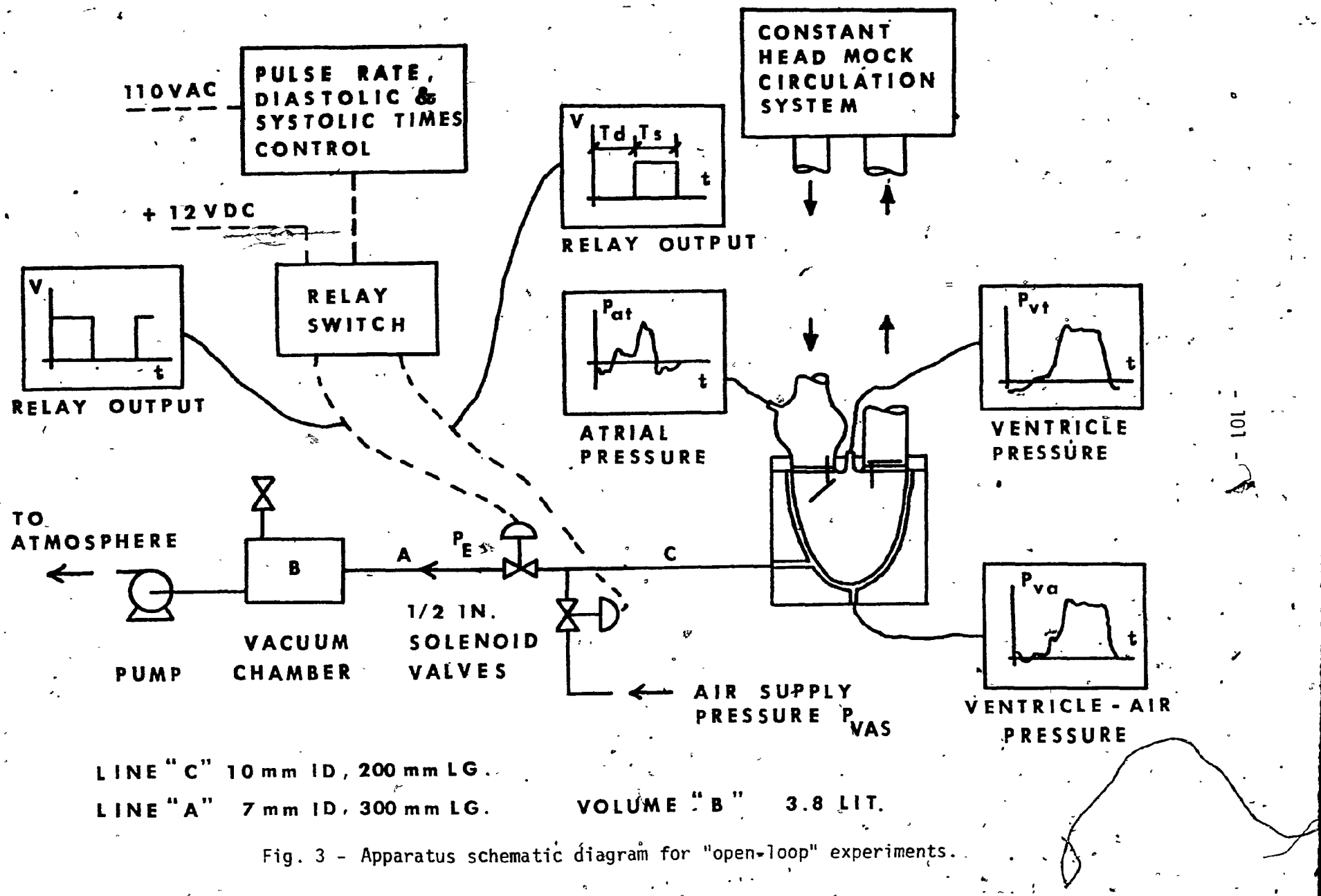

Fig. 3 - Apparatus schematic diagram for "open-loop" experiments.

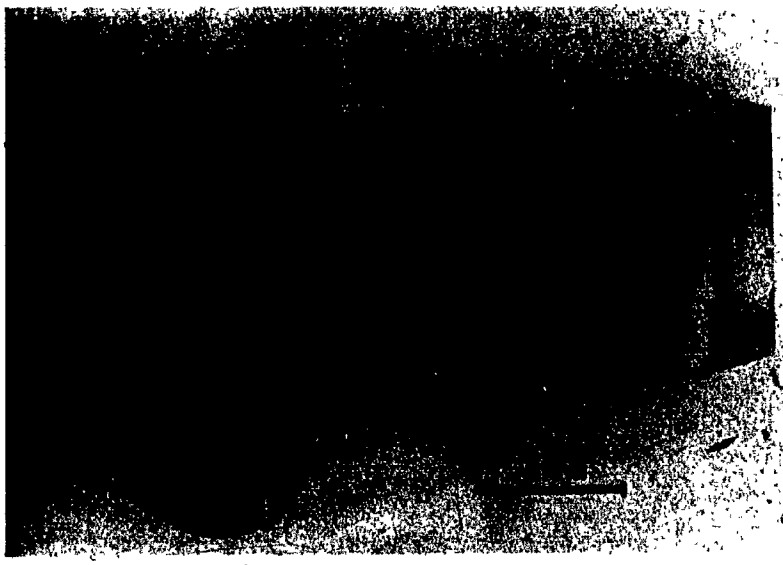

Fig. 4 - Artificial ventricle assembly.

Fig. 5 - Original plasticine model of the ventricle (dark) and the plaster of paris mold.

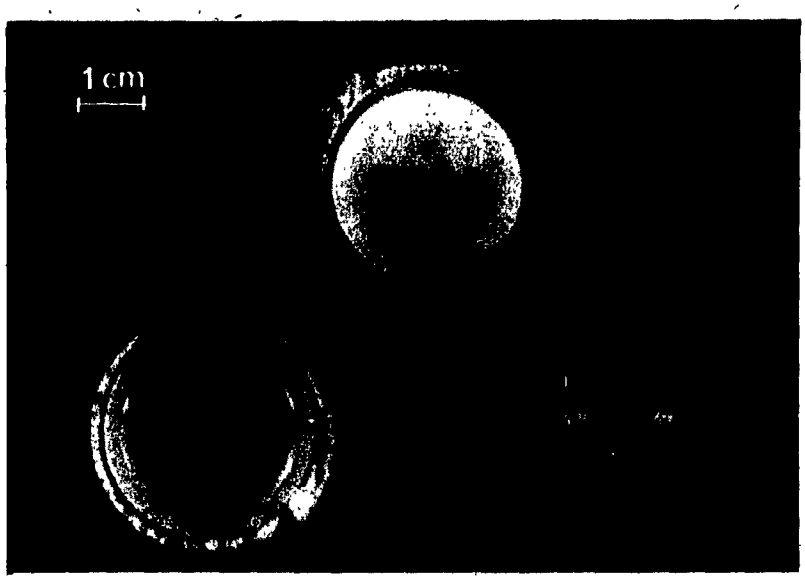

Fig. 6 - Hinged disc valve.

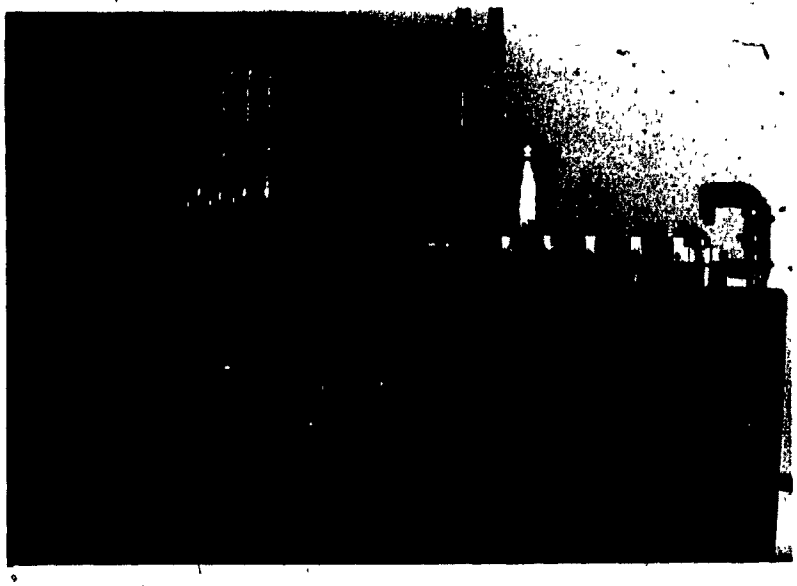

Fig. 7 - Mock circulatory system and the experimental apparatus.

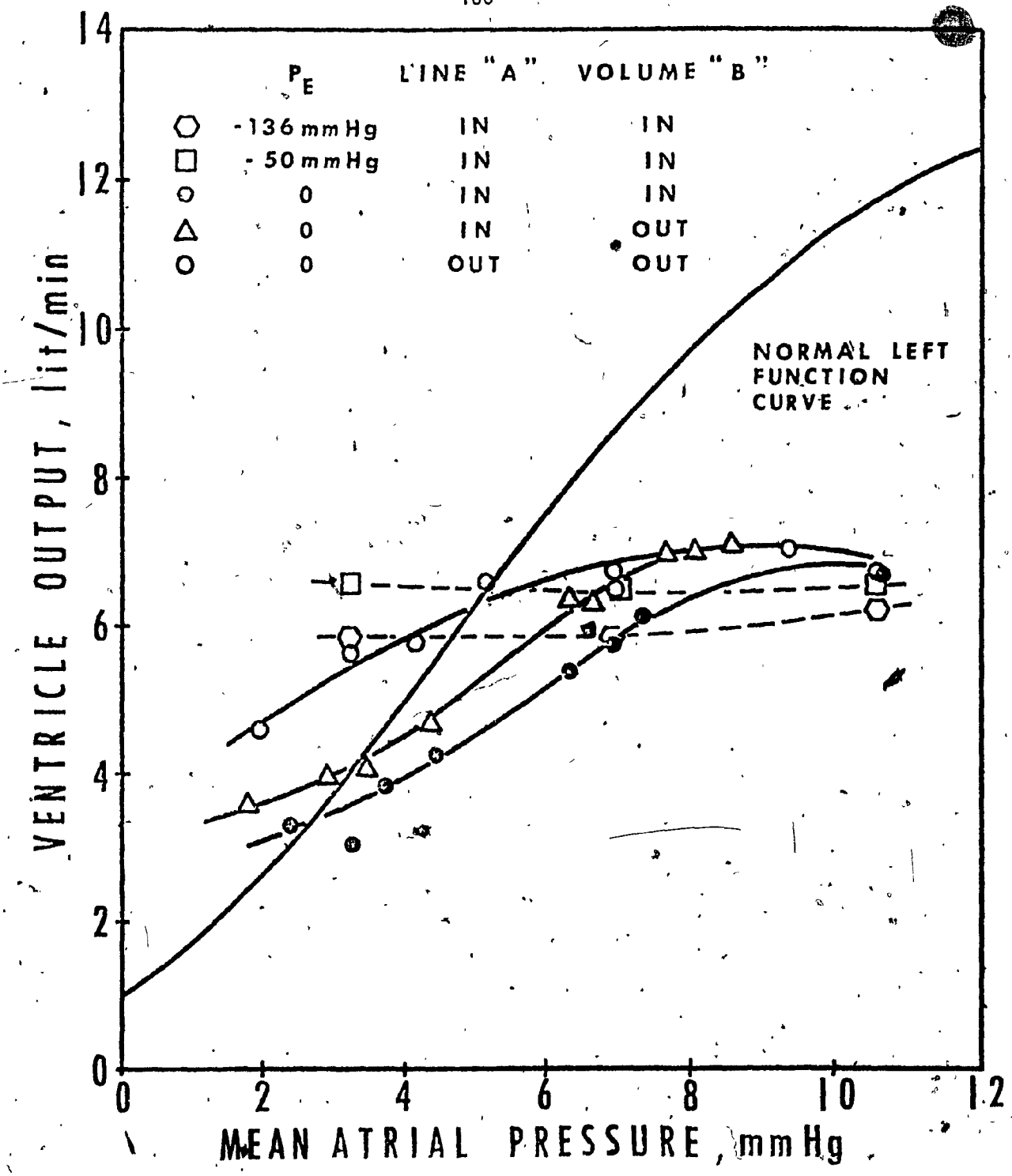

Fig. 8 - Effects of air evacuation rate during diastole on ventricle output at different mean atrial pressures, mean ventricle output pressure = 115 mm Hg, heart rate = 75 beats/min, systolic/diastolic ratio = 1.0, and P_{VAS} = 250 mm Hg.

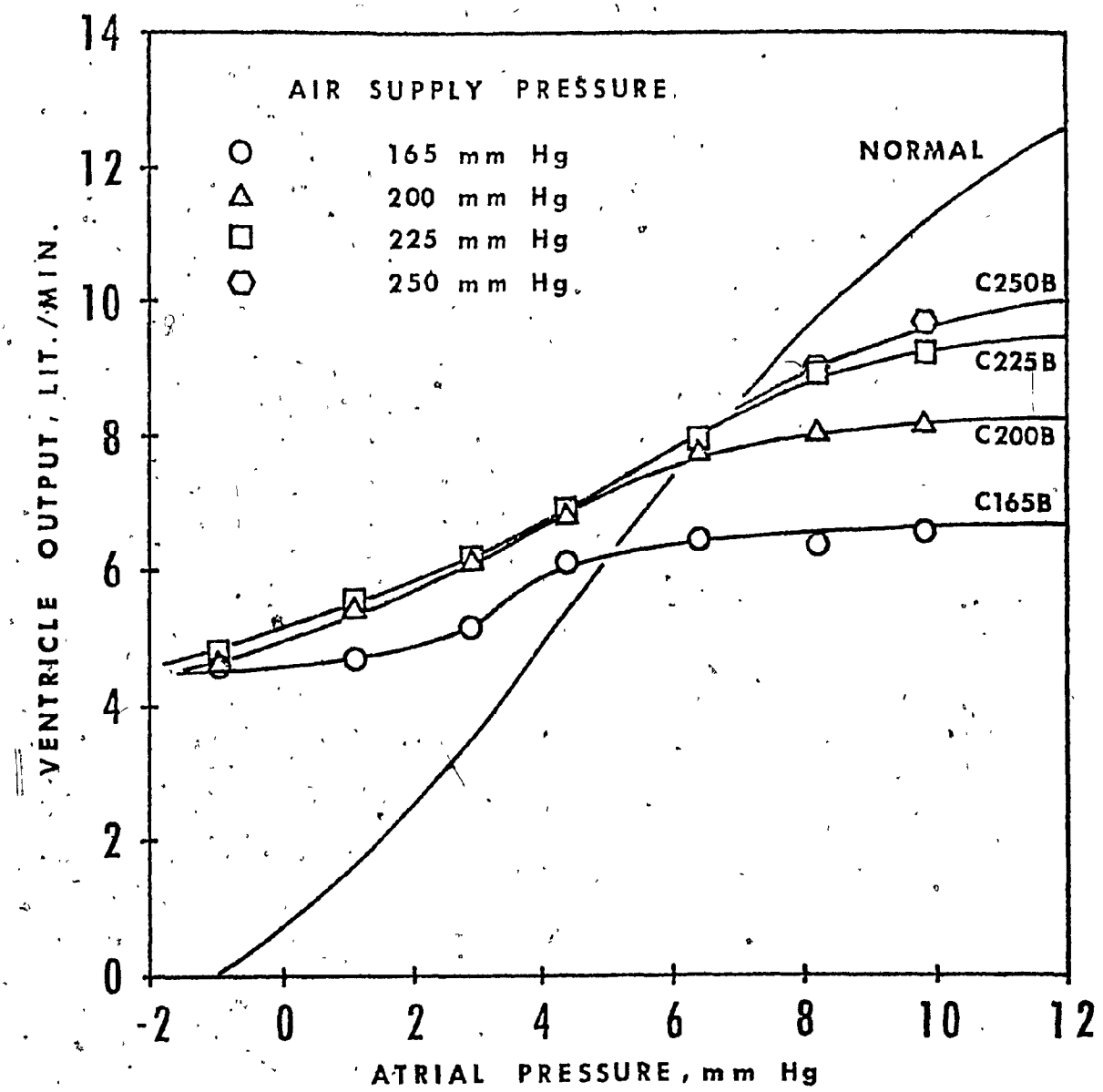

Fig. 9 - Effects of air supply pressure (driving pressure) on mean ventricle output at different mean atrial pressures, mean ventricle output pressure = 100 mm Hg, heart rate = 75 beats/min, systolic/diastolic ratio = 1.0, and P_E = atm.

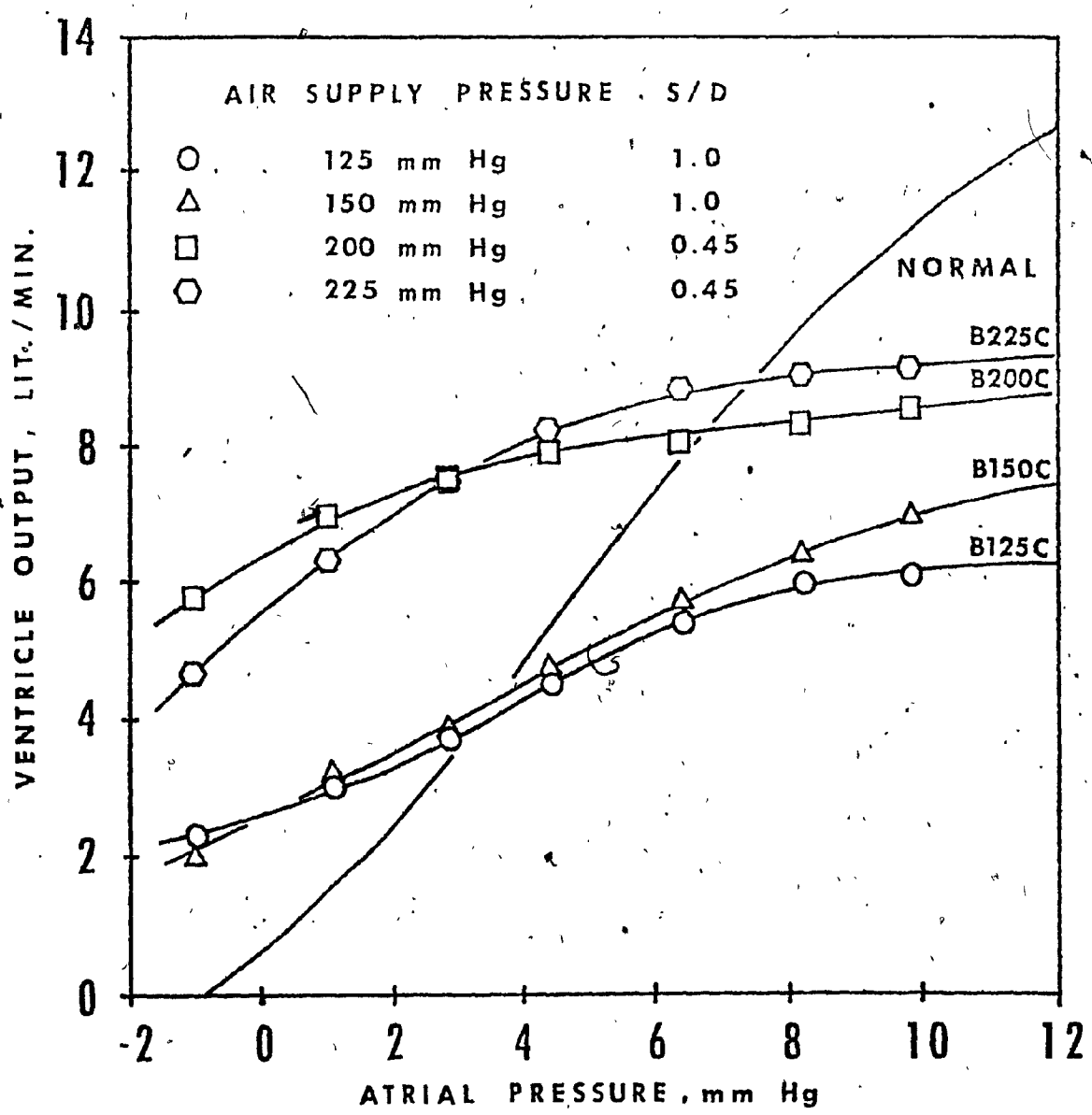

Fig. 10 - Effects of systolic/diastolic ratio on mean ventricle output at different mean atrial pressures, mean ventricle output pres[redacted] = 100 mm Hg, heart rate = 75 beats/min, and P_E = a[redacted].

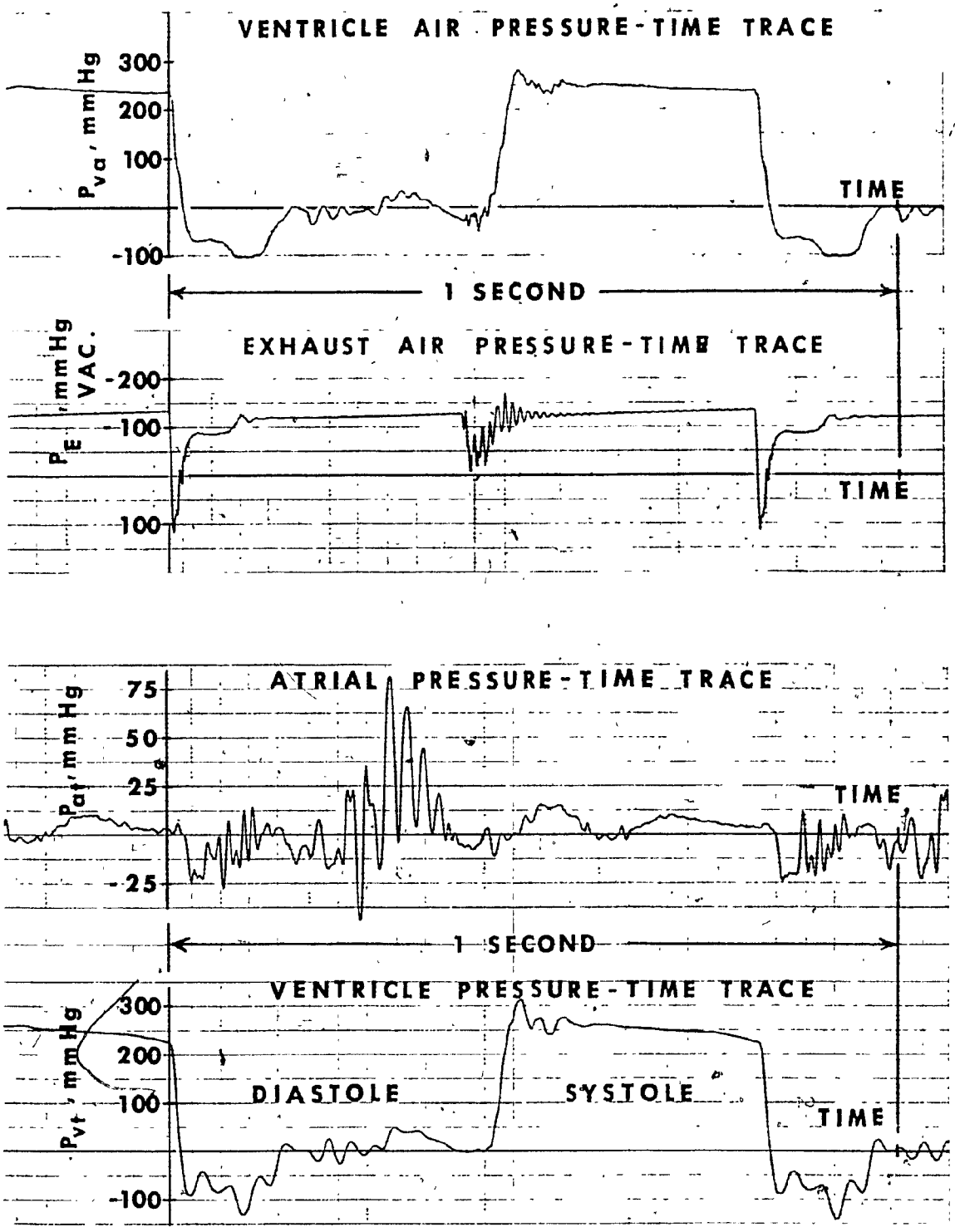

Fig. 11 - Typical dynamic pressure traces at mean ventricle output pressure = 115 mm Hg, heart rate = 75 beats/min, systolic/diastolic ratio = 1.0, P_{VAS} = 250 mm Hg, P_E = - 136 mm Hg, $\overline{P}_{at}$ = 7 mm Hg, line "A" in, and volume "B" in.

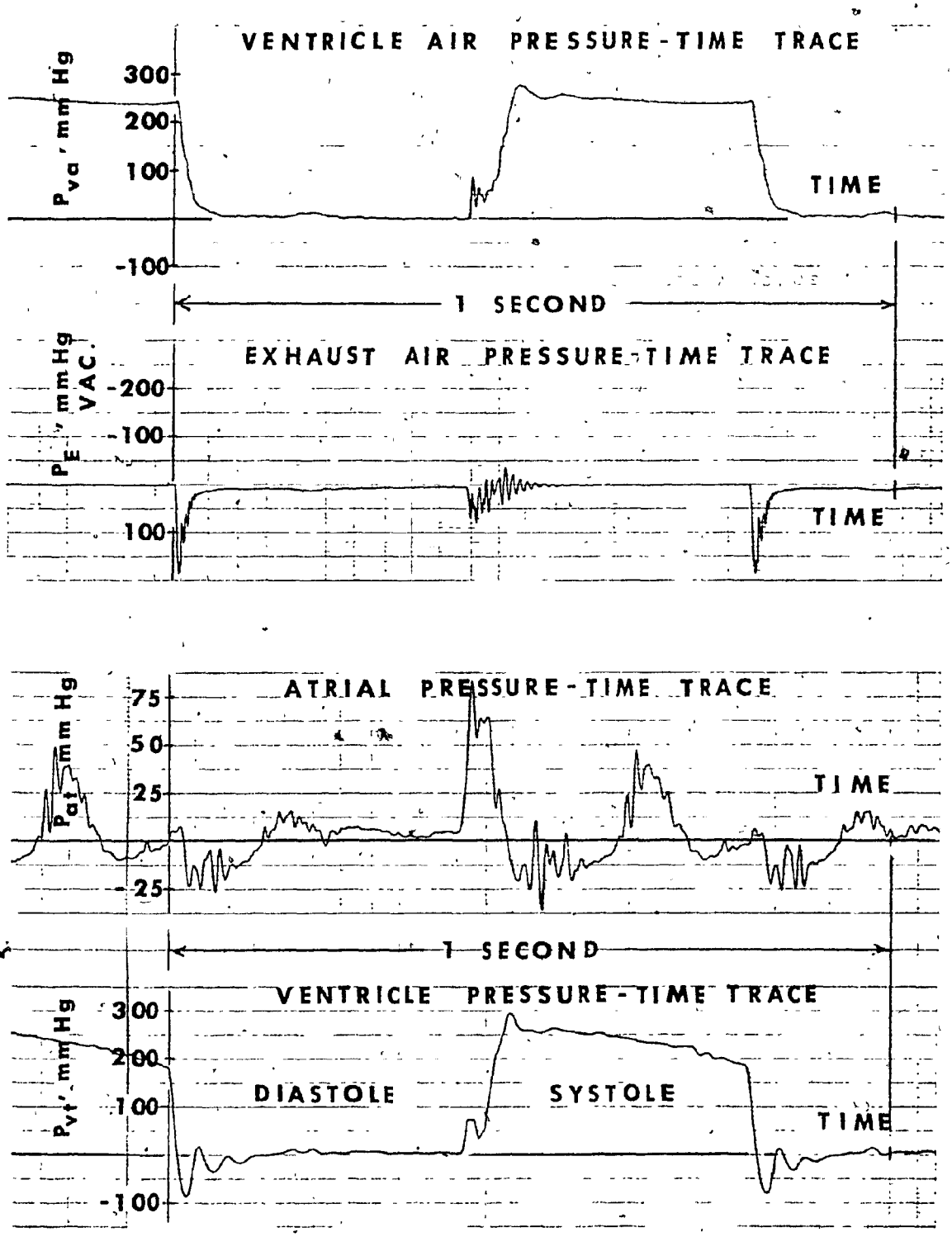

Fig. 12 - Typical dynamic pressure traces at mean ventricle output pressure = 115 mm Hg, heart rate = 75 beats/min, systolic/diastolic ratio = 1.0, P_{VAS} = 250 mm Hg, P_E = atm., $\bar{P}_{at}$ = 7 mm Hg, line "A" in, and volume "B" in.

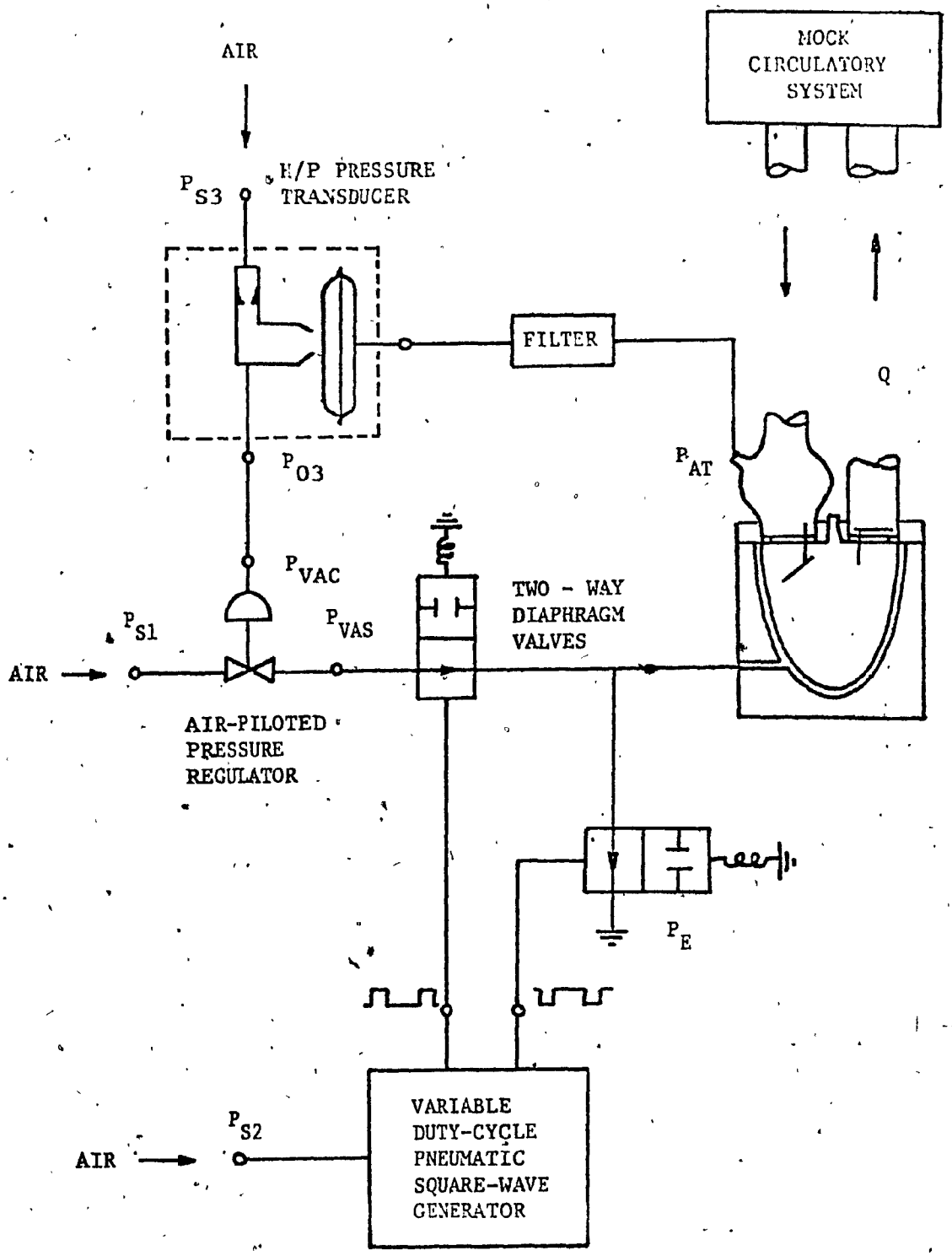

Fig. 13 - Schematic diagram of pneumatic driving system for sac-type artificial ventricle.

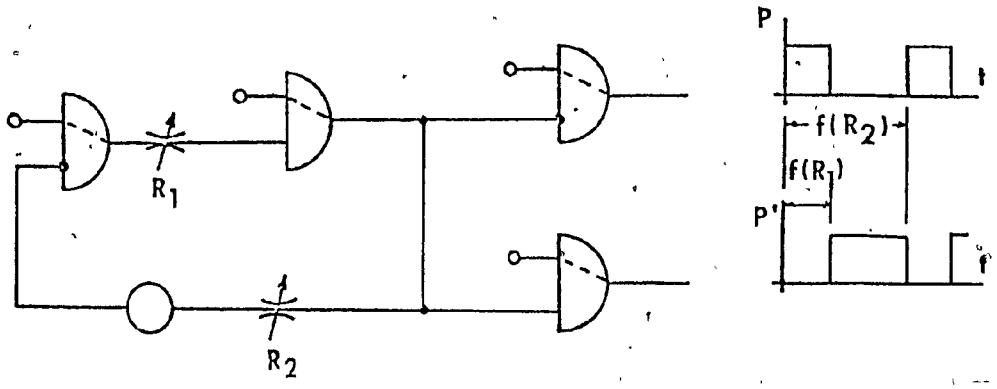

Fig. 14 - Pneumatic square-wave signal generator #1 circuit diagram.

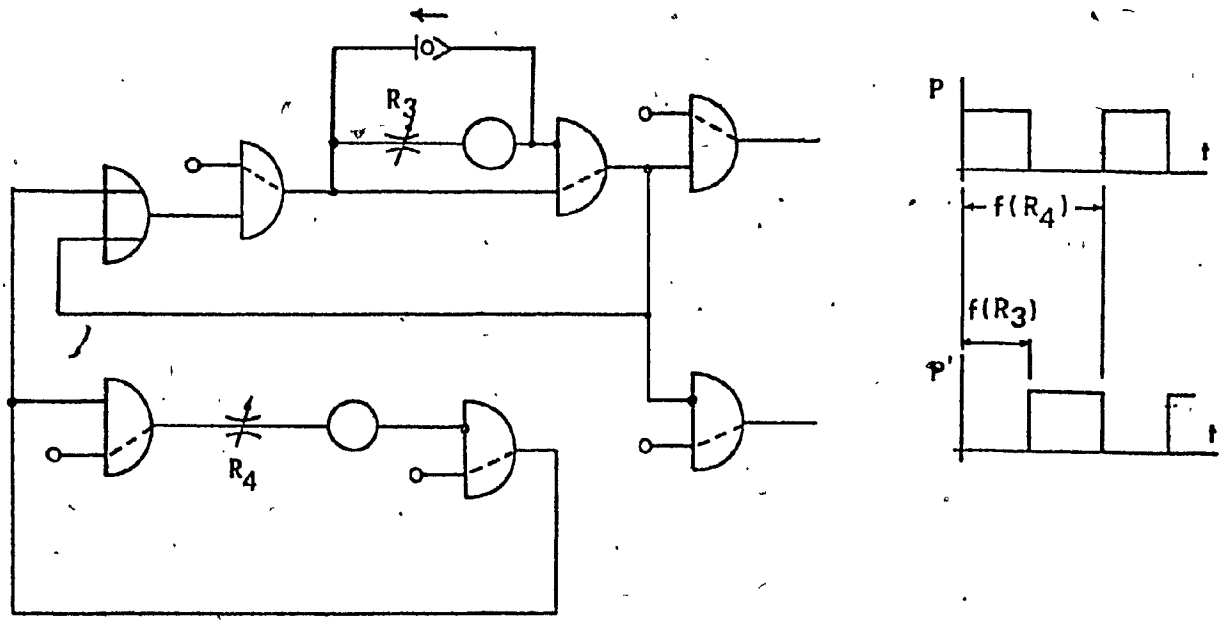

Fig. 15 - Pneumatic square-wave signal generator #2 circuit diagram.

Fig. 16 - Pneumatic square-wave signal generator #1.

FRONT VIEW

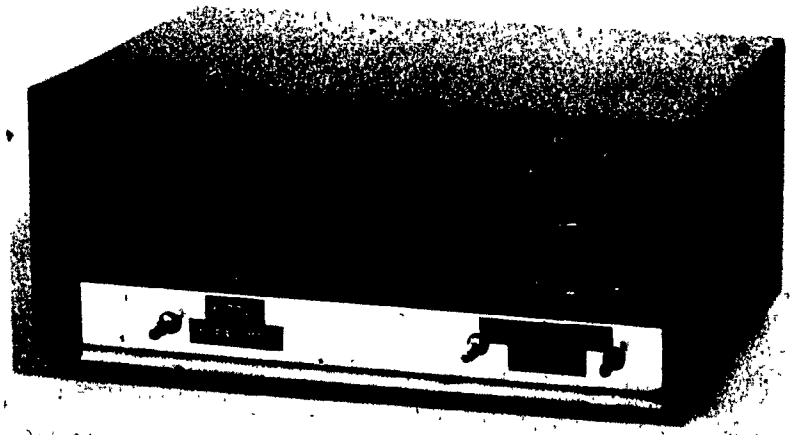

BACK VIEW

Fig. 17 - Pneumatic square-wave signal generator #2.

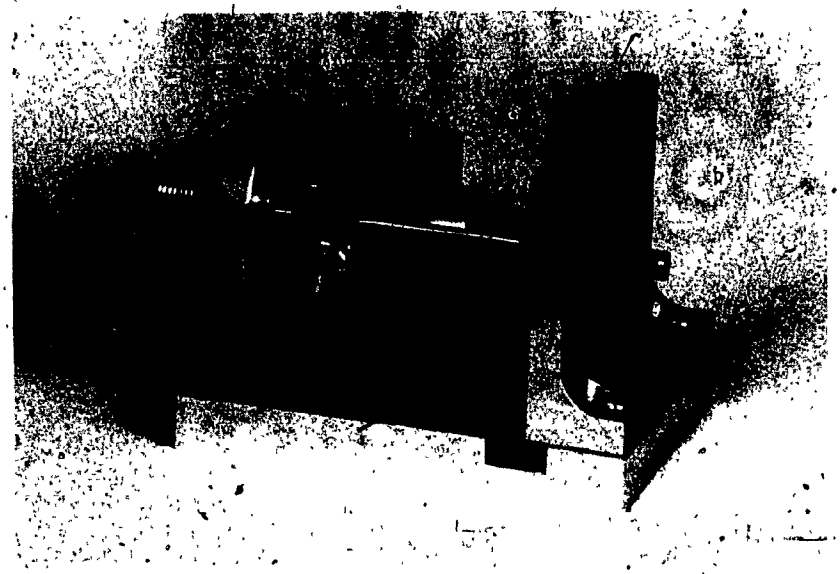

Fig. 18 - Hydraulic/pneumatic pressure transducer with ejector-sensor.

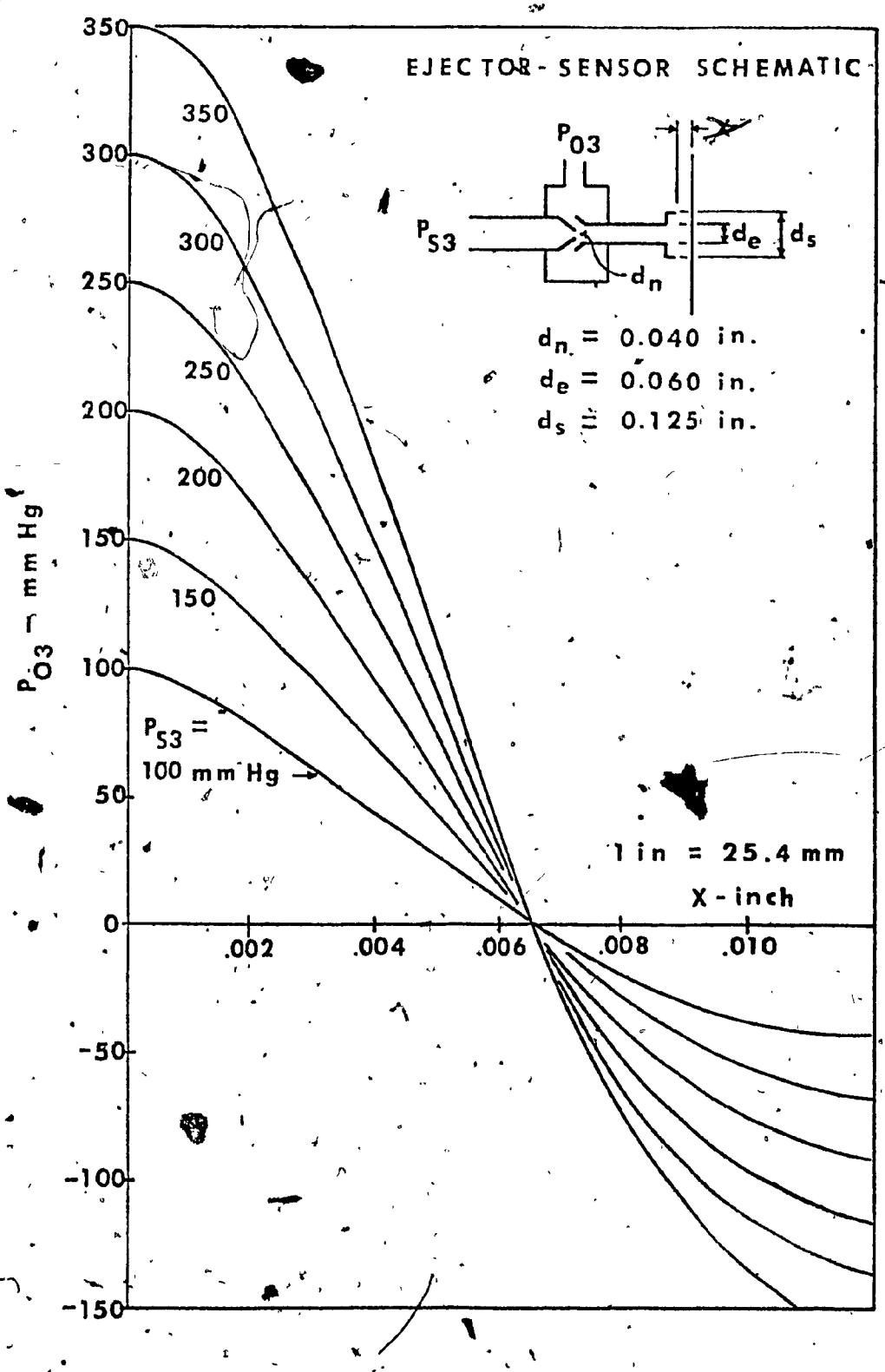

Fig. 19 - Ejector-sensor characteristics.

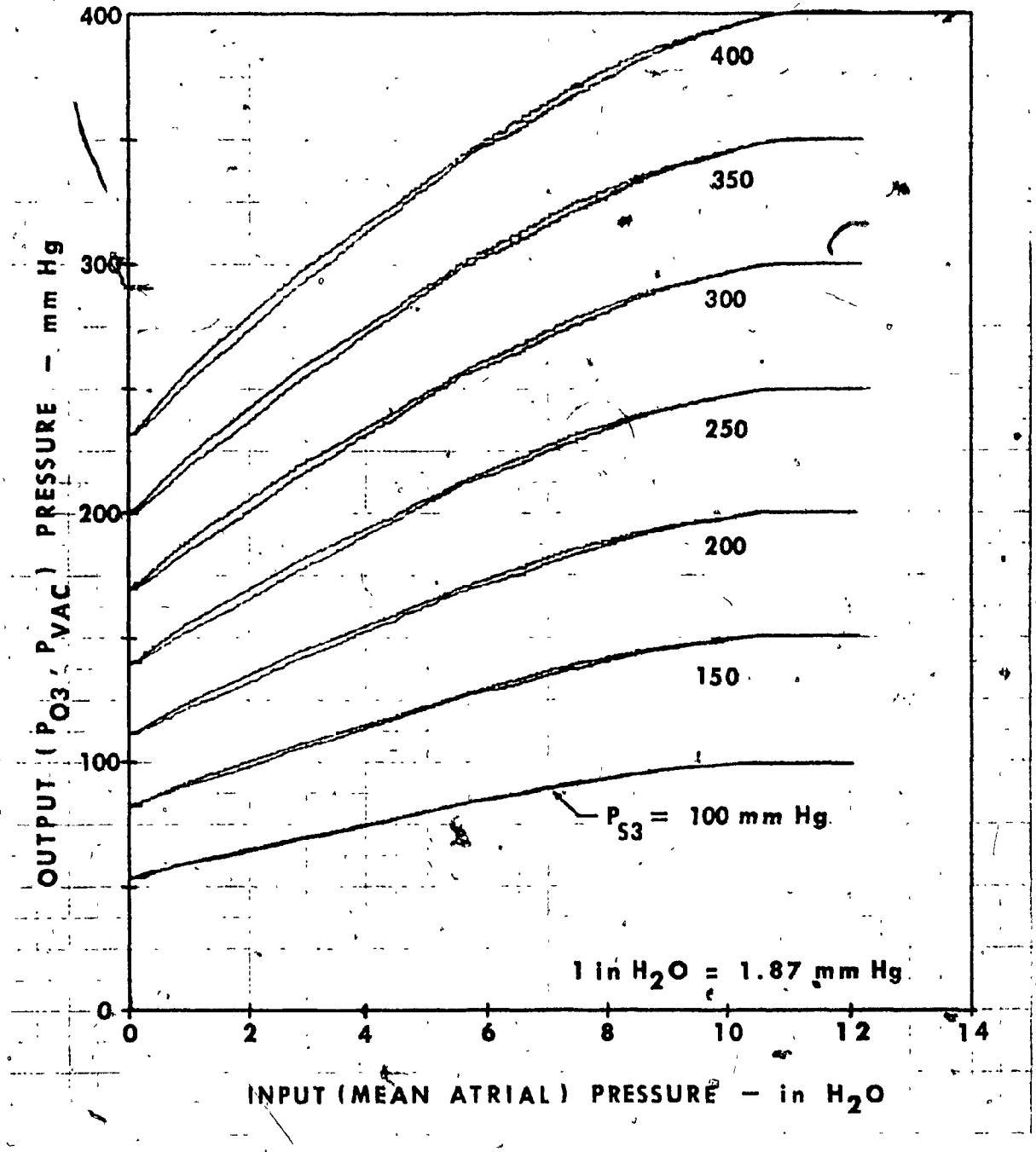

Fig. 20 - Hydraulic/Pneumatic pressure transducer (with ejector-sensor) characteristics, X_o = 0.090 mm.

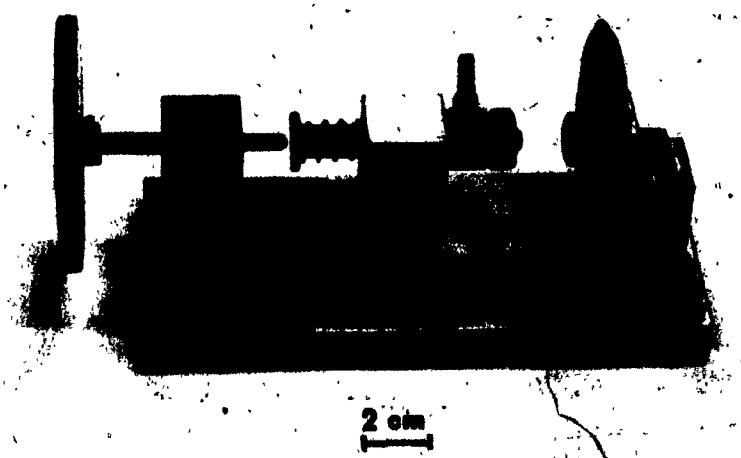

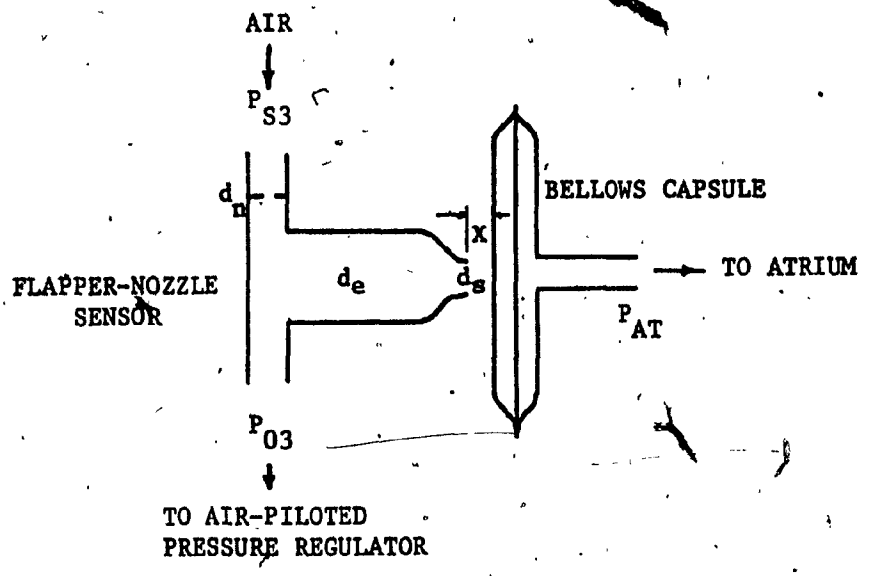

Fig. 21 - Hydraulic/pneumatic pressure transducer with flapper-nozzle sensor and its schematic diagram.

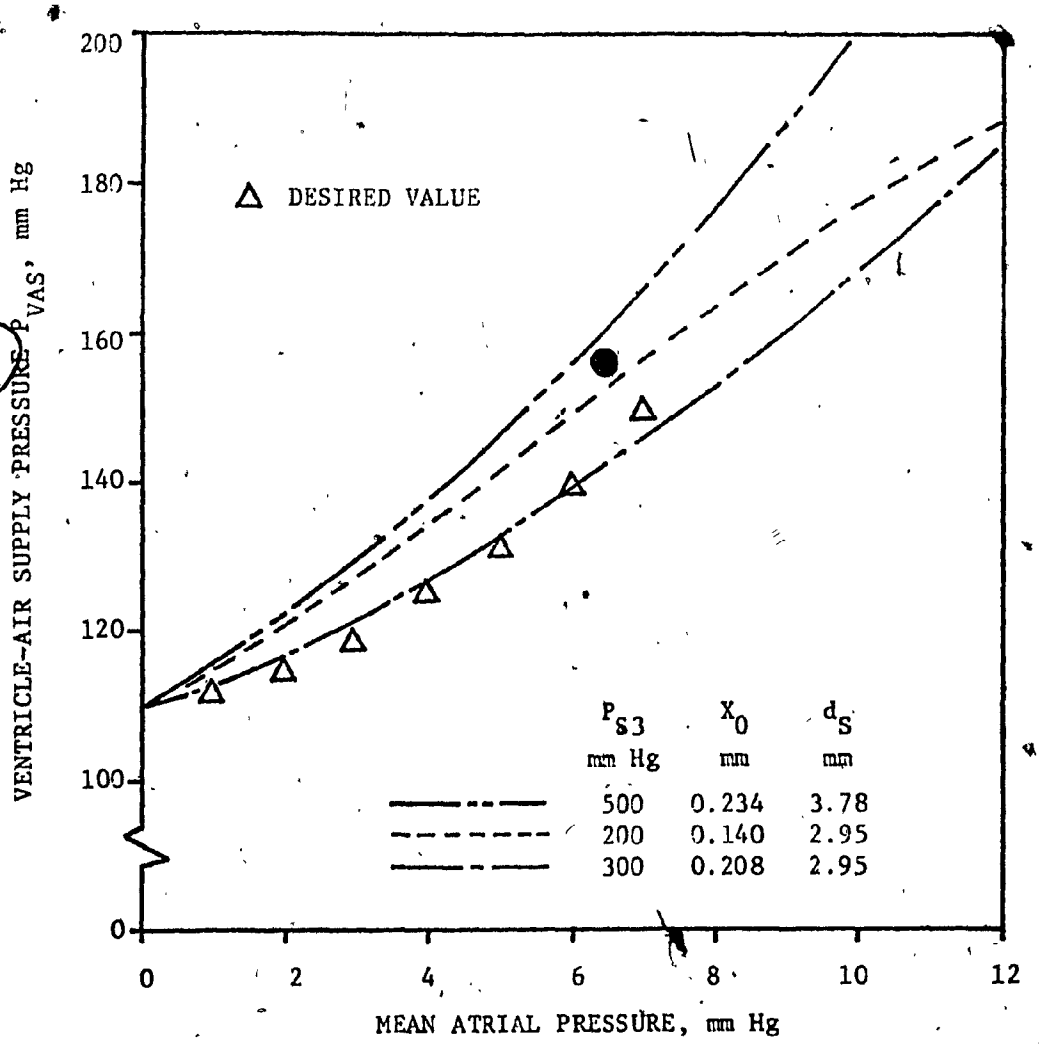

Fig. 22 - Ventricle-air supply pressure characteristics obtained from the H/P pressure transduder with the flapper-nozzle sensor.

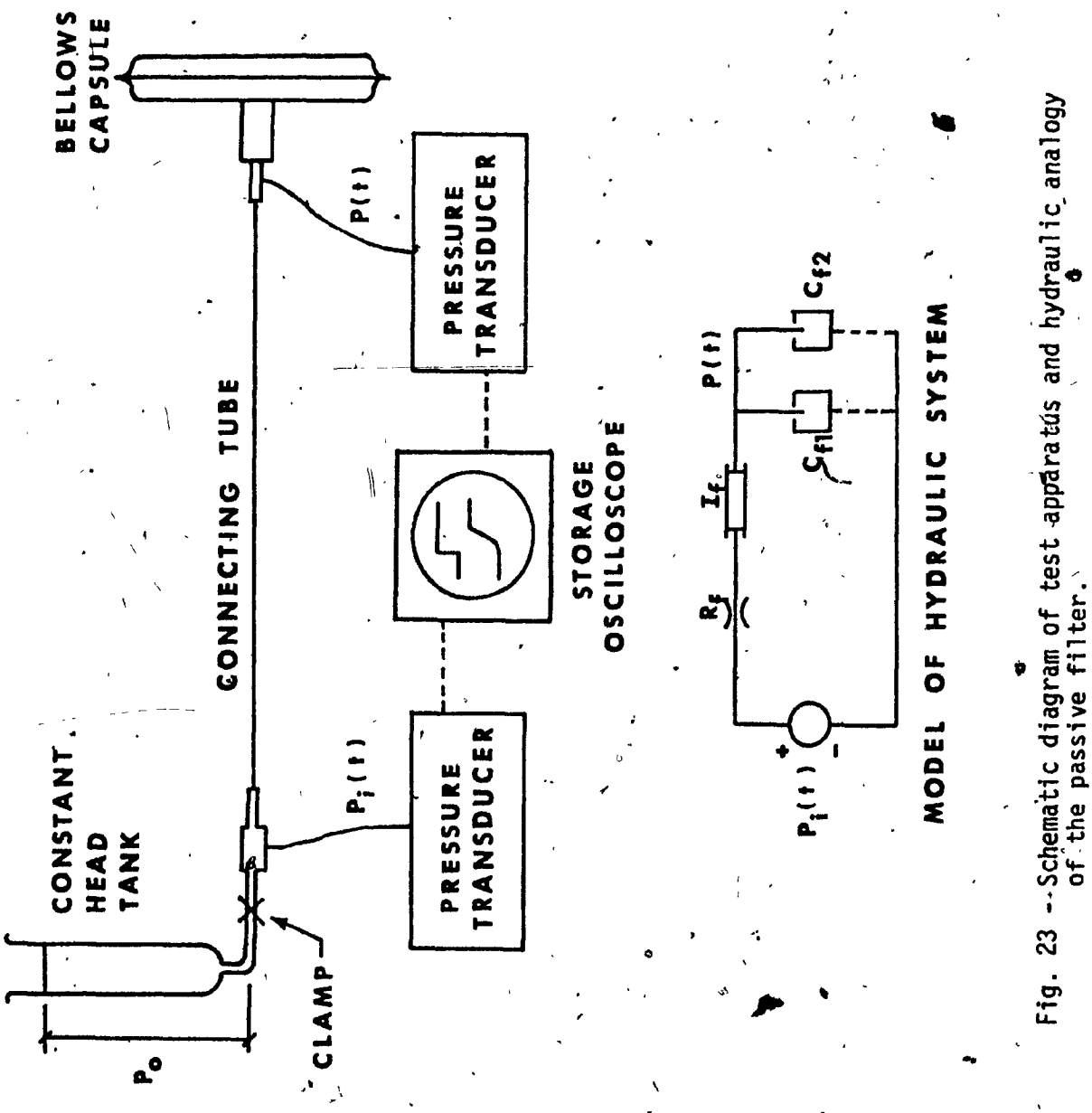

Fig. 23 -- Schematic diagram of test apparatus and hydraulic analogy of the passive filter.

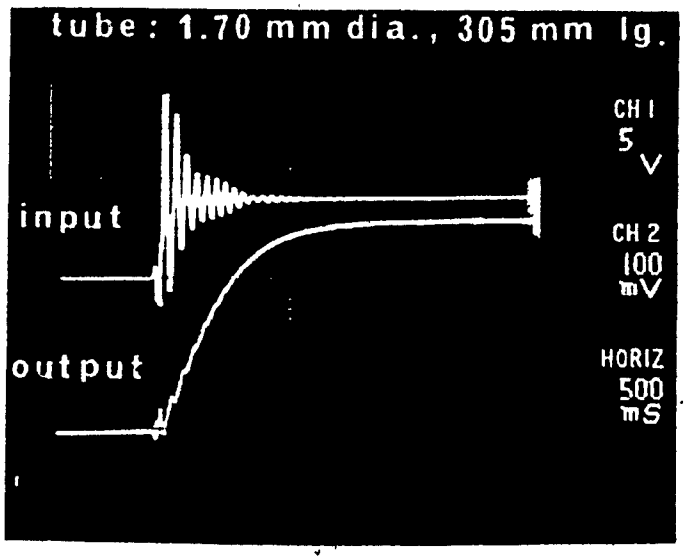

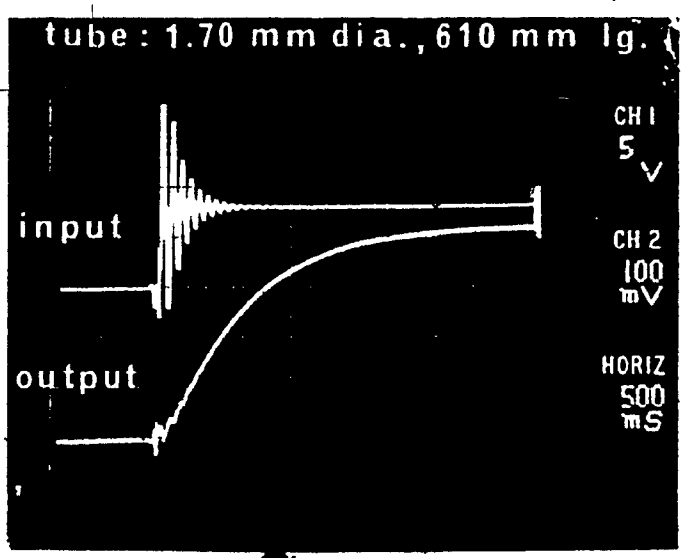

Fig. 24 - Oscilloscope traces at input and output ports of the hydraulic filter.

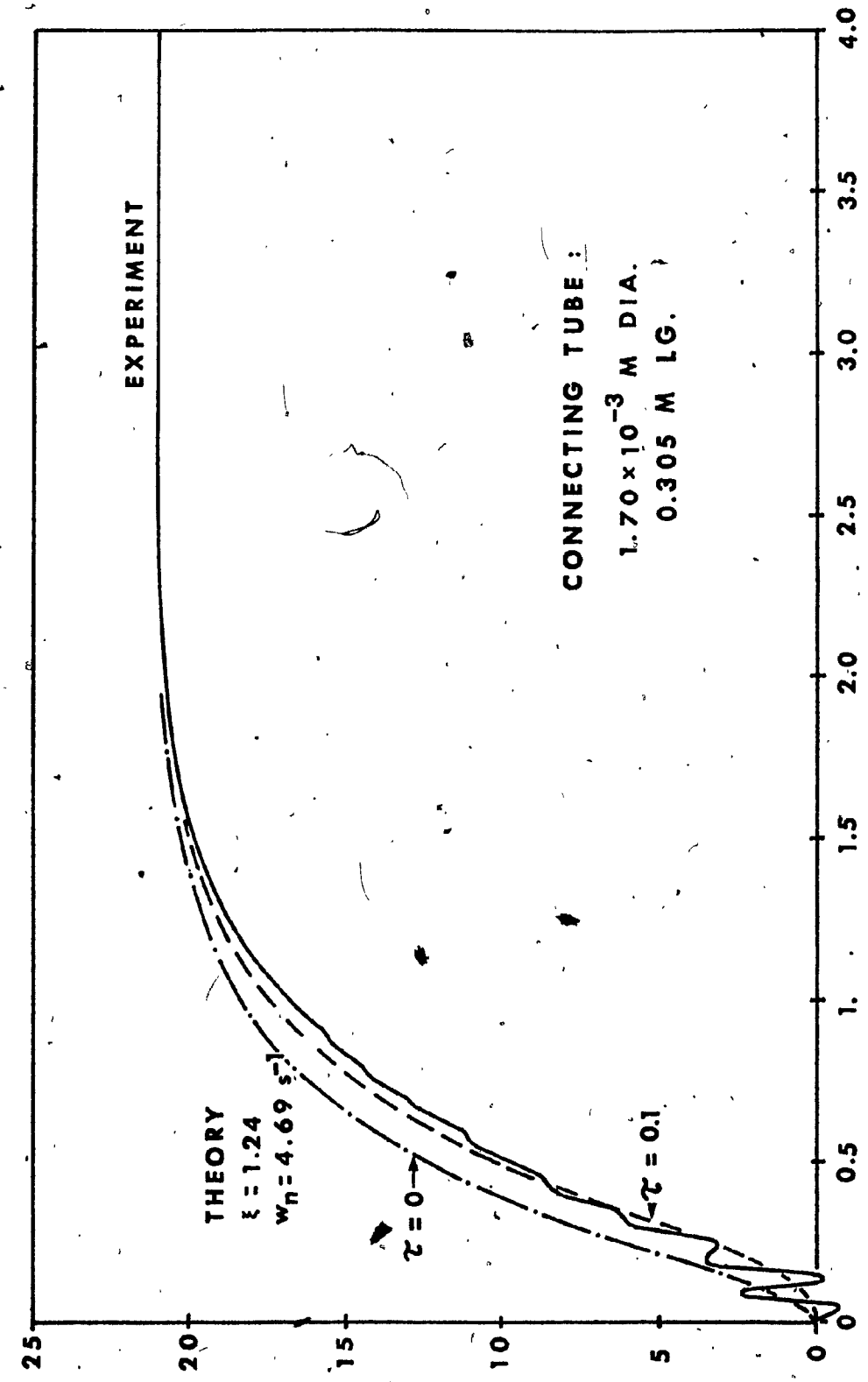

Fig. 25 - Predicted dynamic response of hydraulic filter in comparison with measurements.

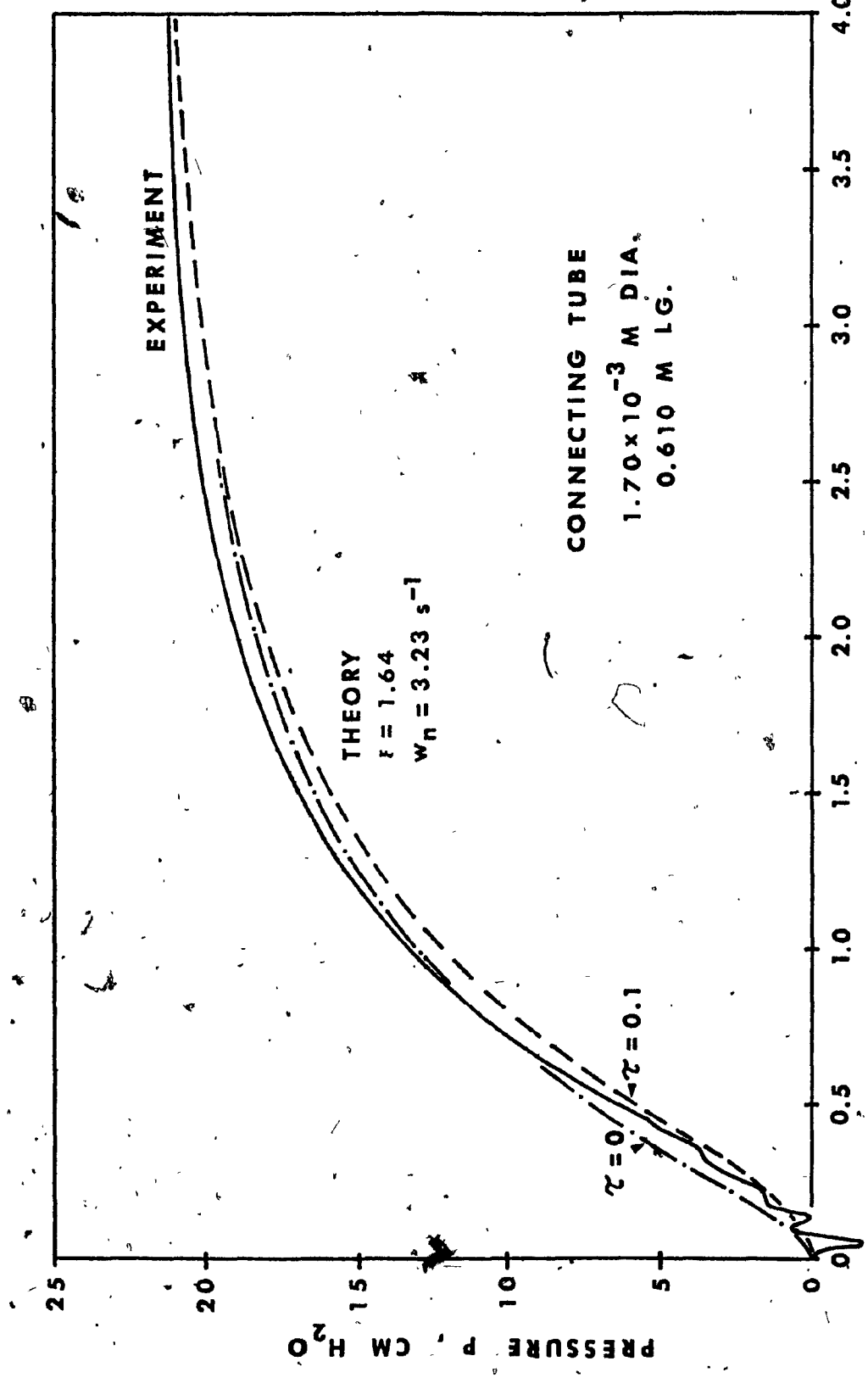

Fig. 26 - Predicted dynamic response of hydraulic filter in comparison with measurements.

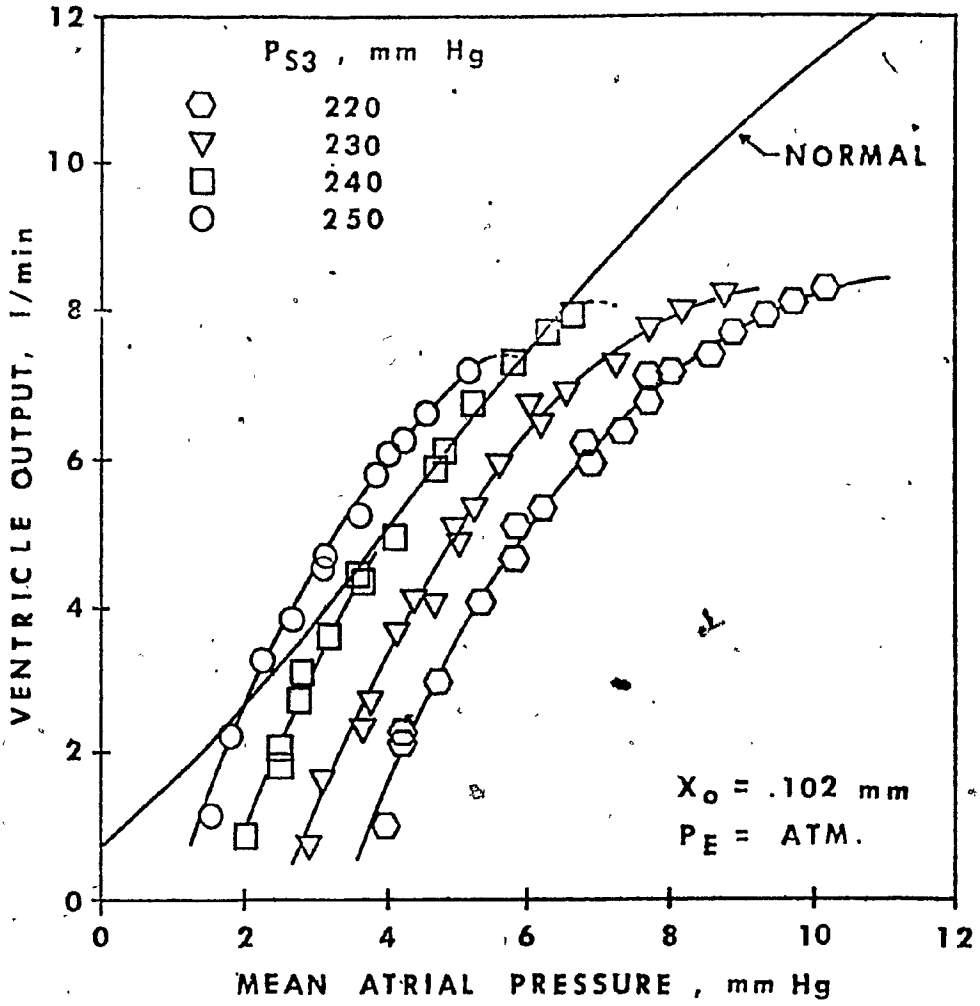

Fig. 27 - Effects of H/P transducer (with ejector-sensor) supply pressure on mean ventricle output at different mean atrial pressures, heart rate = 75 beats/min, systolic time = 0.32 sec, and mean ventricle output pressure = 100 mm Hg.

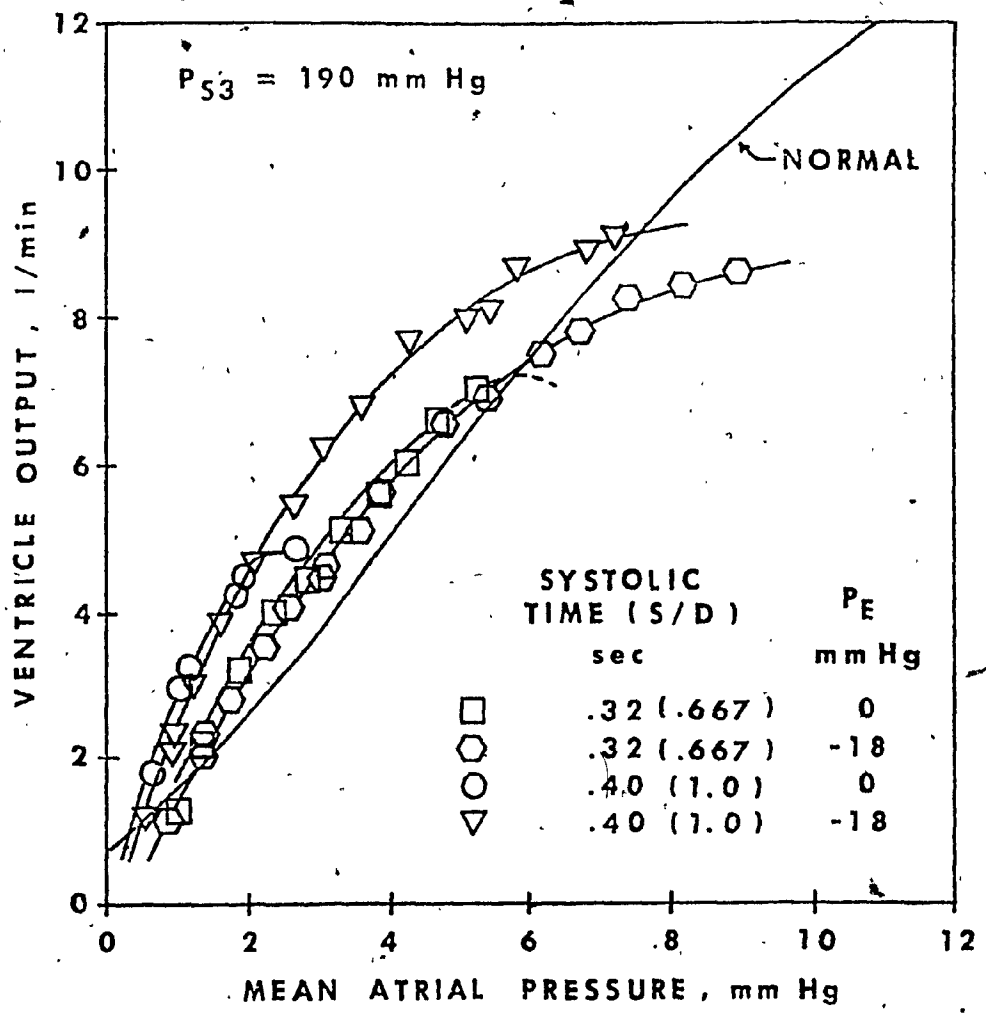

Fig. 28 - Effects of systolic time and exhaust pressure on mean ventricle output at different mean atrial pressures, heart rate = 75 beats/min, mean ventricle output pressure = 100 mm Hg, and X_o = 0.075 mm.

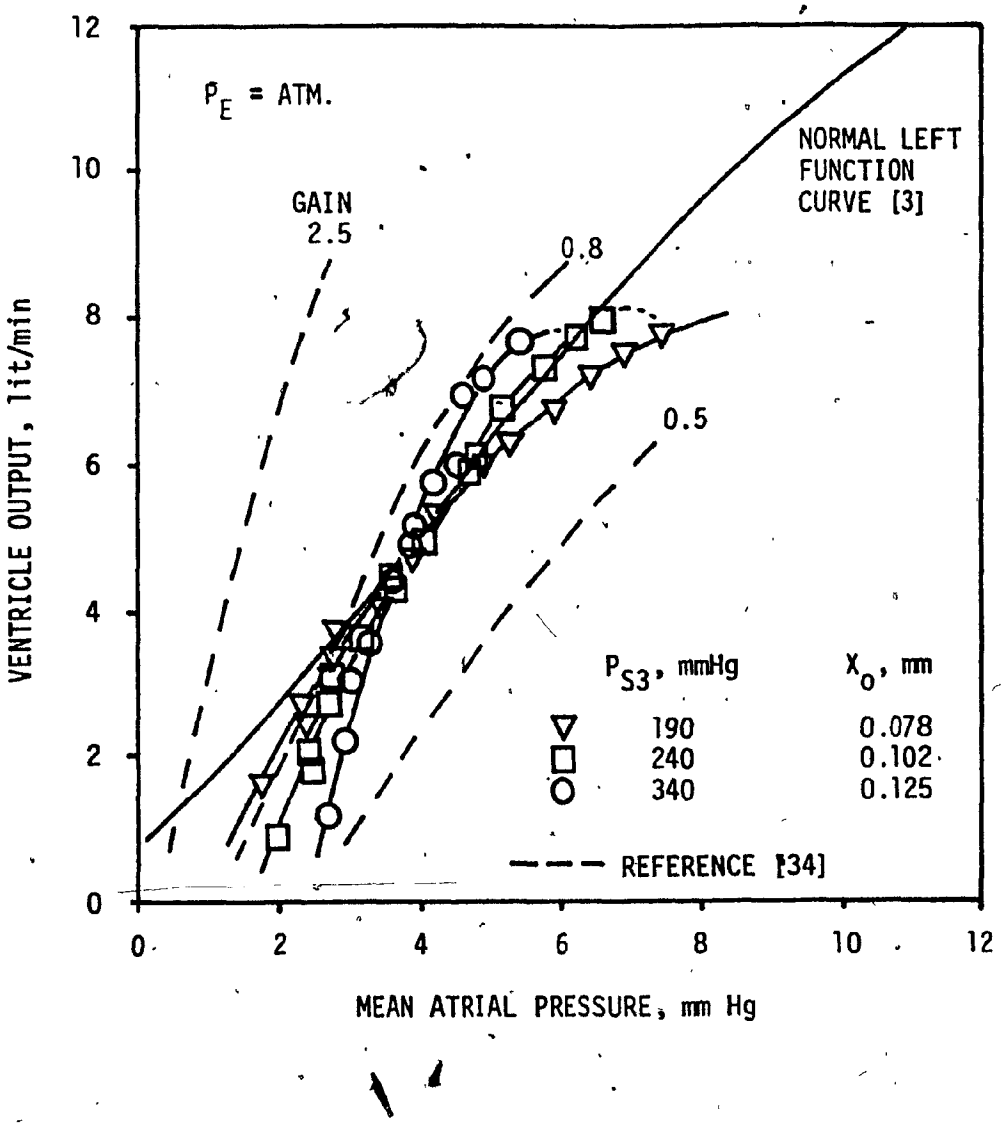

Fig. 29 - Mean ventricle output at different mean atrial pressures, heart rate = 75 beats/min, systolic time = 0.32 sec, and mean ventricle output pressure = 100 mm Hg (with the ejector-sensor H/P pressure transducer).

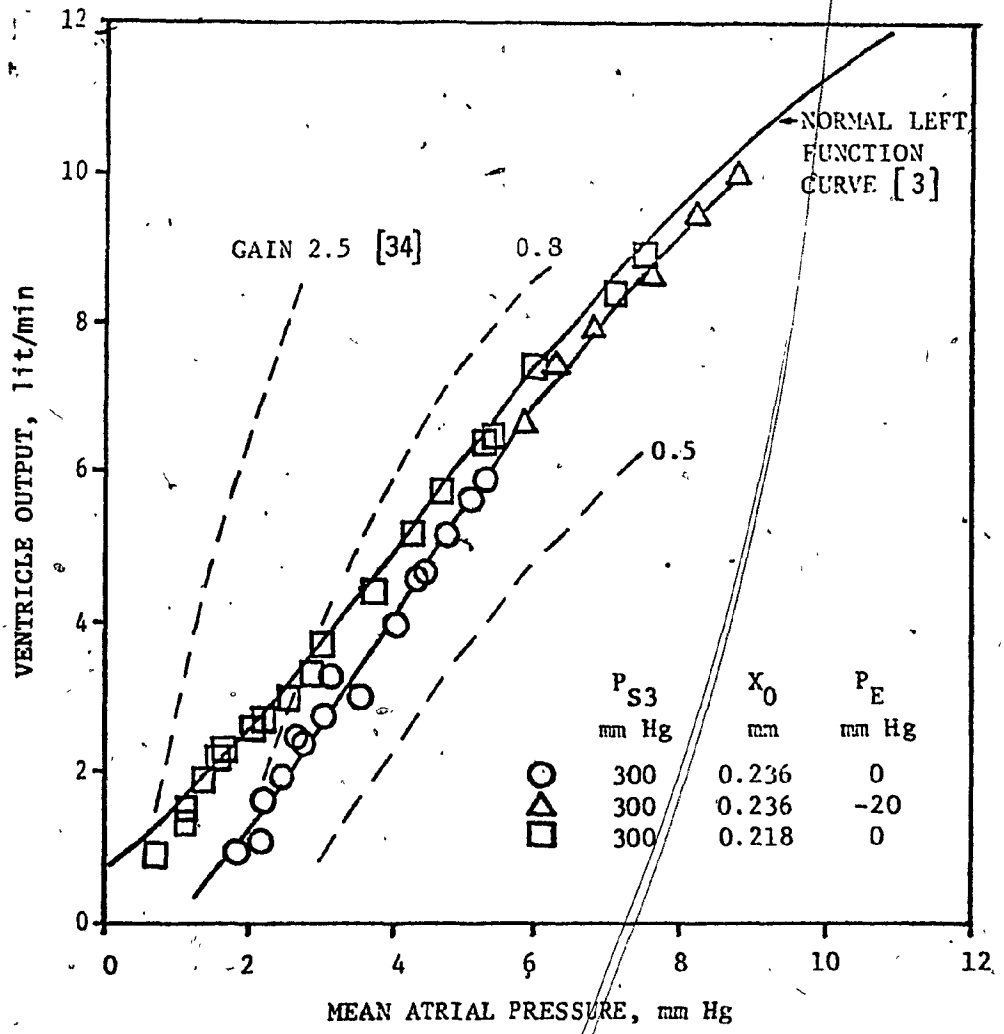

Fig. 30 - Mean ventricle output at different mean atrial pressure, heart rate = 75 beats/min, systolic time = 0.32 sec, and mean ventricle output pressure = 100 mm Hg (with the flapper-nozzle sensor H/P pressure transducer, d_s = 2.95 mm).

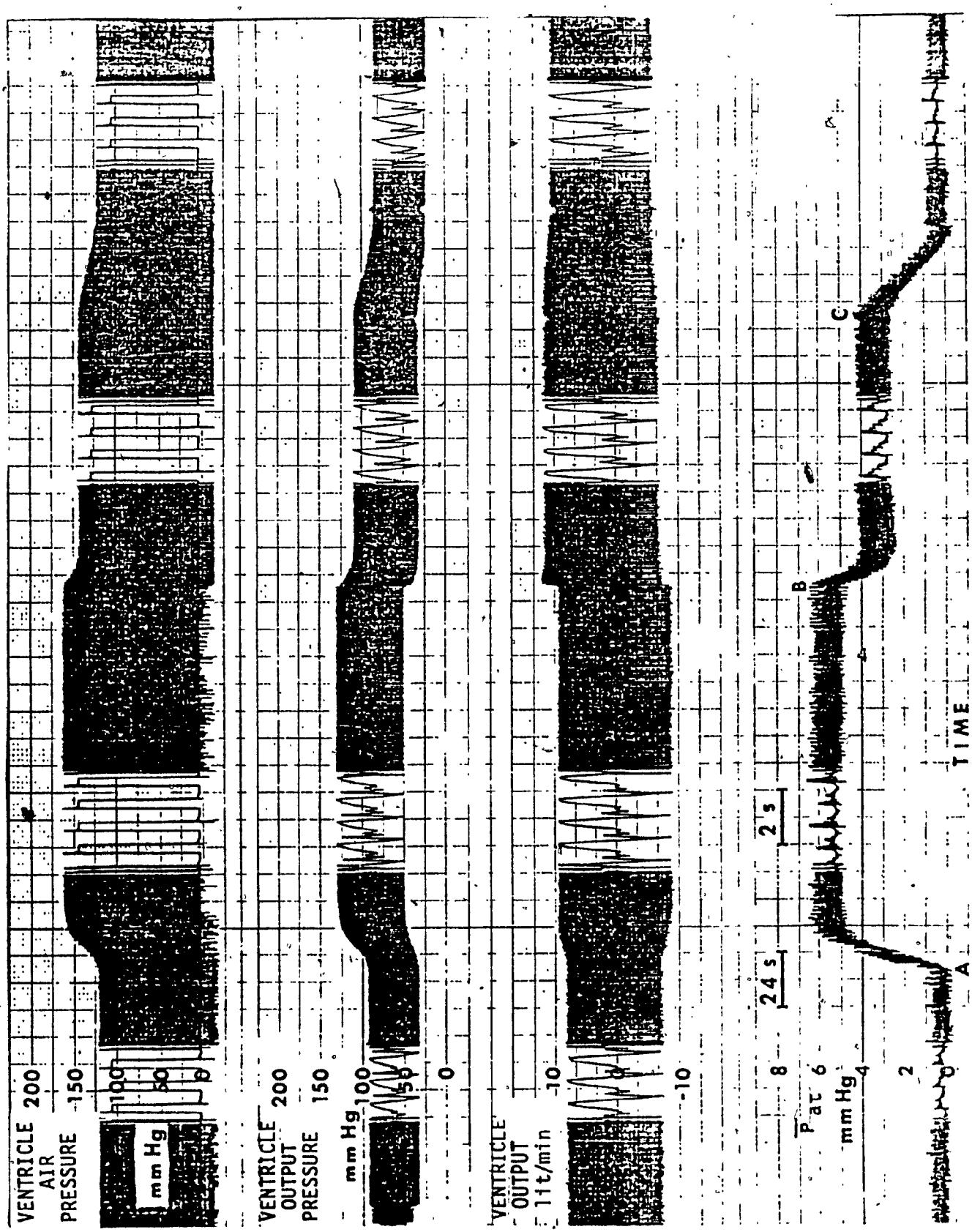

Fig. 31 - Typical dynamic response of the all-pneumatic driving system.

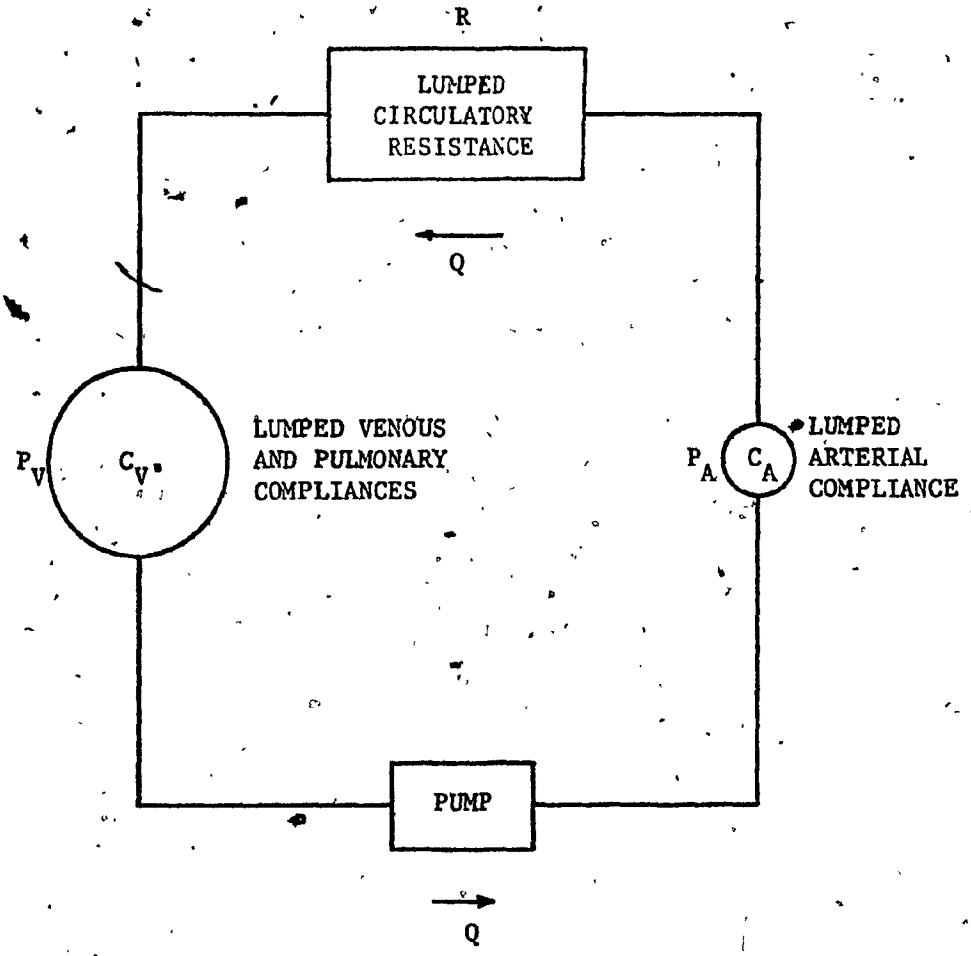

Fig. 32 - Simple model of the cardiovascular system.

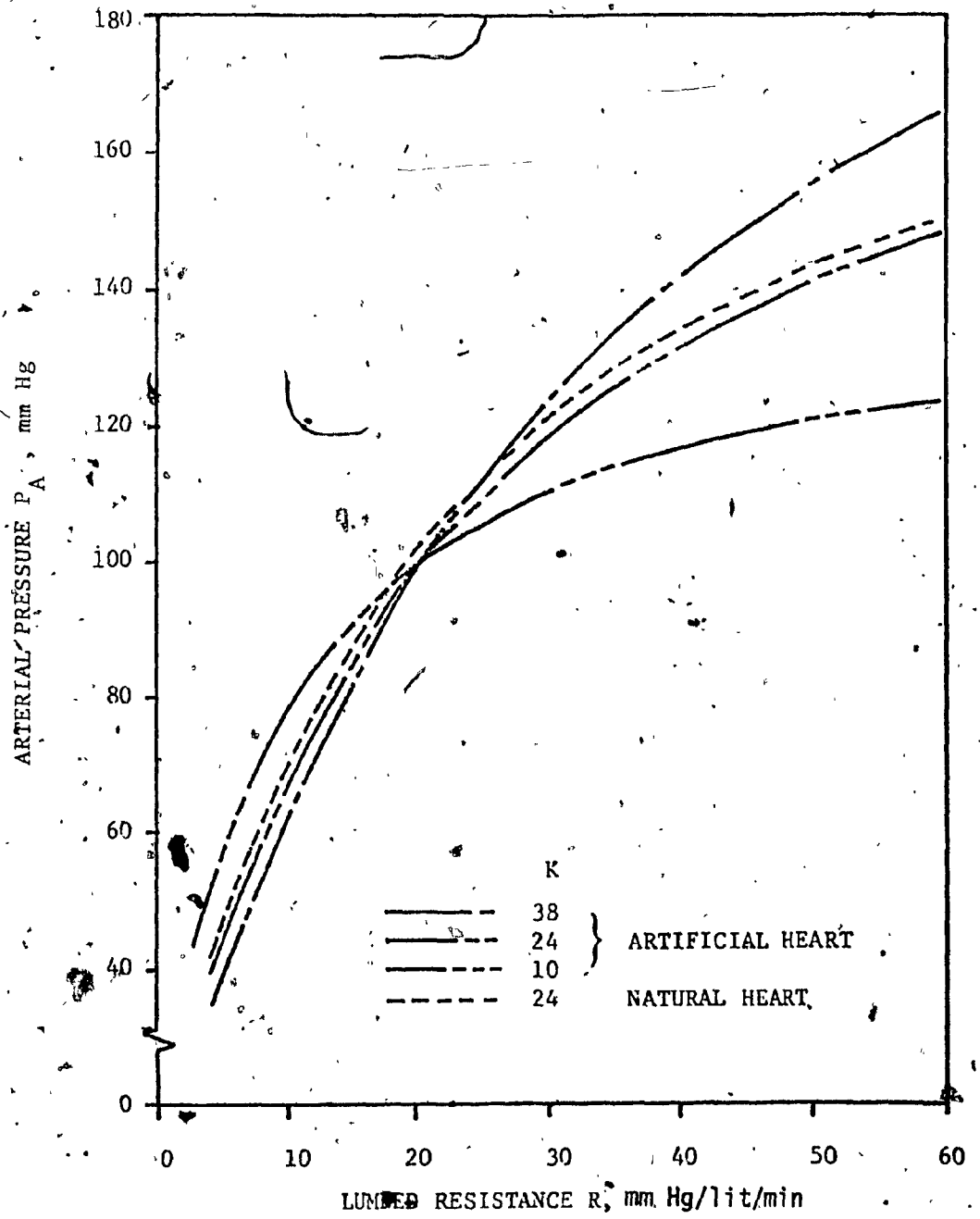

Fig. 33 - Effects of compliance ratio (K) on arterial pressure (P_A) as lumped resistance (R) is varied.

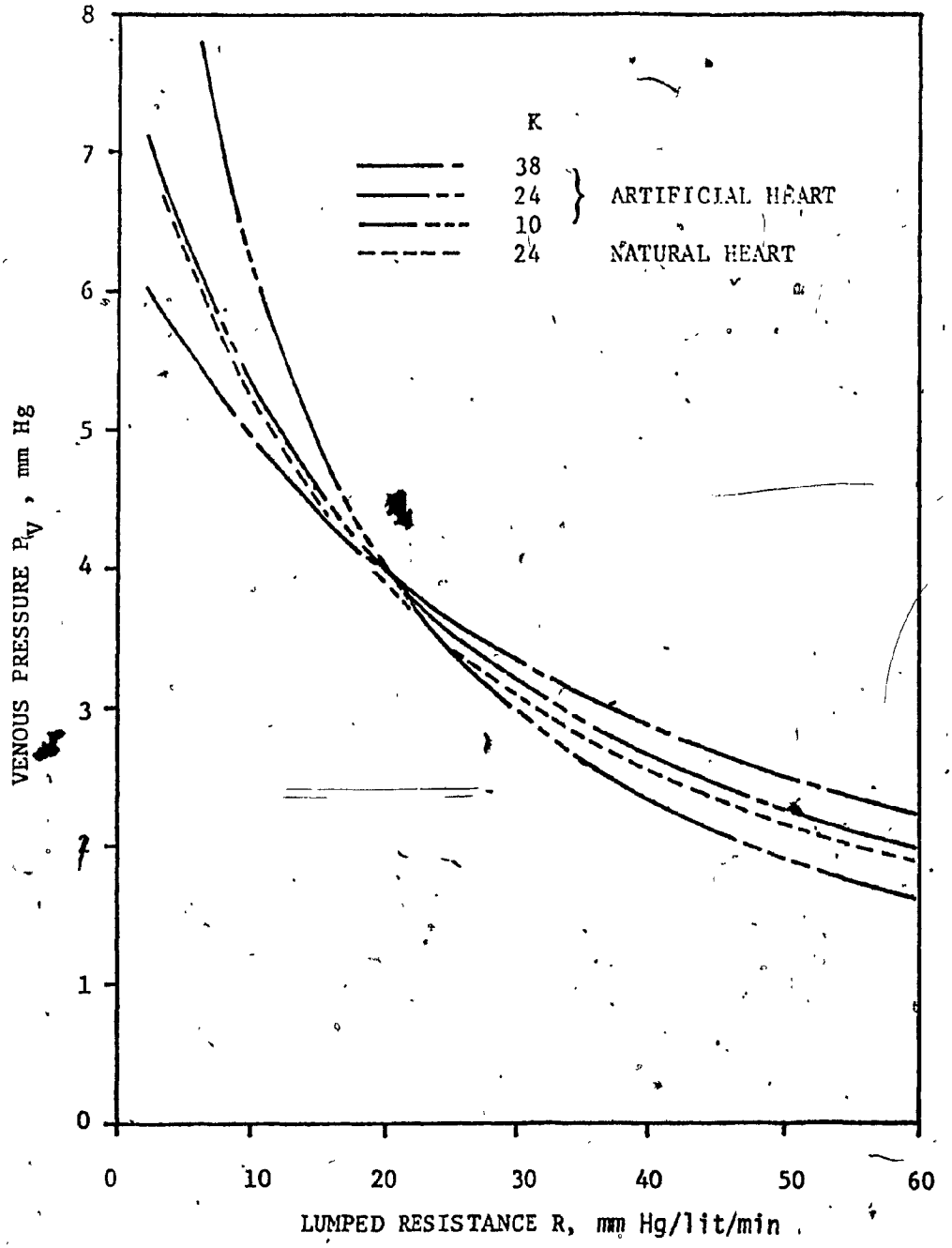

Fig. 34 - Effects of compliance ratio (K) on venous pressure (P_V) as lumped resistance (R) is varied.

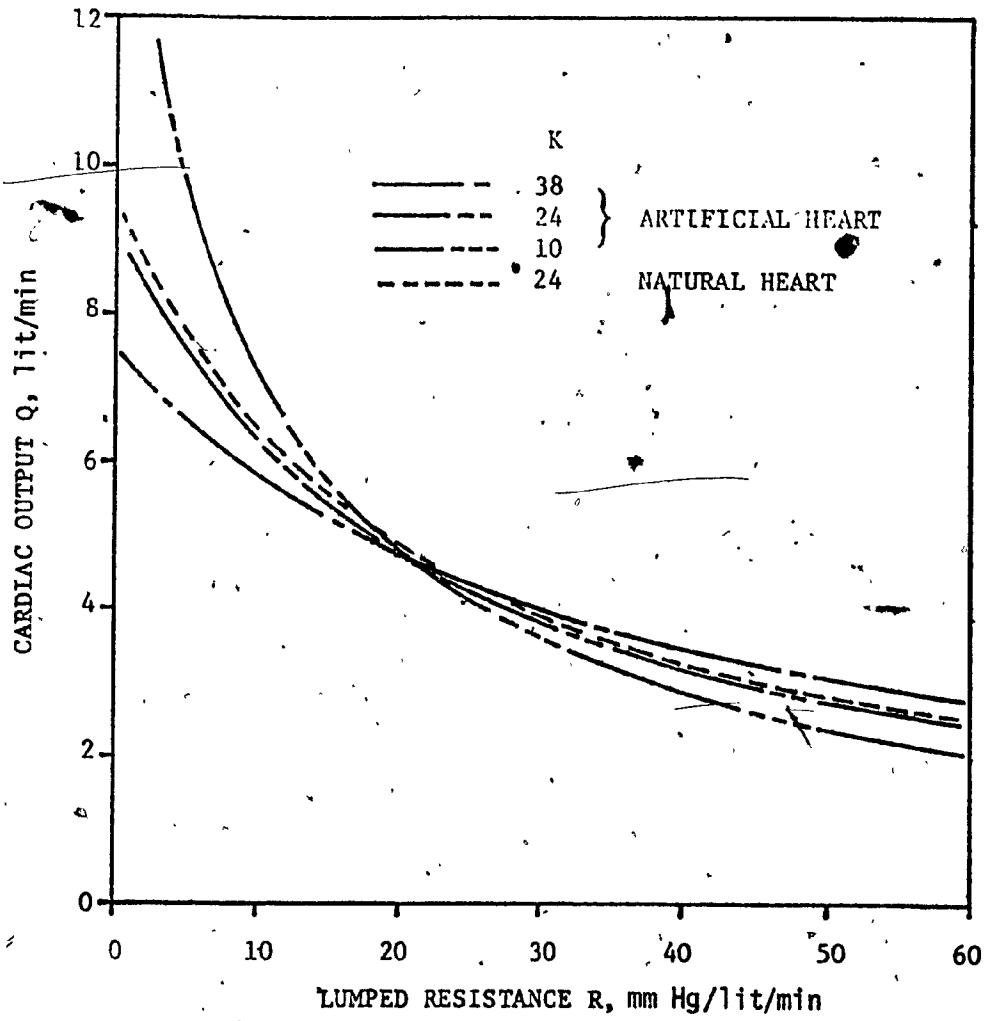

Fig. 35 - Effects of compliance ratio (K) on cardiac output (Q) as lumped resistance (R) is varied.

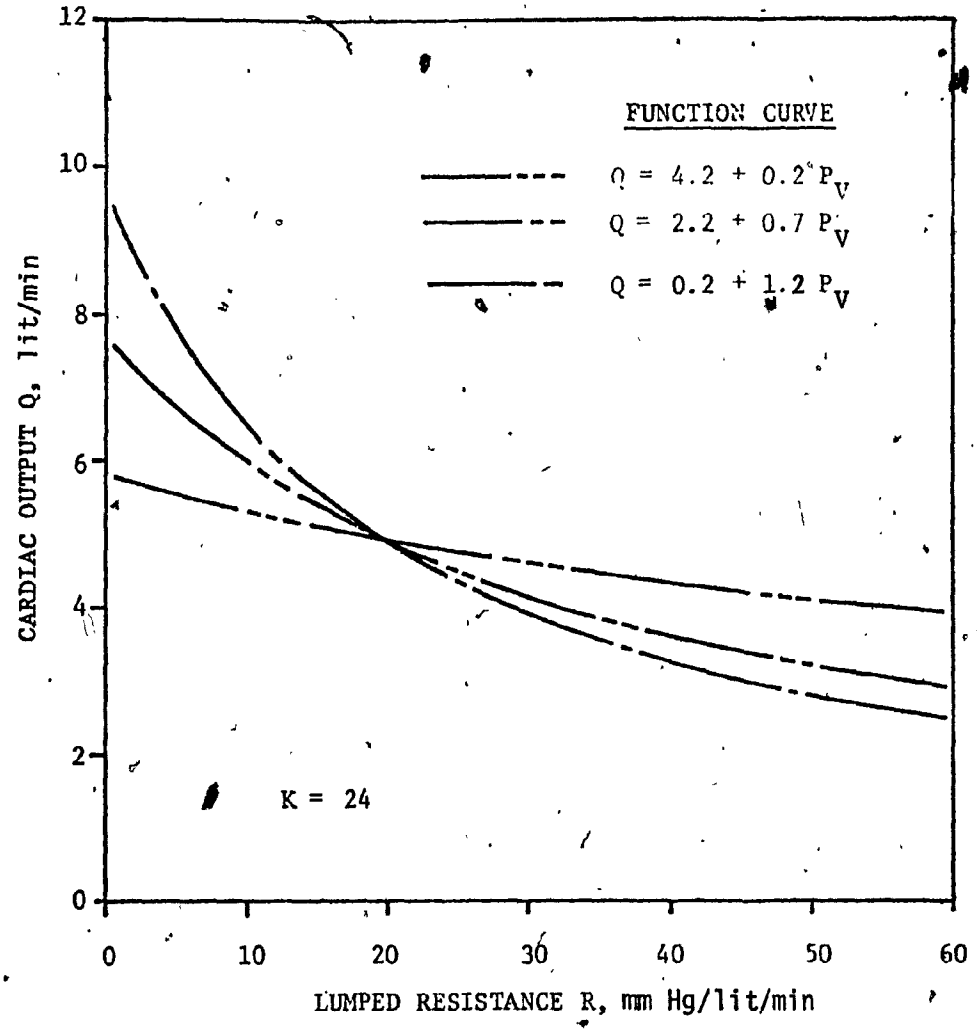

Fig. 36 - Effects of artificial heart sensitivity (K) on cardiac output (Q) as lumped resistance (R) is varied.

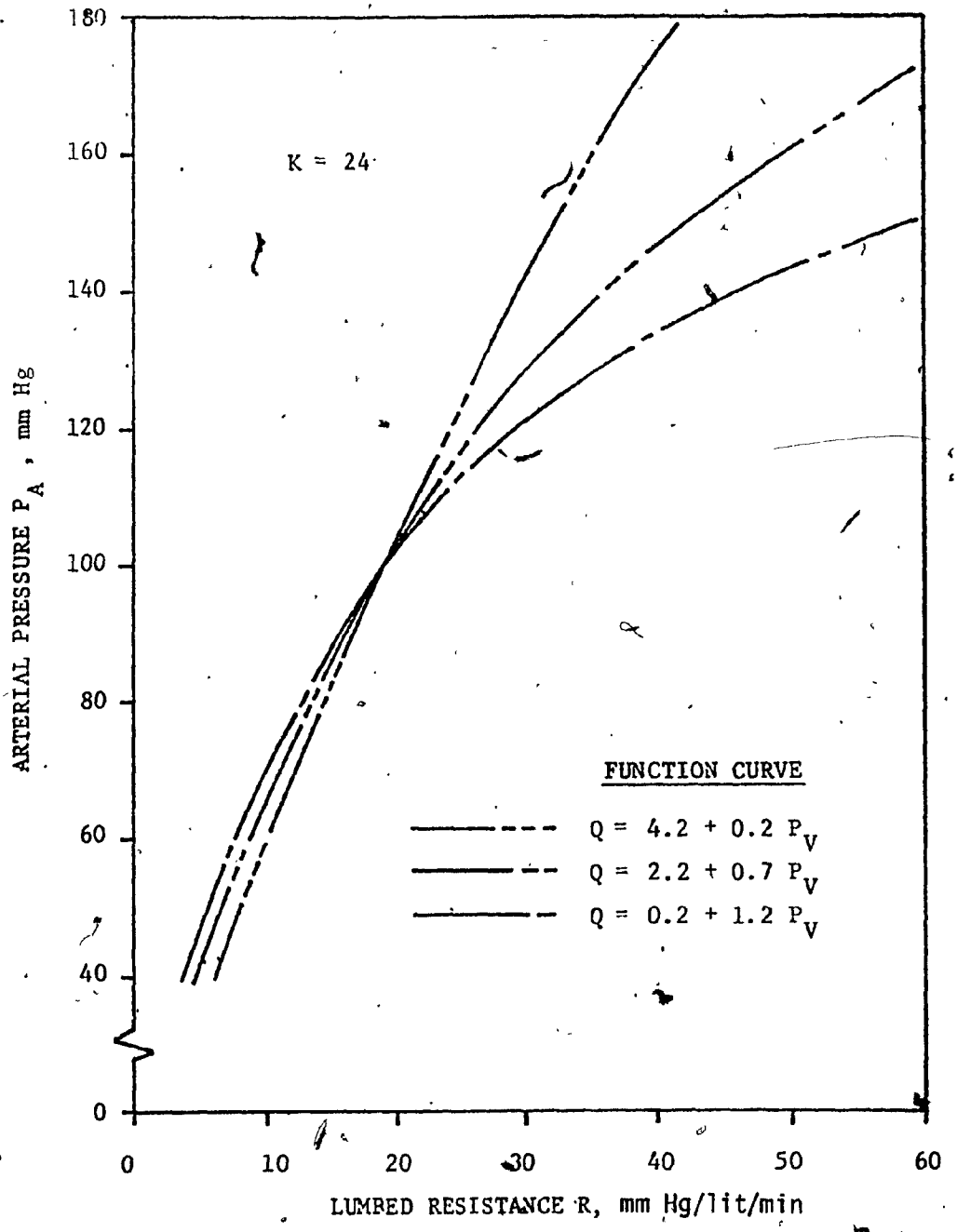

Fig. 37 - Effects of artificial heart sensitivity (B) on arterial pressure (P_A) as lumped resistance (R) is varied.

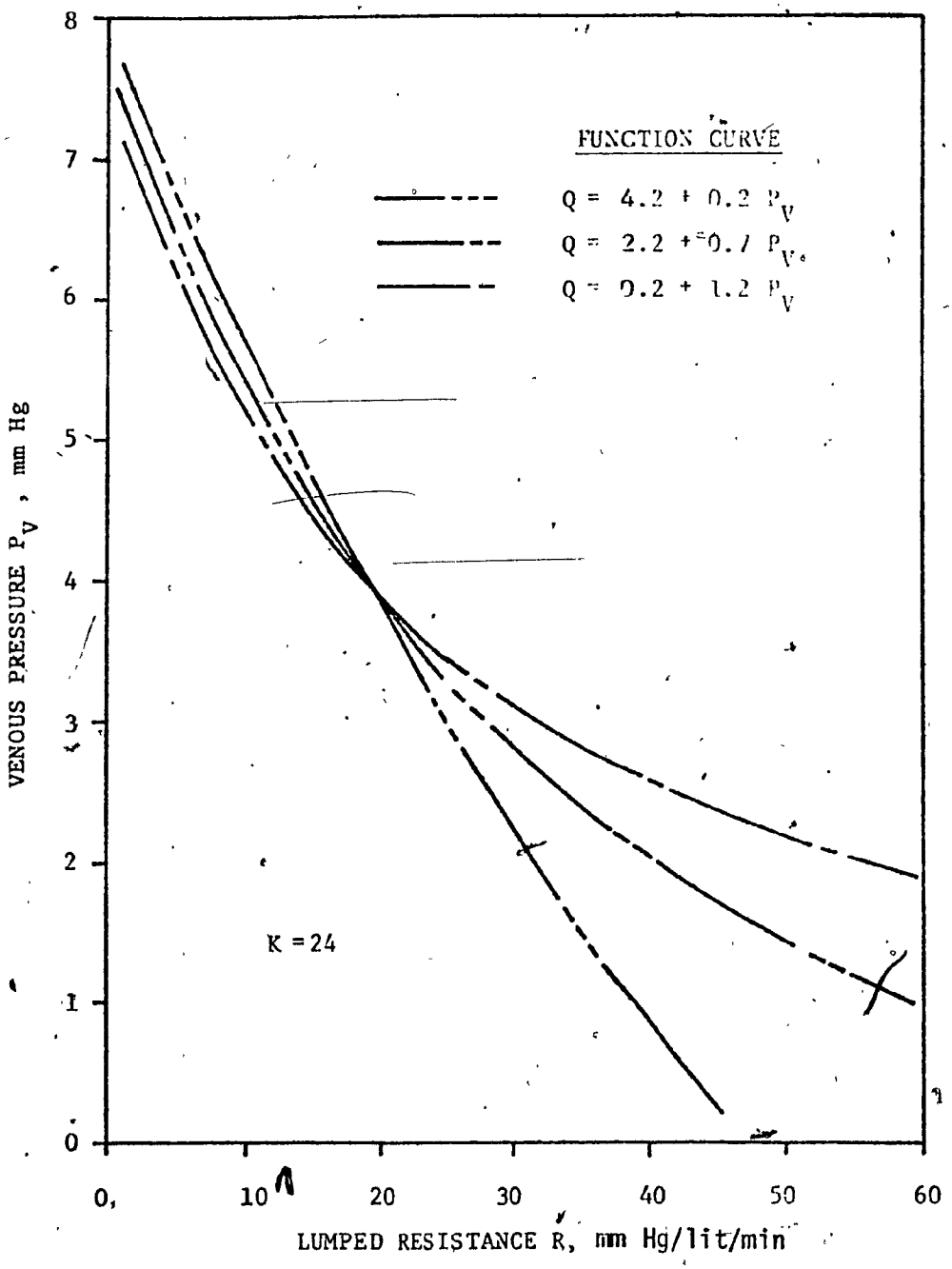

Fig. 38 - Effects of artificial heart sensitivity (B) on venous pressure (P_V) as lumped resistance (R) is varied.

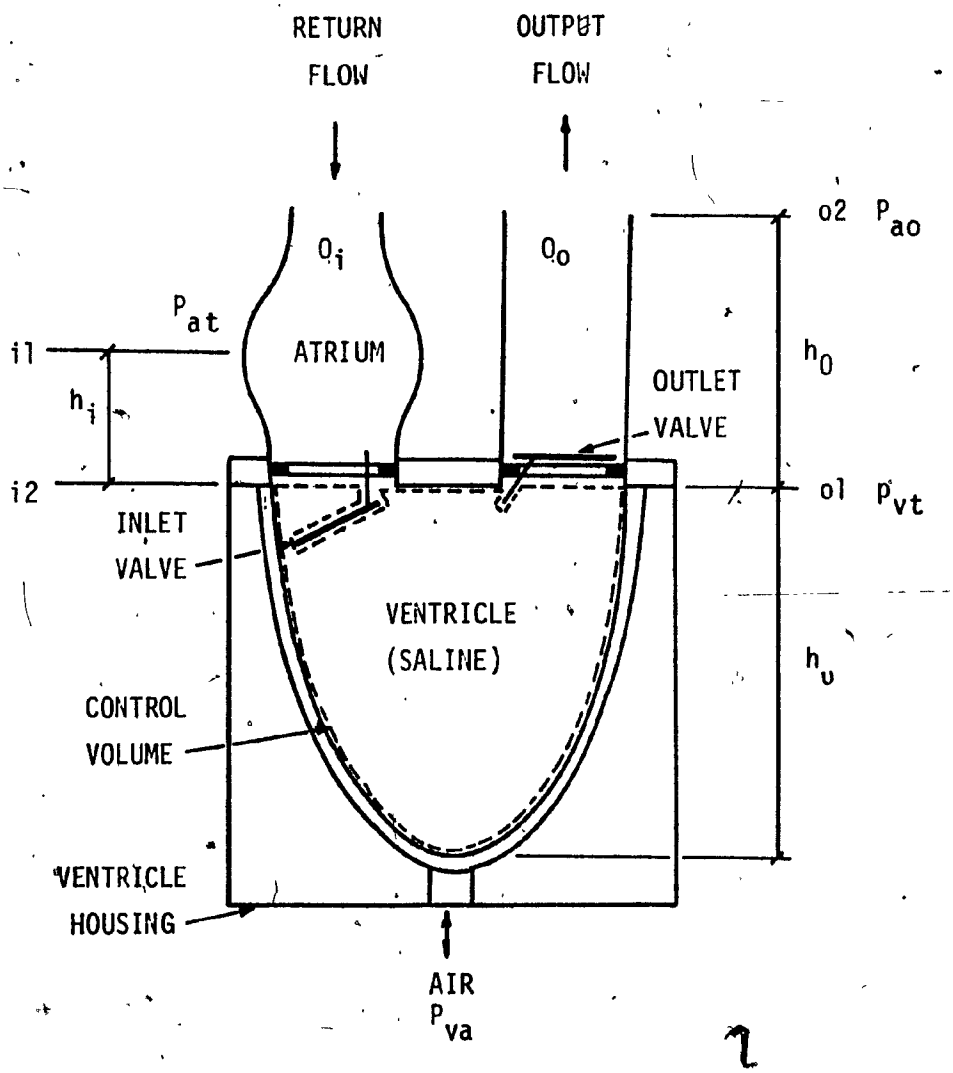

Fig. 39 - Artificial ventricle assembly.

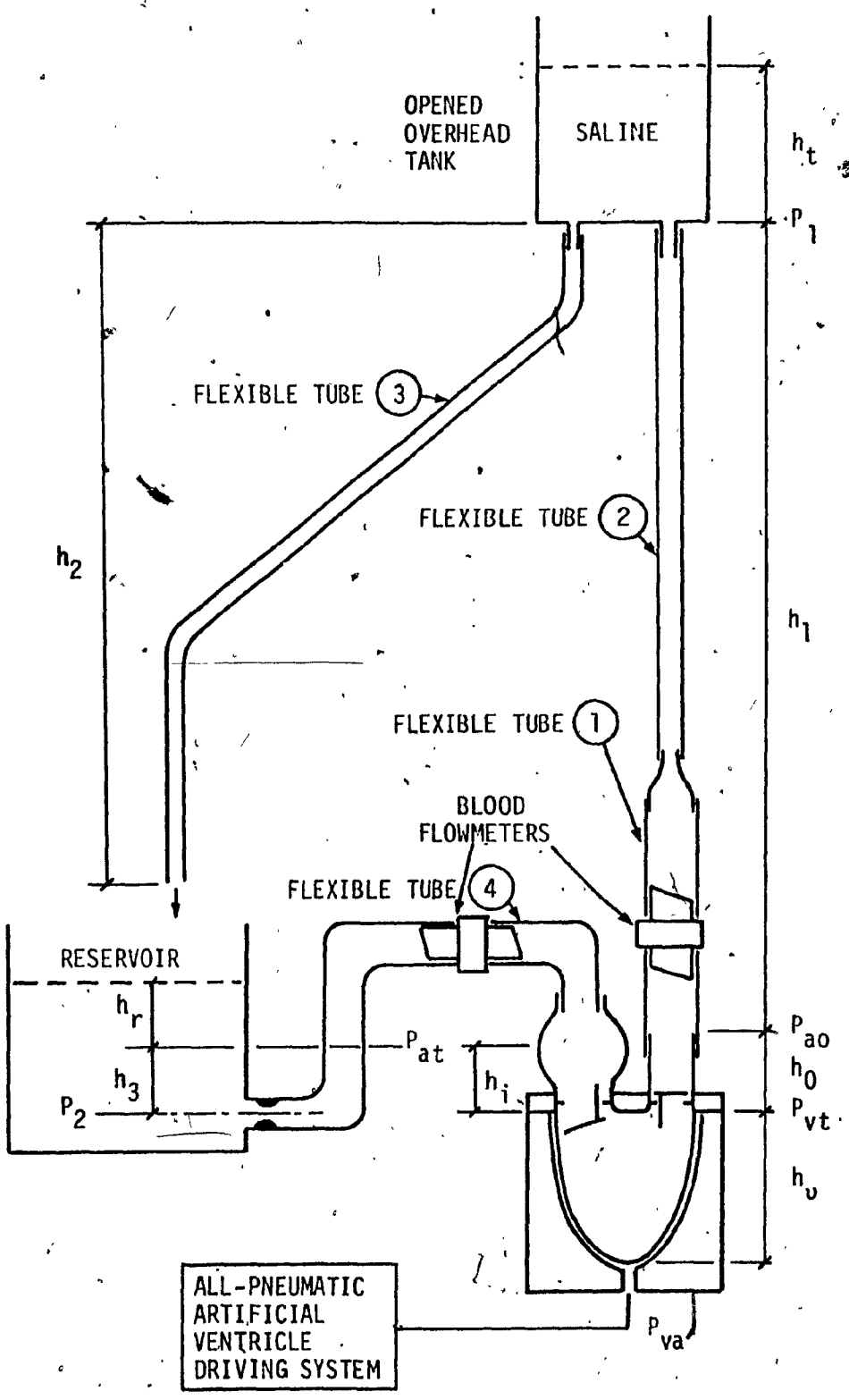

Fig. 40 - Schematic diagram of an artificial ventricle in mock circulation.

Fig. 41 - New artificial ventricle assembly with an air piloted diaphragm exhaust valve.

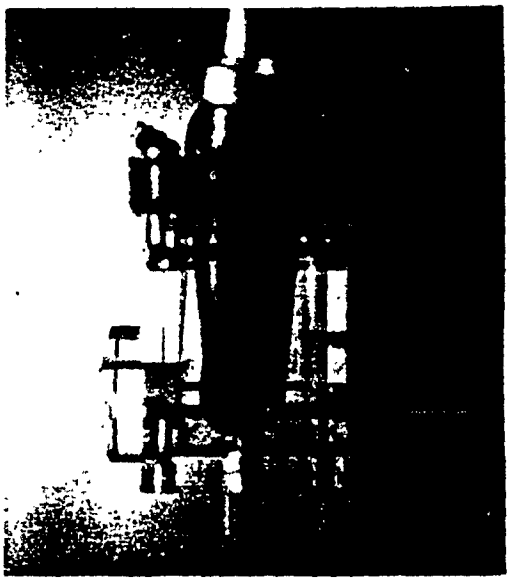

$P_\sigma = 0.24\ kN/m^2$, $V_\upsilon = 135\ ml$

$P_\sigma = 2.22\ kN/m^2$, $V_\upsilon = 8\ ml$

INCREASING PRESSURE

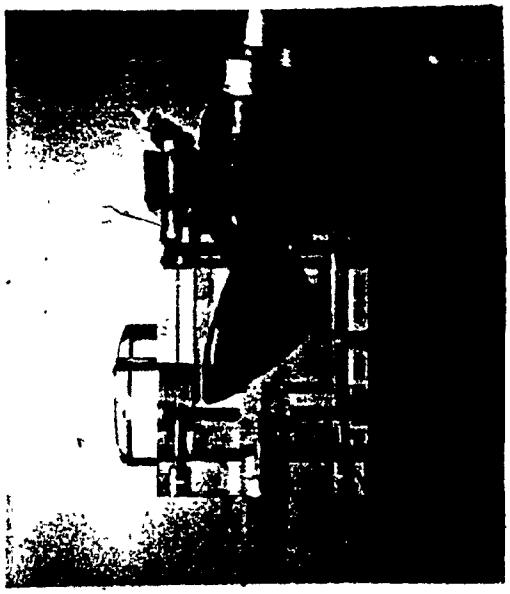

$P_\sigma = 0.37\ kN/m^2$, $V_\upsilon = 26\ ml$

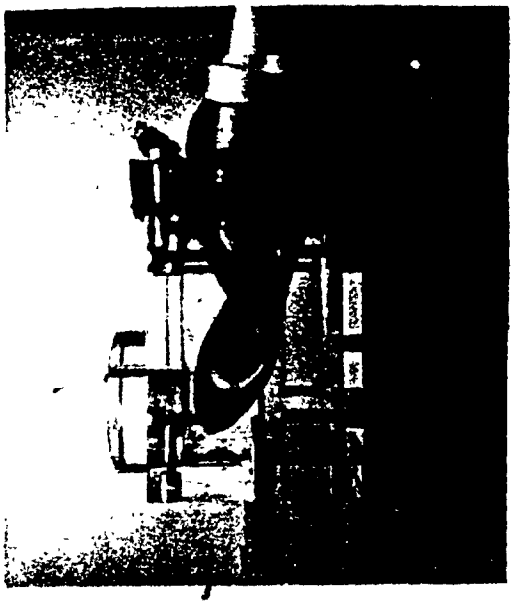

$P_\sigma = 0.24\ kN/m^2$, $V_\upsilon = 53\ ml$

DECREASING PRESSURE

Fig. 42 - Typical photographs of ventricle at different states of pressure equilibrium.

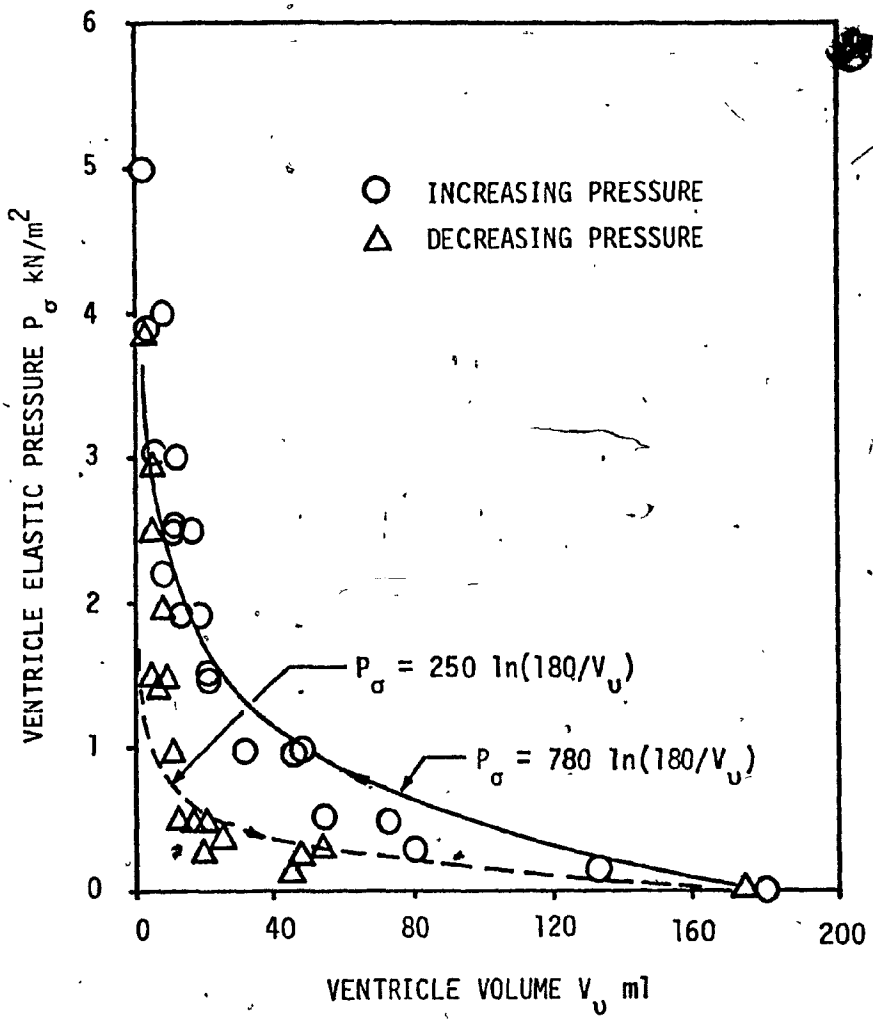

Fig. 43 - Ventricle elastic pressure-volume characteristics.

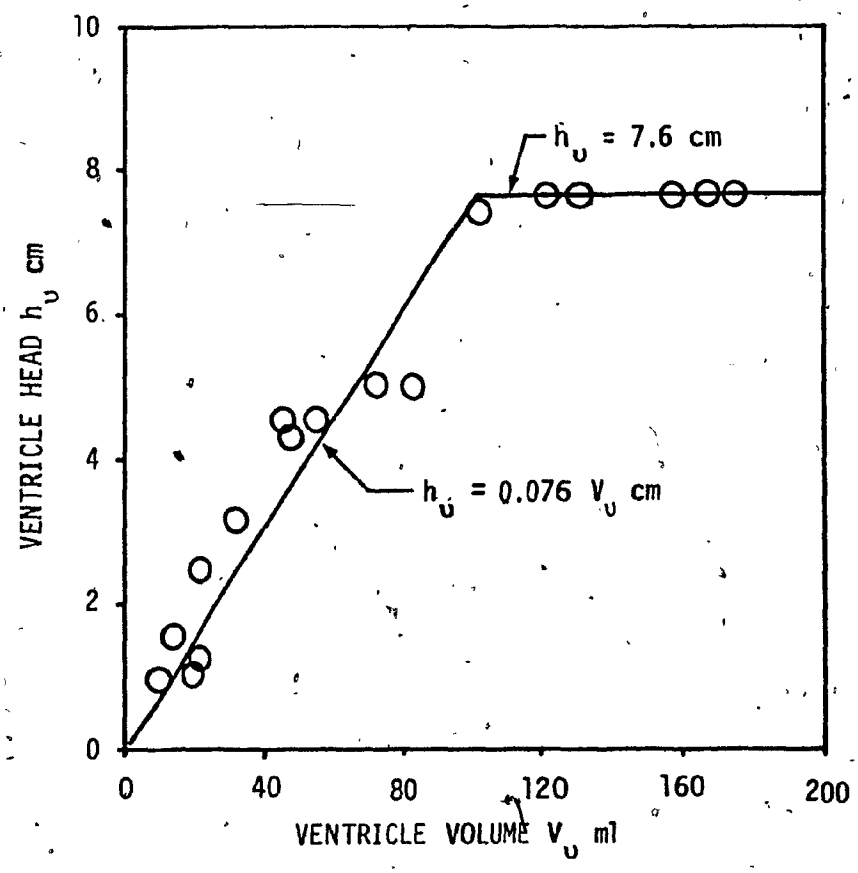

Fig. 44 - Ventricle head-volume characteristics.

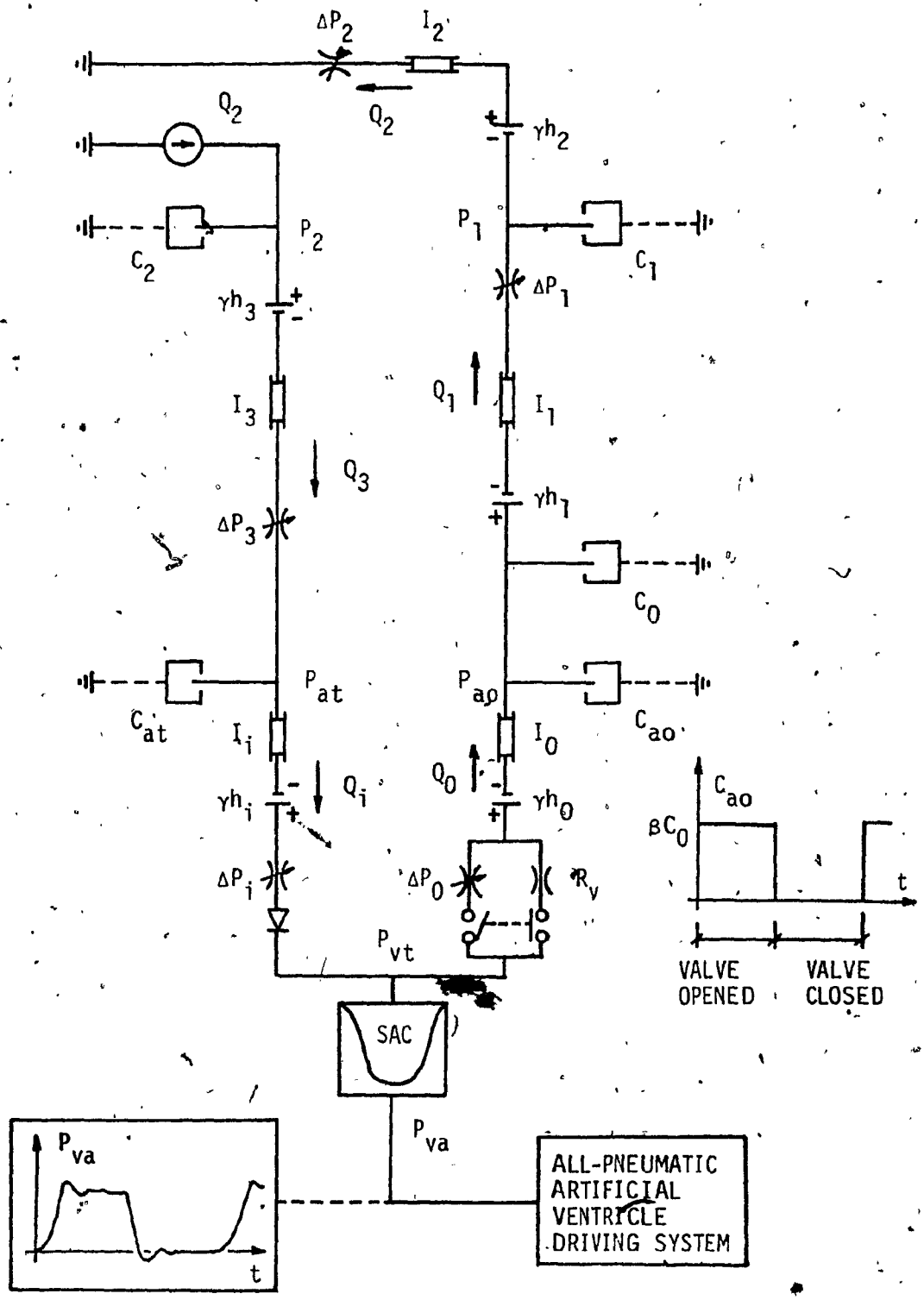

Fig. 45 - Symbolic circuit analogy of the artificial ventricle in mock circulation.

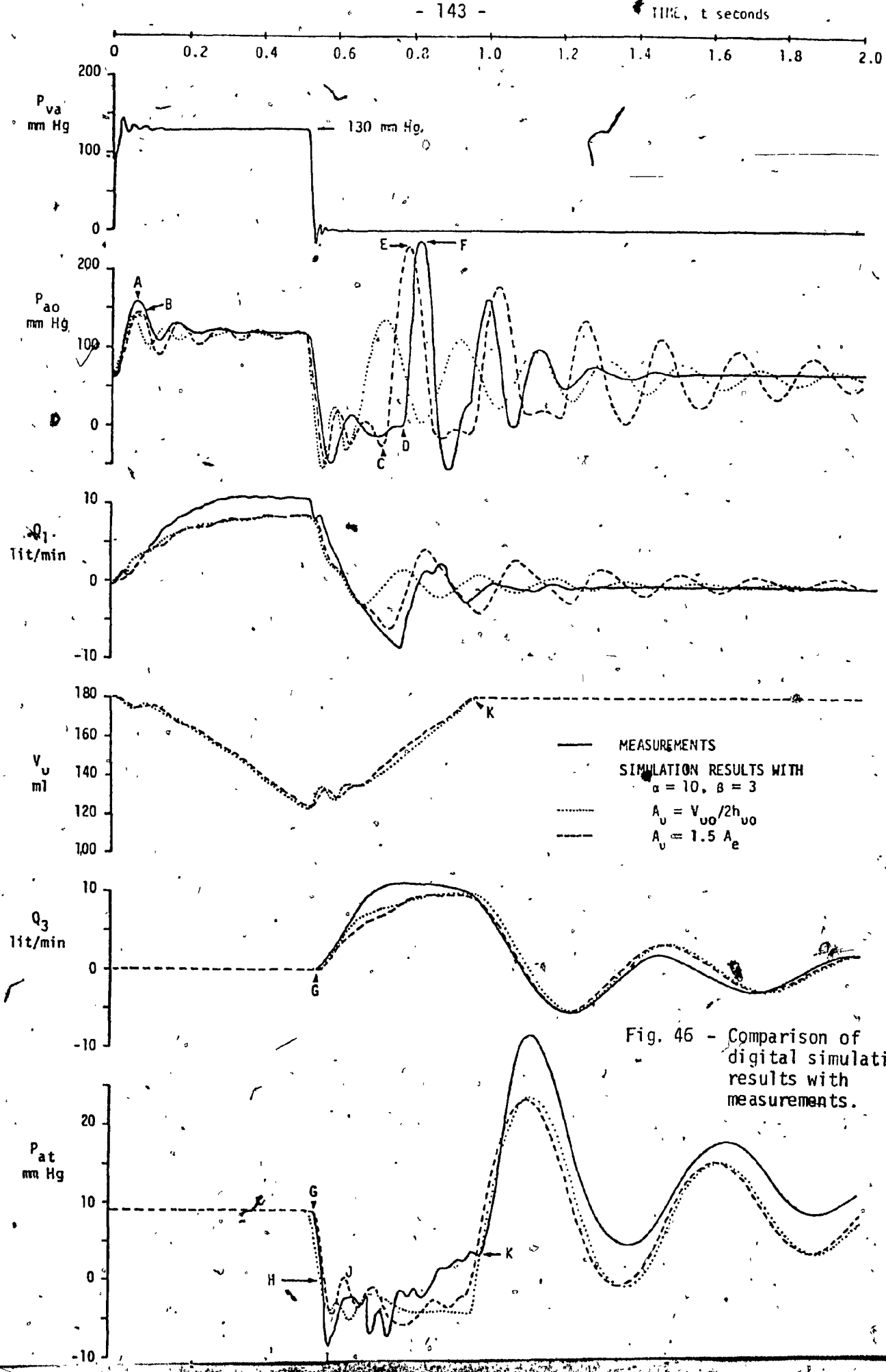

Fig. 46 - Comparison of digital simulation results with measurements.

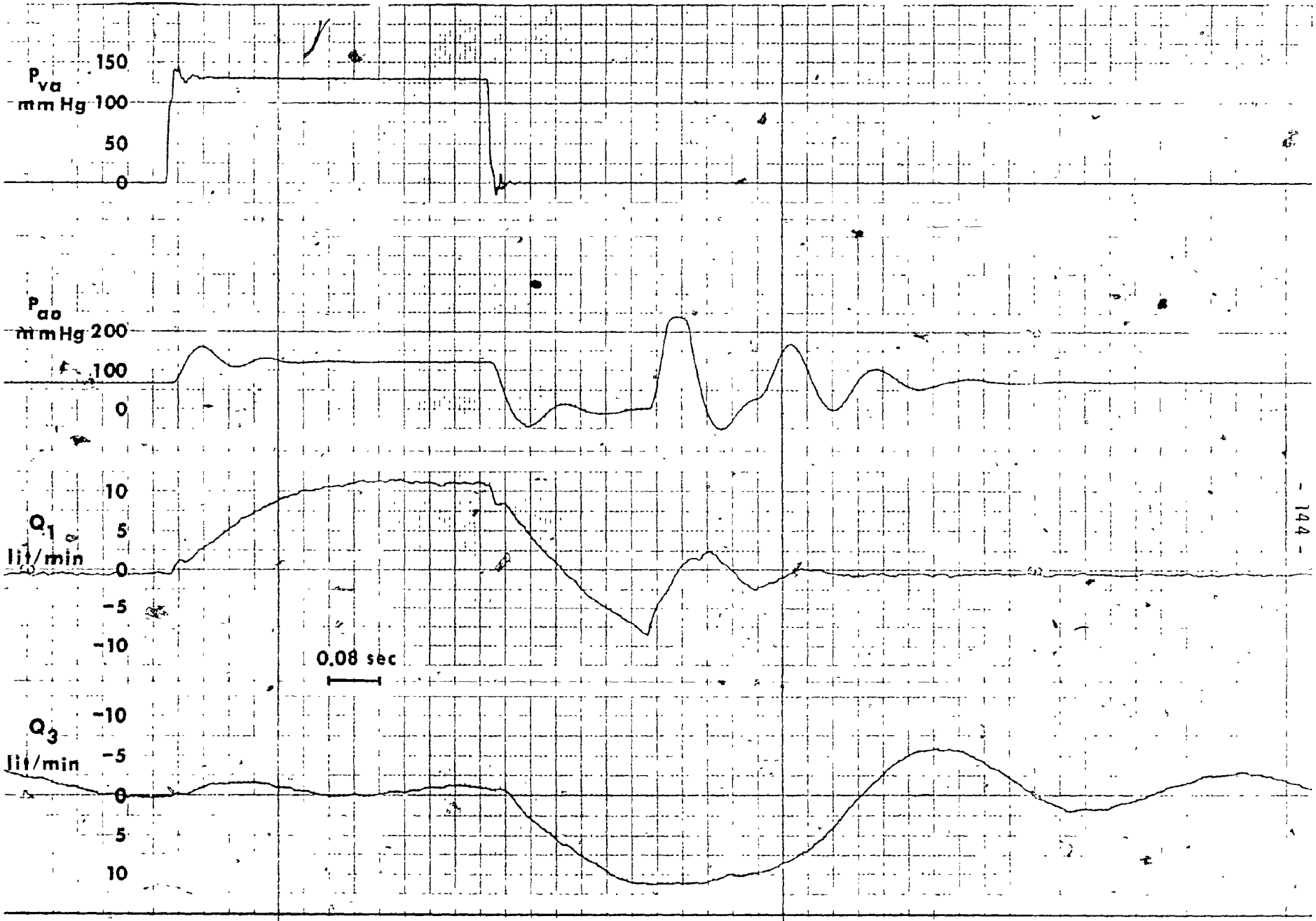

Fig. 47 - Typical measured dynamic stripchart recordings.

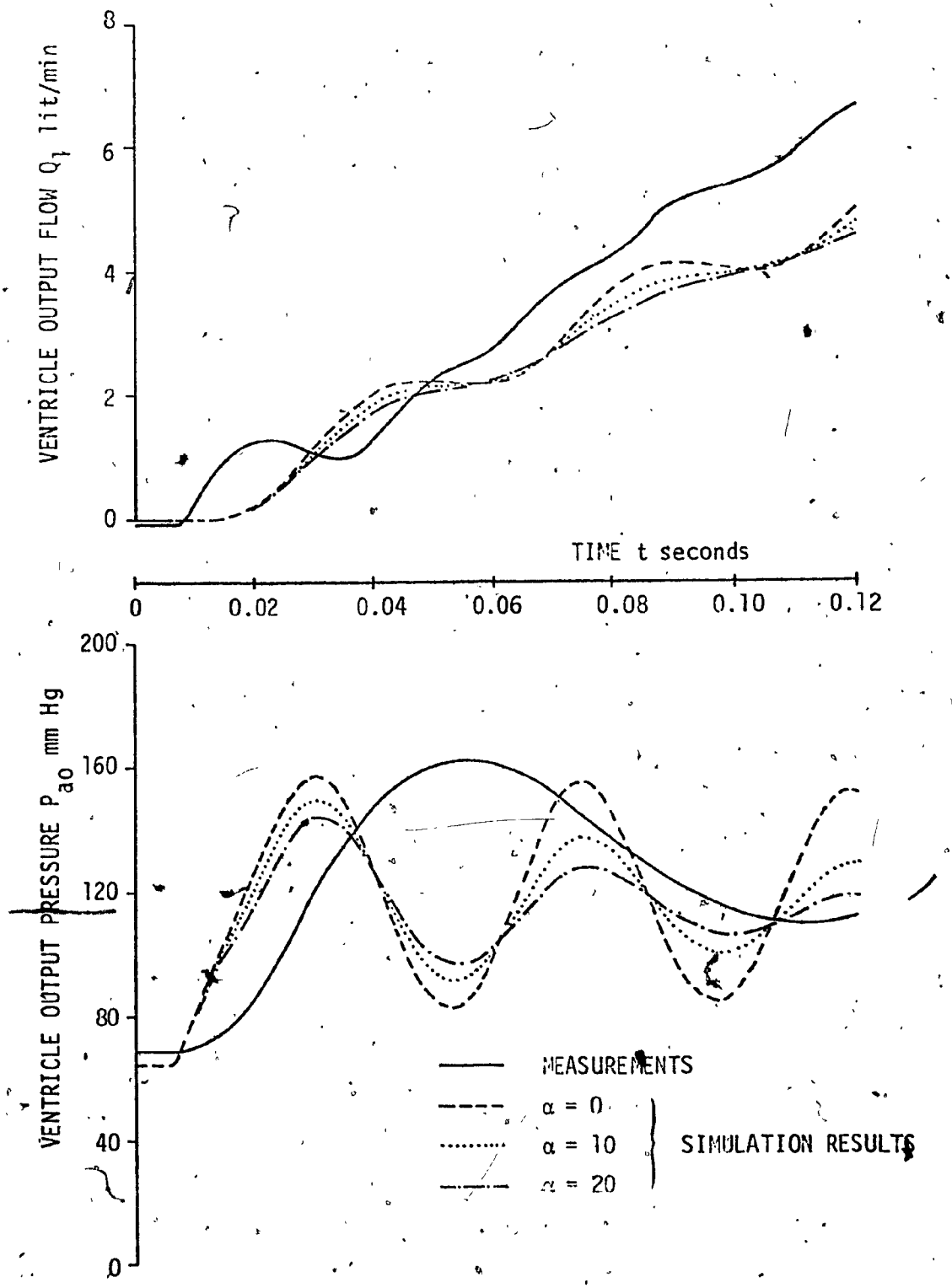

Fig. 48 - Comparison of simulation results with measurements: Effects of α with $\beta = 0$ and $A_U = V_{UO} / 2h_{UO}$.

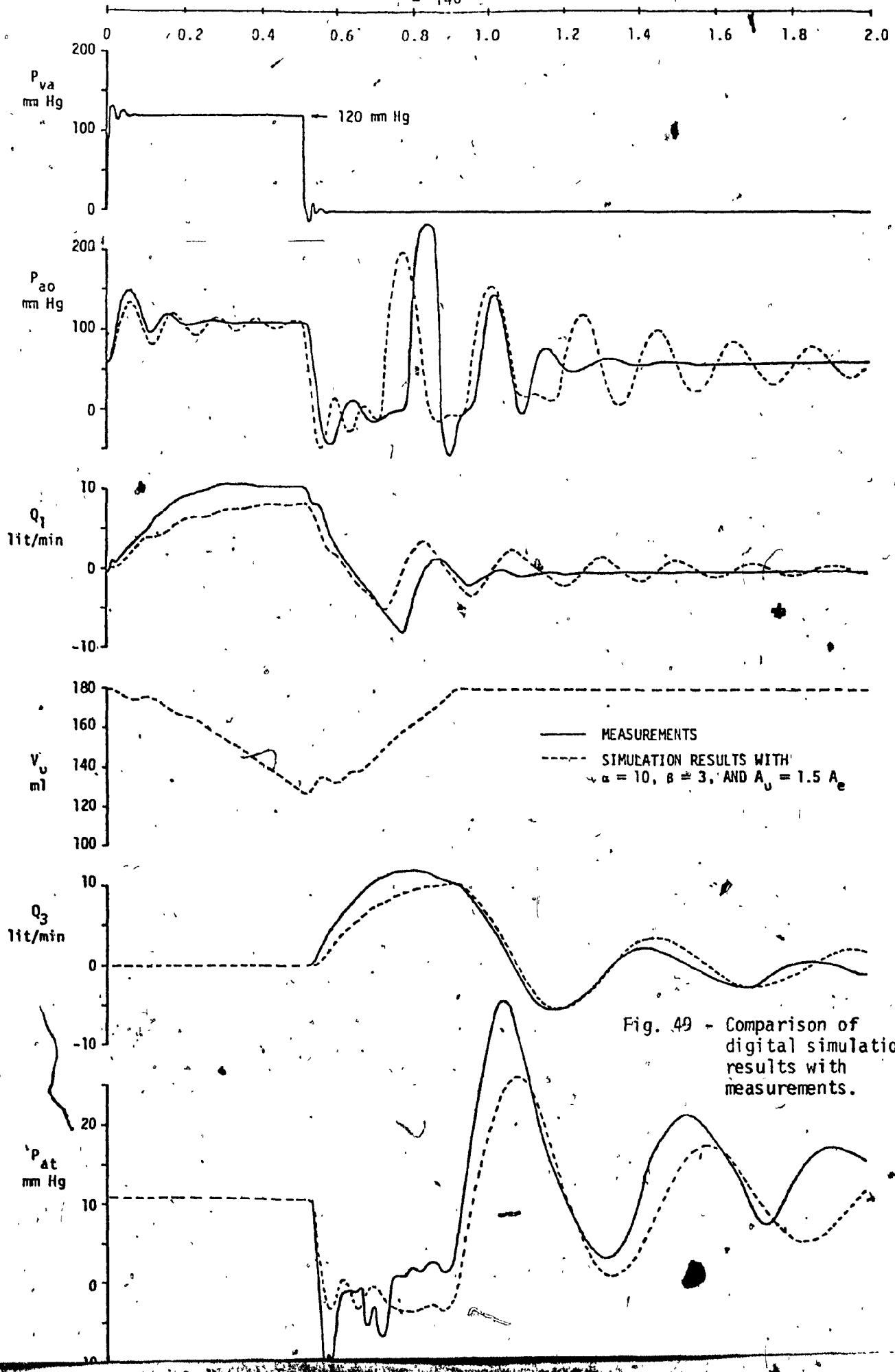

Fig. 49 - Comparison of digital simulation results with measurements.

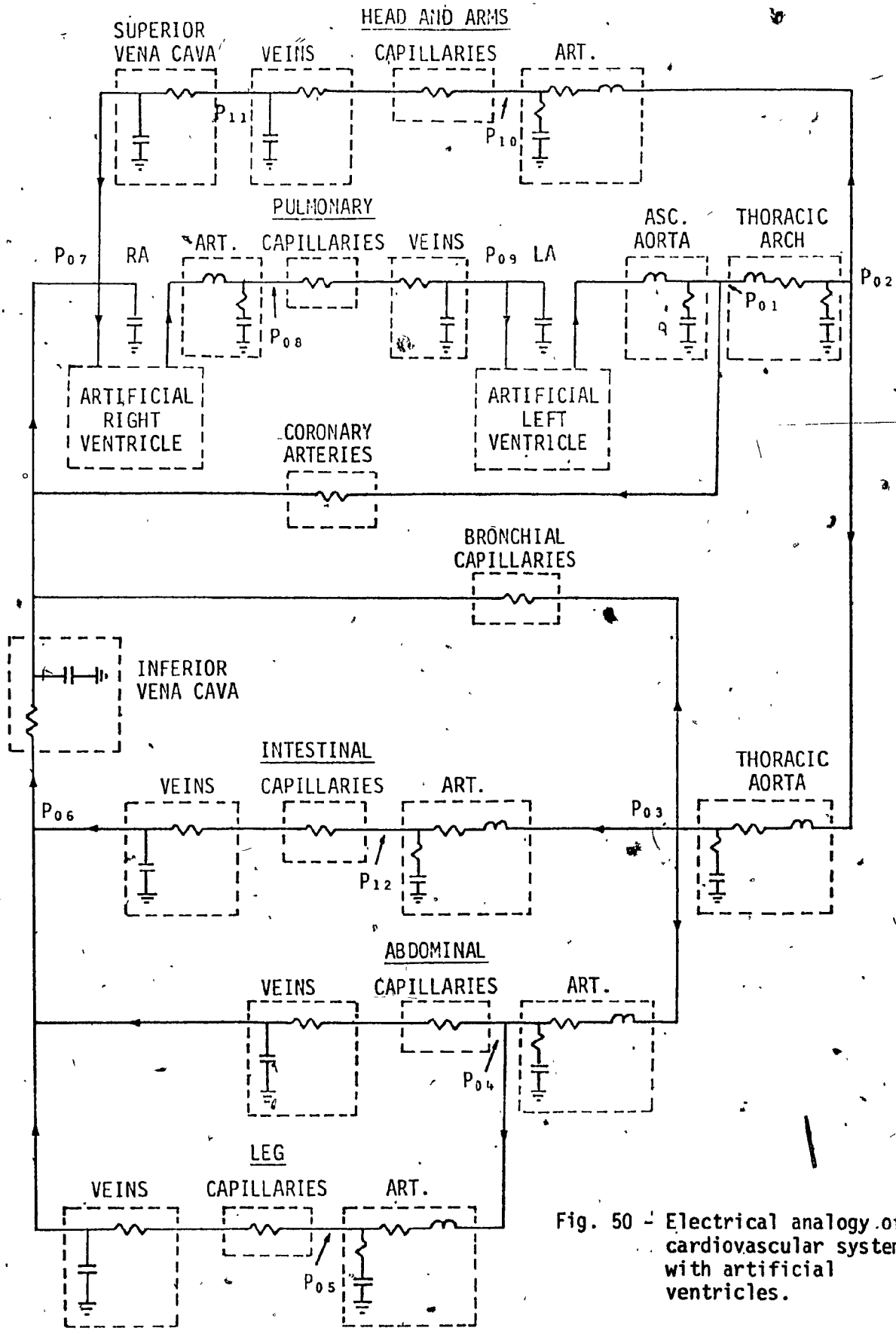

Fig. 50 - Electrical analogy of cardiovascular system with artificial ventricles.

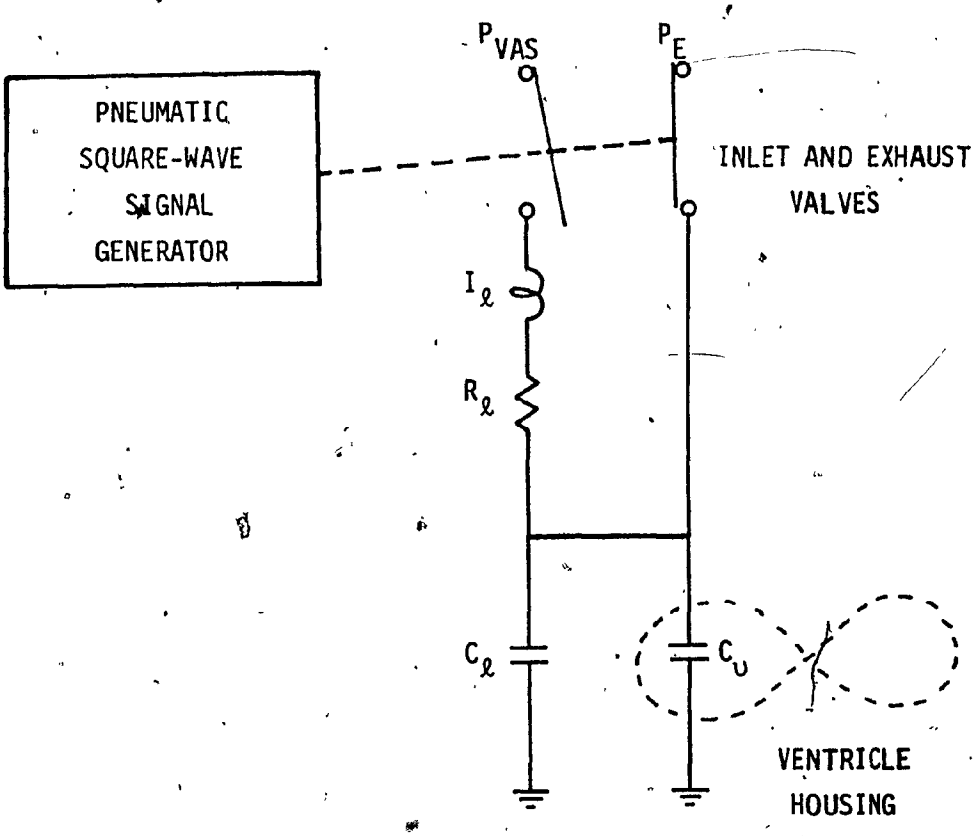

Fig. 51 - Schematic diagram of artificial ventricle driving system.

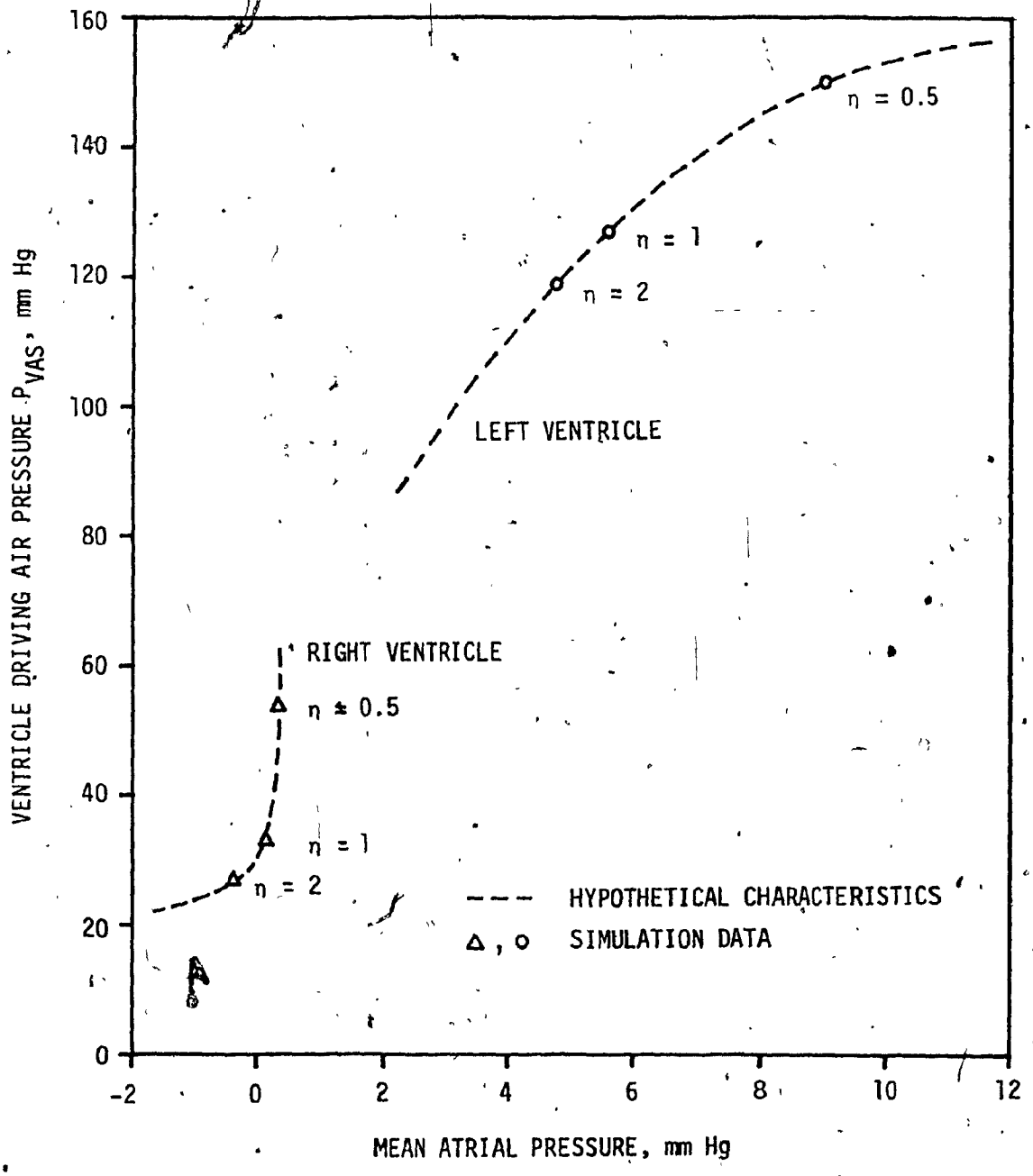

Fig. 52 - Left and right ventricle driving air pressures for η = 0.5, 1 and 2 at different mean atrial pressures.

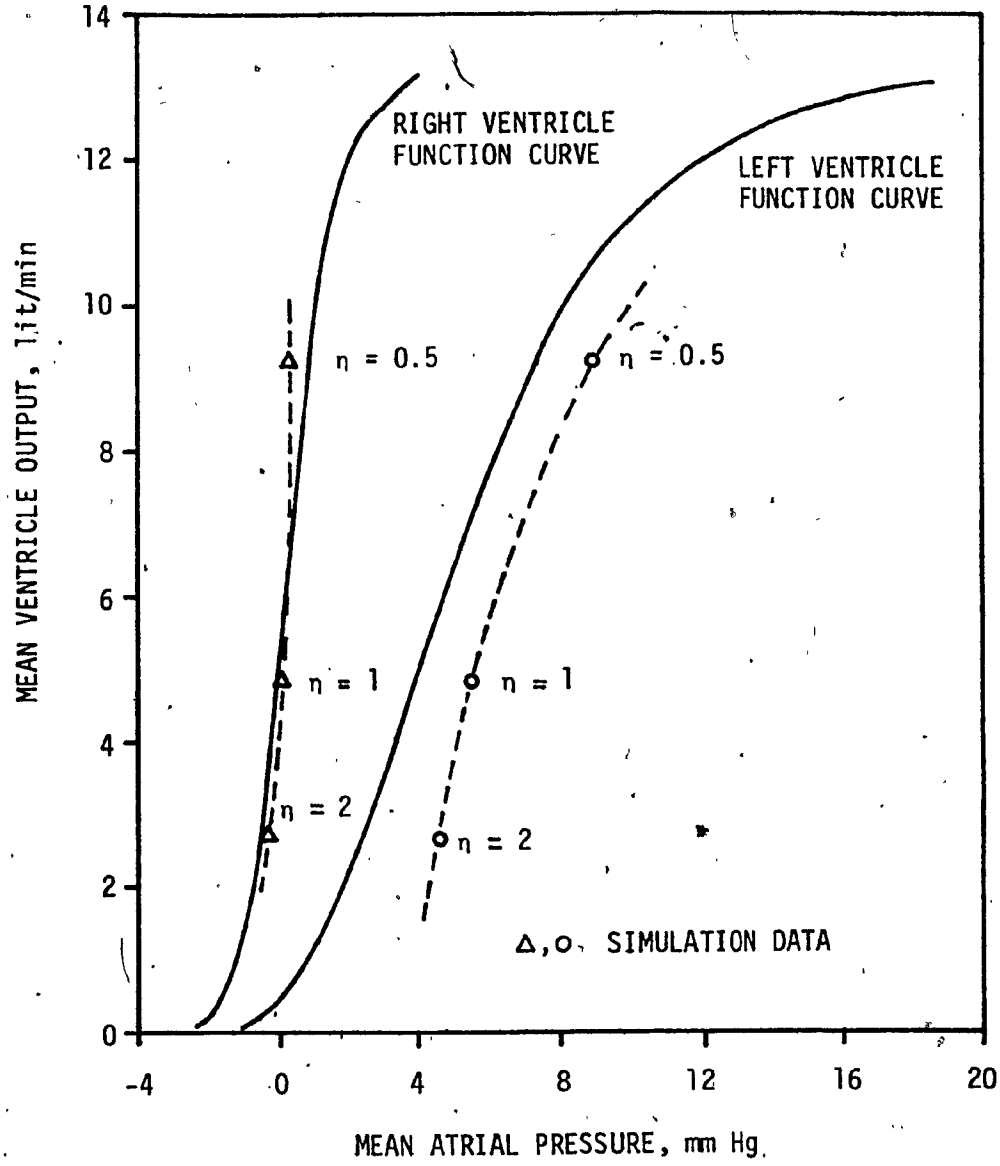

Fig. 53 - Comparison of simulated mean ventricle outputs with the function curves of the normal physiological heart [3] at different mean atrial pressures.

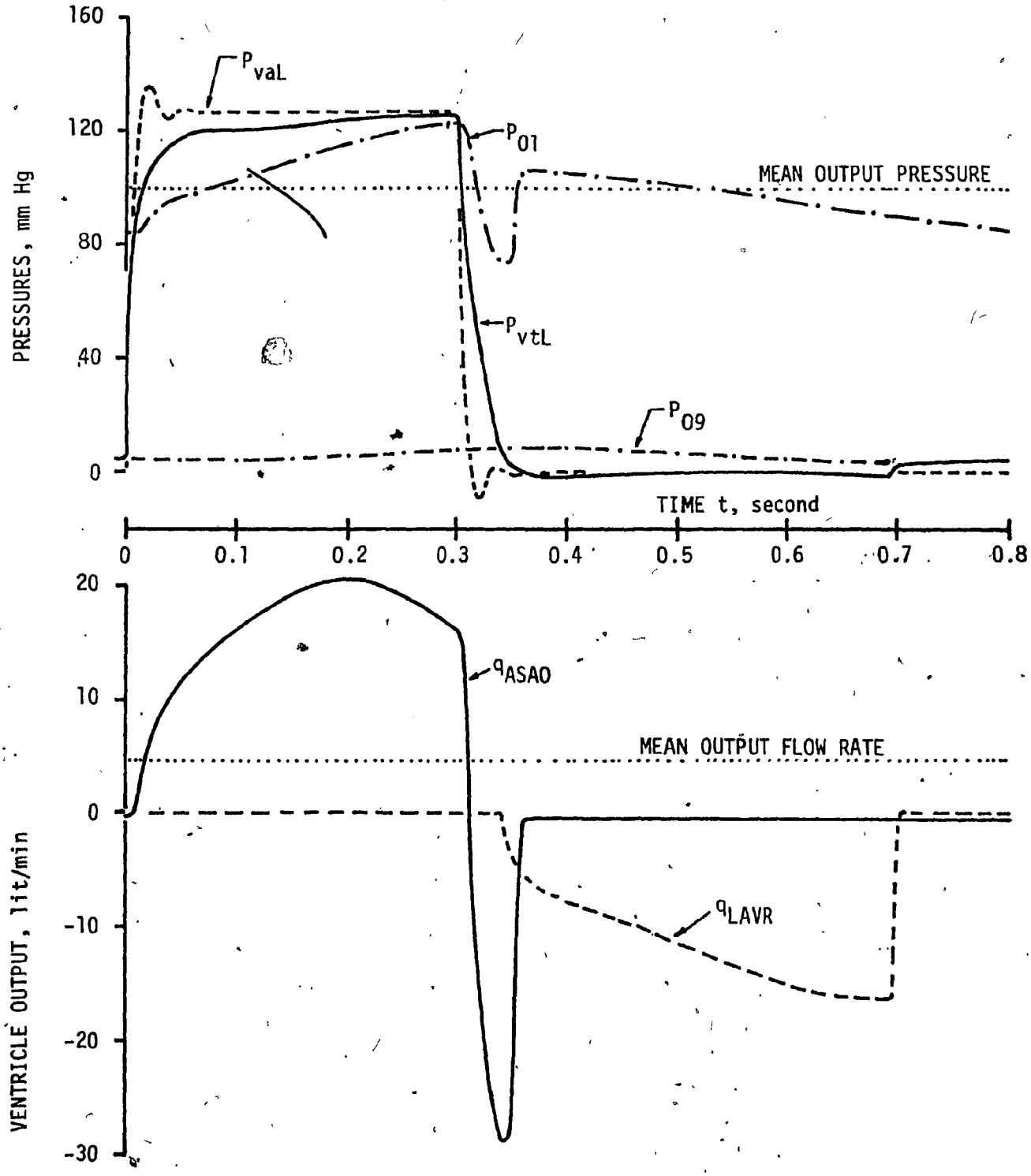

Fig. 54a - Typical simulated pressures and flows dynamic traces from the left ventricle side with normal vascular resistances (n = 1).

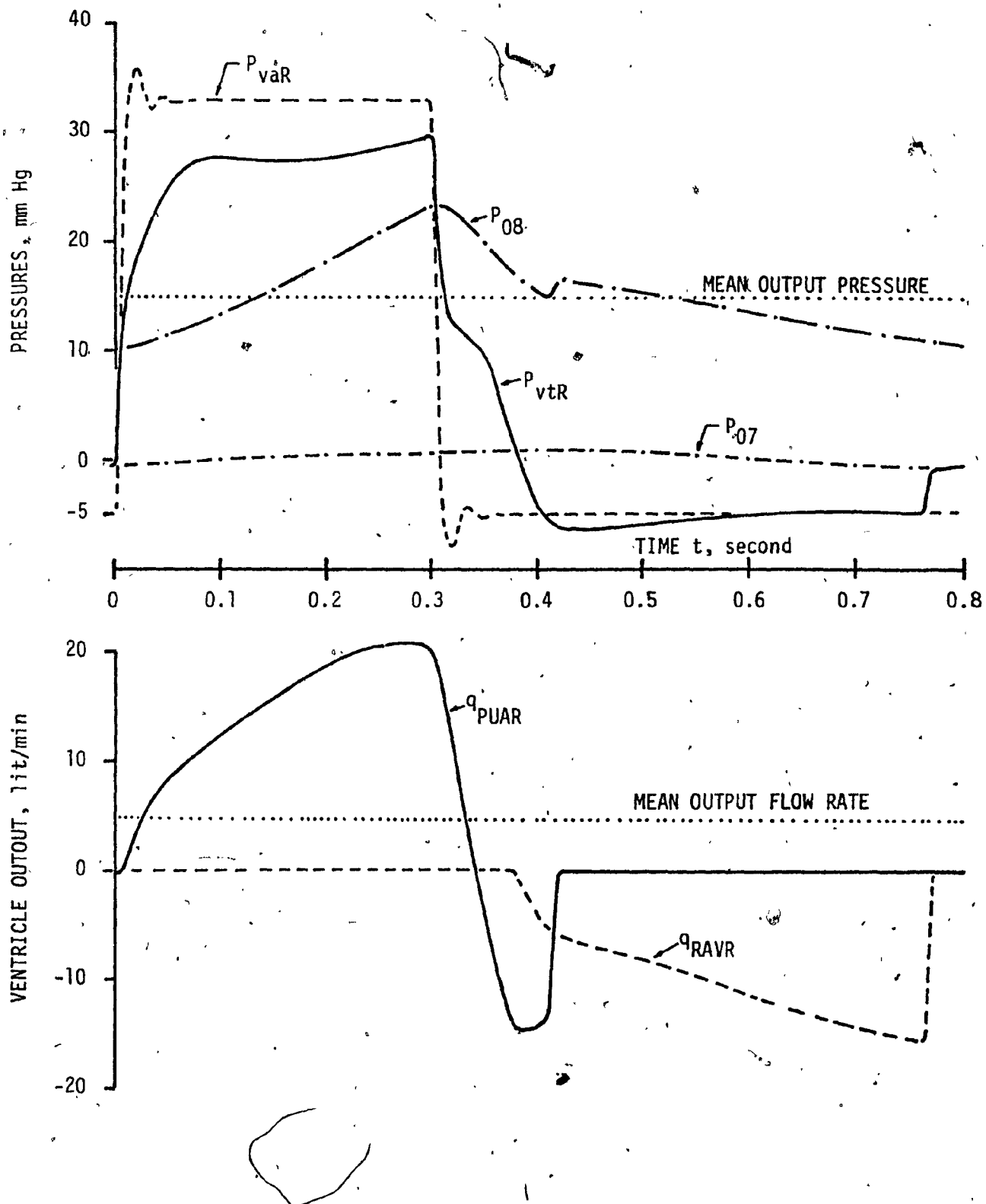

Fig. 54b - Typical simulated pressures and flows dynamic traces from the right ventricle side with normal vascular resistances ($n = 1$).

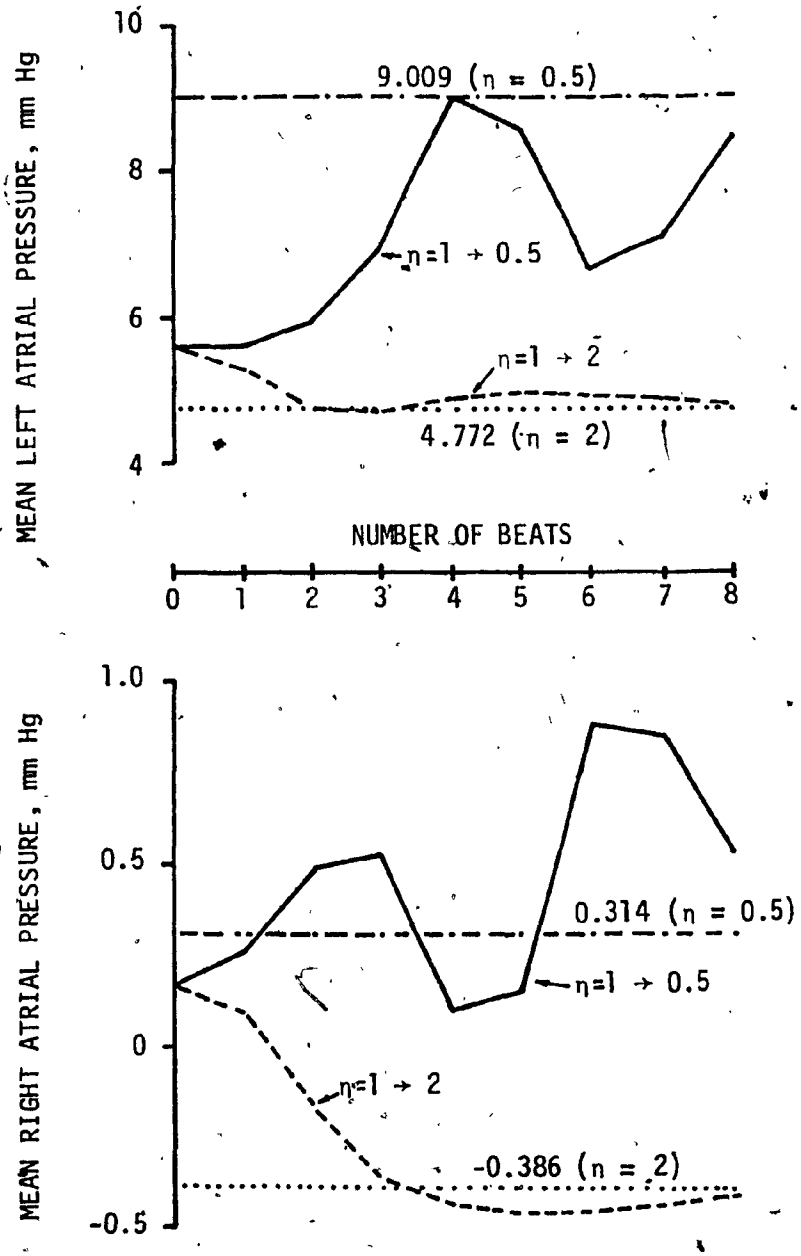

Fig. 55 - Variation of mean left and right atrial pressures as vascular resistances are varied exponentially with time by a factor of 0.5, and 2.

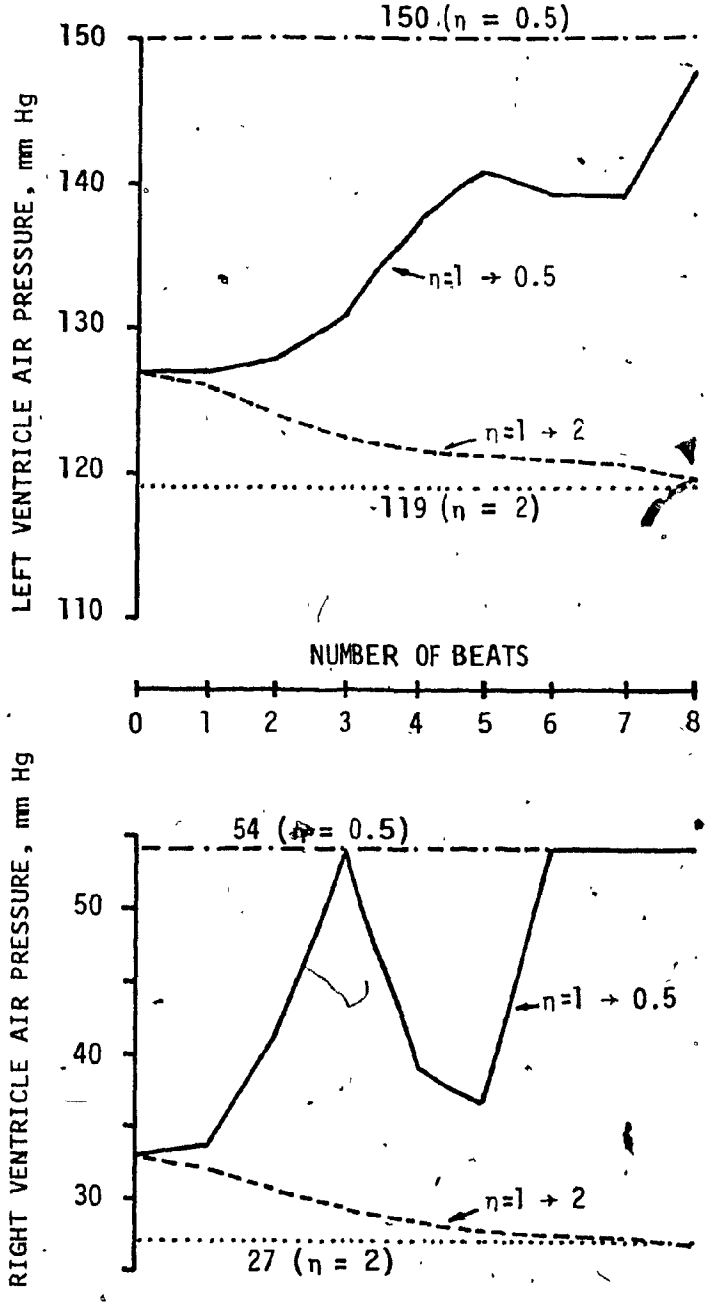

Fig. 56 - Variation of left and right ventricle driving air pressures as vascular resistances are varied exponentially with time by a factor of 0.5, and 2.

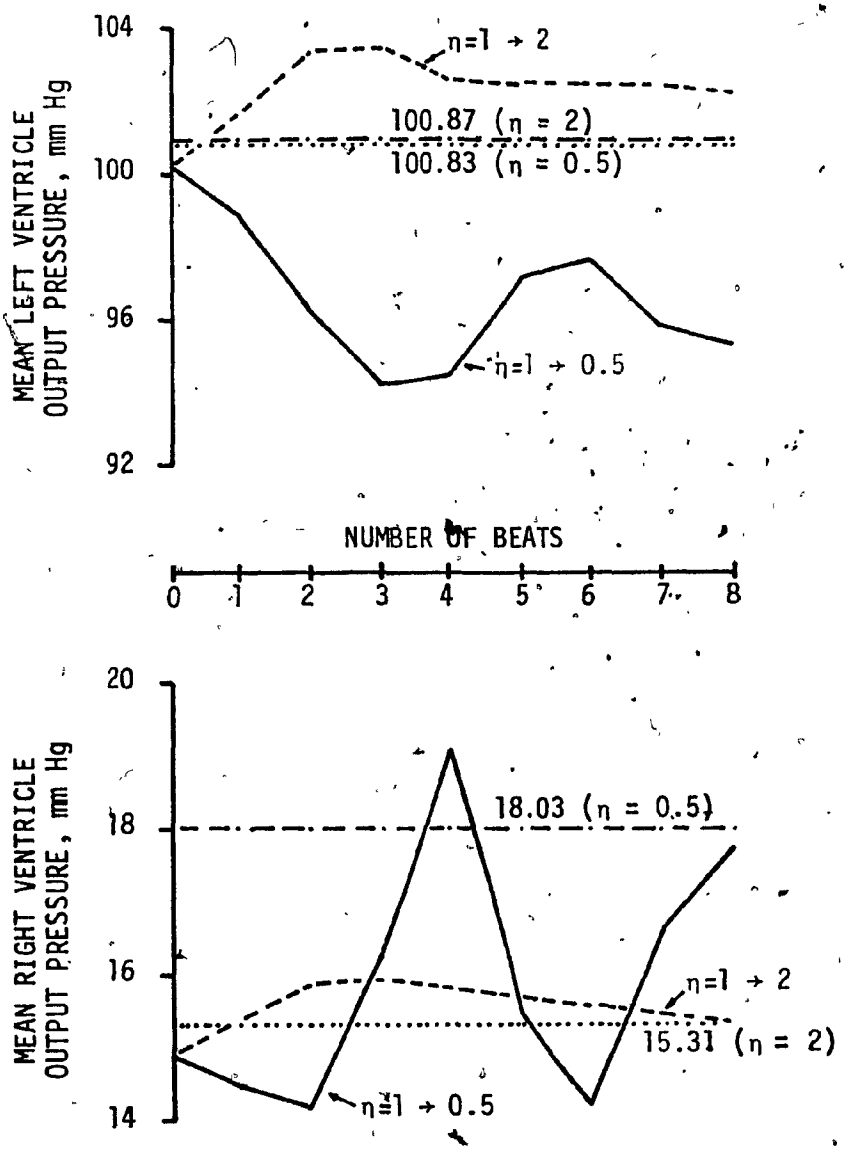

Fig. 57 - Variation of mean left and right ventricle output pressures as vascular resistances are varied exponentially with time by a factor of 0.5, and 2.

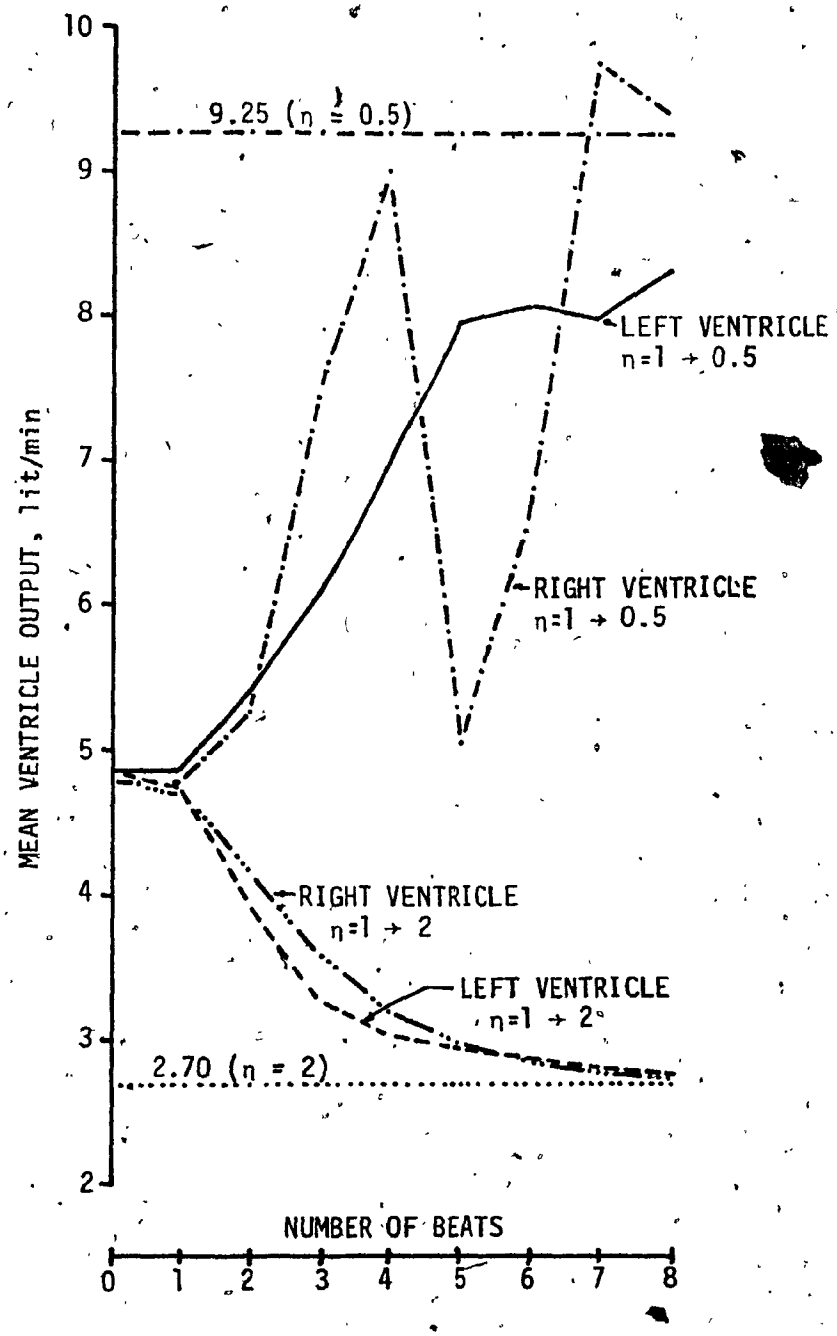

Fig. 58 - Variation of mean left and right ventricle outputs as vascular resistances are varied exponentially with time by a factor of 0.5, and 2.

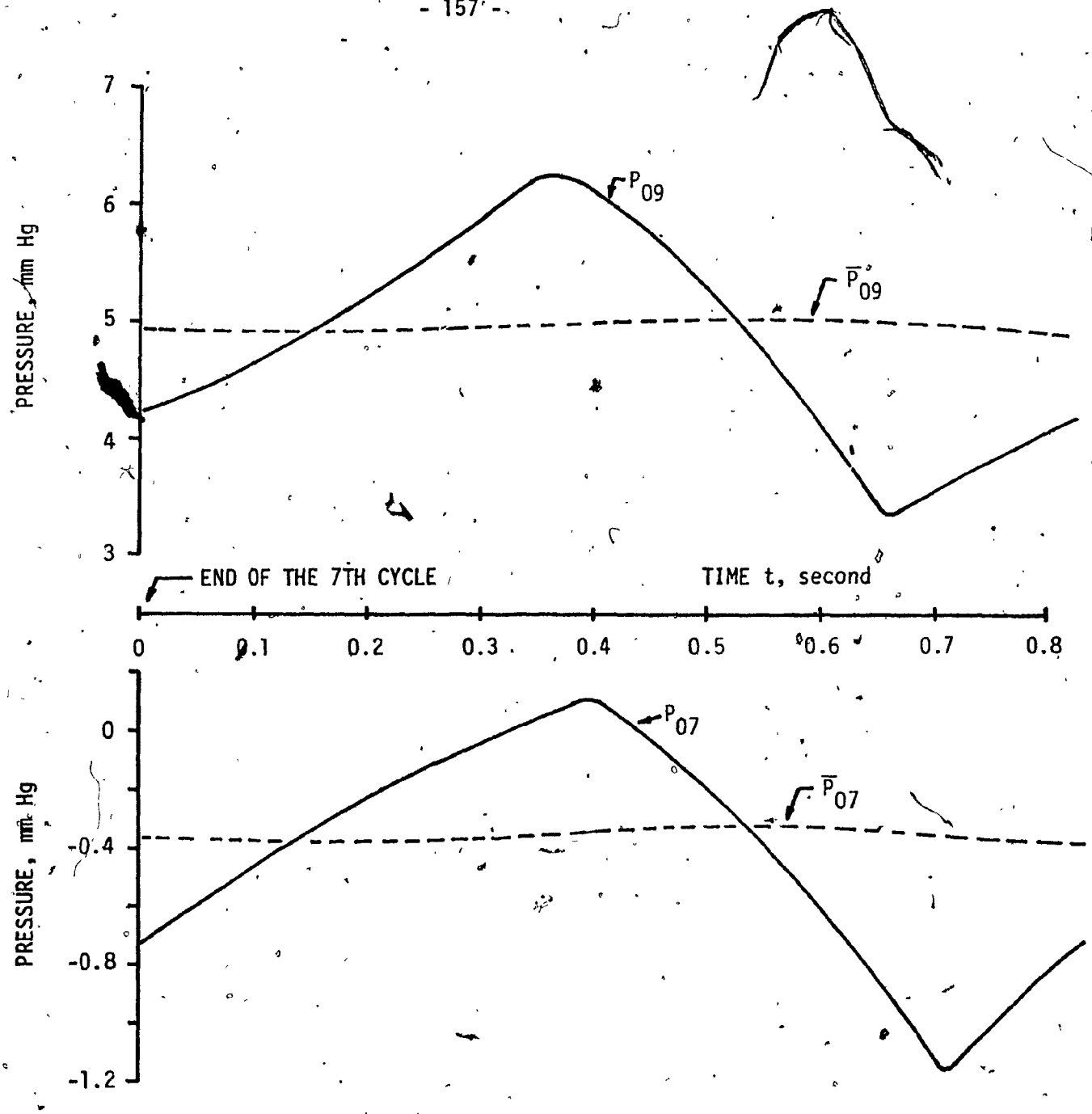

Fig. 59 - Comparison of left and right atrial pressures with the corresponding pressures at output of the passive filter. (The pressures are predicted from the model during the 8th pumping cycle from start-up when n is varied exponentially with time from 1 to 2.)

APPENDIX A

The following figure is a detailed sketch of the connecting tube and fittings. The relevant dimensions, water density and viscosity are given in British units. Resistances and inertances of the tube assembly are first calculated in British units. They are then converted into the Metric units which are consistently used throughout the thesis. Minor losses are neglected in the calculation of the overall lumped resistance.

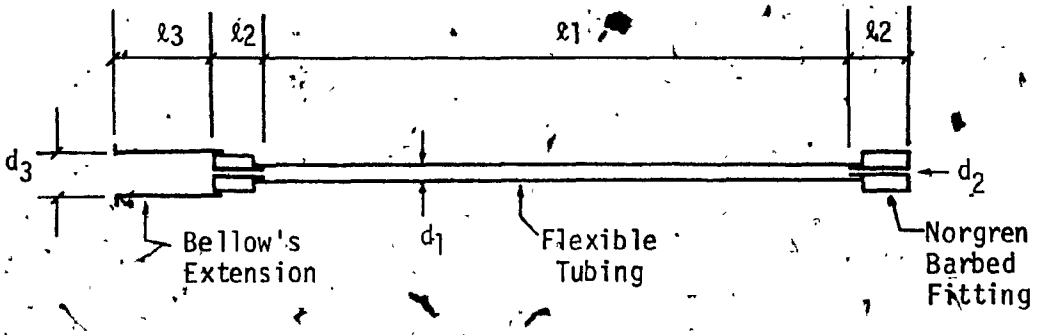

$d_1 = 0.067$ in. $\quad \ell 1 = 12$ in.

$d_2 = 0.043$ in. $\quad \ell 2 = 0.545$ in.

$d_3 = 0.088$ in. $\quad \ell 3 = 0.667$ in.

Resistance

$$\mu(\text{water}) = 1.64 \times 10^{-7}\ \text{lb}_f\text{-sec/in}^2$$

$$R_{\ell 1} = \frac{128(1.64 \times 10^{-7})(12)}{\pi(0.67 \times 10^{-1})^4} = 3.980\ \text{lb}_f\text{-sec/in}^5$$

$$R_{\ell 2} = \frac{128(1.64 \times 10^{-7})(0.545)}{\pi(0.43 \times 10^{-1})^4} = 1.065\ \text{lb}_f\text{-sec/in}^5$$

$$R_{\ell 3} = \frac{128(1.64 \times 10^{-7})(0.667)}{\pi(0.88 \times 10^{-1})^4} = 0.074\ \text{lb}_f\text{-sec/in}^5$$

The lumped resistance:

$$R_f = R_{\ell 1} + 2R_{\ell 2} + R_{\ell 3} = \underline{\underline{6.184\ \text{lb}_f\text{-sec/in}^5}}$$

or

$$R_f = 6.184\ \frac{\text{lb}_f\text{-sec}}{\text{in}^5} \times 4.448\ \frac{\text{N}}{\text{lb}_f} \times \left(\frac{1}{0.0254}\right)^5 \frac{\text{in}^5}{\text{m}^5}$$

$$= \underline{\underline{2.60 \times 10^9\ \text{N-sec/m}^5}}$$

Inertance

$$\rho(\text{water}) = 9.36 \times 10^{-5}\ \text{lb}_f\text{-sec/in}^4$$

$$I_{\ell 1} = \frac{4(9.36 \times 10^{-5})(12)}{\pi(0.67 \times 10^{-1})^2} = 0.3187\ \text{lb}_f\text{-sec}^2\text{/in}^5$$

$$I_{\ell 2} = \frac{4(9.36 \times 10^{-5})(0.545)}{\pi(0.43 \times 10^{-1})^2} = 0.0351 \text{ lb}_f\text{-sec}^2/\text{in}^5$$

$$I_{\ell 3} = \frac{4(9.36 \times 10^{-5})(0.667)}{\pi(0.88 \times 10^{-1})^2} = 0.0103 \text{ lb}_f\text{-sec}^2/\text{in}^5$$

The lumped inertance:

$$I_f = \frac{4}{3}(I_{\ell 1} + 2I_{\ell 2} + I_{\ell 3}) = \underline{\underline{0.5323 \text{ lb}_f\text{-sec}^2/\text{in}^5}}$$

or

$$I_f = 0.5323 \frac{\text{lb}_f\text{-sec}^2}{\text{in}^5} \times 4.448 \frac{\text{N}}{\text{lb}_f} \times \left(\frac{1}{0.0254}\right)^5 \frac{\text{in}^5}{\text{m}^5}$$

$$= \underline{\underline{2.24 \times 10^8 \text{ N-sec}^2/\text{m}^5}}$$

APPENDIX B

From static measurements, the pressure-displacement characteristics of the bellows capsule shown in Figure B.1, are obtained. The displacement was measured with a traversing microscope. The inverse of the slope of the characteristic curve gives the spring constant of the bellows capsule, i.e.

$$k_{bs} = \frac{\Delta P}{\Delta X} = \frac{4 \text{ in } H_2O}{0.00277 \text{ in}} \times 0.0361 \frac{lb_f/in^2}{\text{in } H_2O}$$

$$= \underline{\underline{52.1 \ lb_f/in^2/in}}$$

or

$$k_{bs} = 52.1 \frac{lb_f}{in^3} \times 6890 \frac{N/m^2}{lb_f/in^2} \times 39.37 \frac{in}{m}$$

$$= \underline{\underline{1.41 \times 10^7 \ N/m^2/m}}$$

The capacitance C_{f1} can be calculated as

$$C_{f1} = \frac{A_{be}}{k_{bs}} = \frac{(0.5)(3.62 \times 10^{-3})}{1.41 \times 10^7} = 1.28 \times 10^{-10} \ m^5/N$$

where $A_{be} = 0.5 \ A_b$ with $A_b = 3.62 \times 10^{-3}$ (the bellows area).

Similarly,

$$C_{f2} = \frac{V_{bo}}{kP_o} = \frac{0.4 \ V_b}{kP_o} = \frac{(0.4)(1.9 \times 10^{-5})}{(1.0)(14.7)(6890)}$$

$$= \underline{\underline{7.5 \times 10^{-11} \ m^5/N}}$$

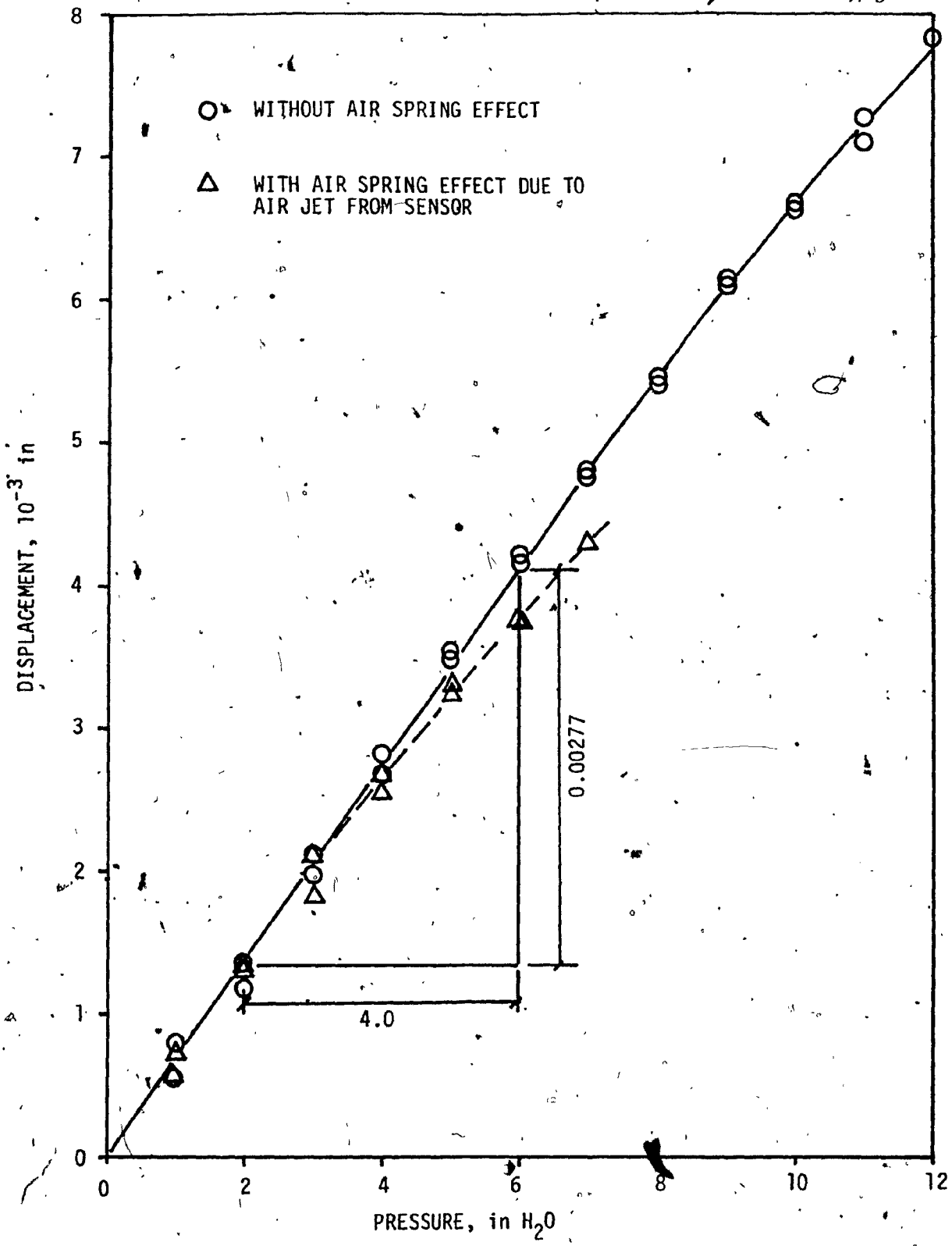

Fig. B.1 - Pressure - displacement characteristics of bellows.

APPENDIX C

By solving the circuit shown in Figure 23 of the text, the following momentum equation is obtained.

$$I_f \frac{dQ}{dt} + R_f Q + \frac{1}{(C_{f1} + C_{f2})} \int_0^t Q \, dt = P_i(t) \qquad (C.1)$$

Let

$$W_n = \sqrt{\frac{1}{I_f(C_{f1} + C_{f2})}} \qquad (C.2)$$

$$\zeta = \frac{R_f}{2}\sqrt{\frac{(C_{f1} + C_{f2})}{I_f}} \qquad (C.3)$$

Equation (C.1) can be written as

$$\frac{dQ}{dt} + 2\zeta W_n Q + W_n^2 \int_0^t Q \, dt = \frac{1}{I_f} P_i(t) \qquad (C.4)$$

For $\zeta > 1$, the natural response (i.e. the homogeneous solution of Equation (C.4)) is

$$Q_n(t) = A_1 e^{r_1 t} + A_2 e^{r_2 t} \qquad (C.5)$$

where A_1 and A_2 are constants to be determined from known boundary conditions, and $r_{1,2} = -\zeta W_n \pm W_n\sqrt{\zeta^2 - 1}$.

For an excitation of

$$P_i(t) = P_o(1 - e^{-t/\tau}) \qquad (C.6)$$

the forced response (i.e. the particular solution of Equation (C.4)) is of the form

$$Q_f(t) = Q_{f0} + Q_{f1}e^{-t/\tau} \tag{C.7}$$

where Q_{f0} and Q_{f1} are constants. By substituting Equation (C.7) into Equation (C.4), it is found that

$$Q_{f0} = 0 \tag{C.8}$$

and

$$Q_{f1} = \frac{P_o\tau}{I_f}\left(\frac{1}{1 - 2\zeta W_n\tau + W_n^2\tau^2}\right) \tag{C.9}$$

That is, with Q_{f0} and Q_{f1} as given by Equations (C.8) and (C.9), respectively, the solution given by Equation (C.7) satisfies the differential equation in Equation (C.4). Therefore, the complete response of the hydraulic circuit is

$$Q(t) = A_1e^{r_1t} + A_2e^{r_2t} + \left(\frac{1}{1 - 2\zeta W_n\tau + W_n^2\tau^2}\right)\frac{P_o\tau}{I_f}e^{-t/\tau} \tag{C.10}$$

Using the boundary conditions $Q(0) = 0$, and $\dot{Q}(0) = 0$, the constants A_1 and A_2 are determined to be:

$$A_1 = \frac{-\frac{P_o}{I_f}(1 + \tau r_2)}{(r_2 - r_1)(1 - 2\zeta W_n\tau + W_n^2\tau^2)} \tag{C.11}$$

$$A_2 = \frac{\frac{P_o}{I_f}(1 + \tau r_1)}{(r_2 - r_1)(1 - 2\zeta W_n\tau + W_n^2\tau^2)} \tag{C.12}$$

Since
$$P(t) = \frac{1}{(C_{f1} + C_{f2})} \int_0^t Q\, dt \tag{C.13}$$

and $P(0) = 0$, the pressure $P(t)$ can be found by integrating Equation (C.10). The result is

$$P(t) = \frac{P_o W_n^2}{1 - 2\zeta W_n \tau + W_n^2 \tau^2} \left\{ \frac{1 + \tau r_1}{r_2(r_1 - r_2)} (1 - e^{r_2 t}) \right.$$
$$\left. - \frac{1 + \tau r_2}{r_1(r_1 - r_2)} (1 - e^{r_1 t}) + \tau^2 (1 - e^{-t/\tau}) \right\} \tag{C.14}$$

APPENDIX D

With the assumptions (Nos. 6, 7 and 8) listed in Section 4.2, the term associated with the rate of change of energy within the control volume can be expanded as follows:

$$\frac{d}{dt}\int_{c} (u + \frac{v^2}{2} + gz)\,\rho dv_c = \Phi = \frac{d}{dt}\left[(\frac{v^2}{2} - \frac{1}{2}gh_v)\,\rho V_v\right]$$

$$= (\frac{1}{2}\rho v^2 - \frac{1}{2}\gamma h_v)\frac{dV_v}{dt} + \rho V_v(v\frac{dv}{dt} - \frac{1}{2}g\frac{dh_v}{dt}) \qquad (D.1)$$

With assumption No. 9, the above equation can be written as

$$\Phi = \{\frac{\rho(Q_o - Q_i)^2}{2A_v^2} - \frac{1}{2}\gamma h_v\}\dot{V}_v$$

$$+ \frac{\rho V_v}{A_v^2}(Q_o - Q_i)(\dot{Q}_o - \dot{Q}_i) - \frac{1}{2}\gamma V_v \dot{h}_v \qquad (D.2)$$

Taking the datum at the non-deformable control surface, and applying assumptions Nos. 1, 6 and 10, the net energy flux leaving the control surface is

$$\int_s (u + \frac{p}{\rho} + \frac{v^2}{2} + gz)\,\rho\vec{V}_r \cdot d\vec{A}$$

$$= \{P_{yt} + \frac{\rho(Q_o - Q_i)^2}{2A_e^2}\}\,(Q_o - Q_i) \qquad (D.3)$$

Using the remaining assumptions (Nos. 2-5), the energy

equation of the deformable control volume becomes

$$- P_\sigma \dot{V}_U + \left\{\frac{\rho(Q_o - Q_i)^2}{2A_U^2} - \frac{1}{2}\gamma h_U\right\} \dot{V}_U$$

$$+ \frac{\rho V_U}{A_U^2}(Q_o - Q_i)(\dot{Q}_o - \dot{Q}_i) - \frac{1}{2}\gamma V_U \dot{h}_U$$

$$+ \left\{P_{vt} + \frac{\rho(Q_o - Q_i)^2}{2A_e^2}\right\}(Q_o - Q_i) + P_{va}\dot{V}_U = 0 \quad (D.4)$$

Dividing by $\dot{V}_U = (Q_i - Q_o)$ given in the text, Equation (D.4) reduces to the following momentum equation

$$P_{va} - P_{vt} - P_\sigma - \frac{1}{2}\gamma\left[h - \frac{V_U}{(Q_o - Q_i)}\dot{h}_U\right] + \frac{1}{2}\frac{\rho(Q_o - Q_i)^2}{A_U^2}$$

$$- \frac{1}{2}\frac{\rho(Q_o - Q_i)^2}{A_e^2} = \frac{\rho V_U}{A_U^2}(\dot{Q}_o - \dot{Q}_i) \quad (D.5)$$